

**BEHAVIOUR OF LATERRALLY LOADED PILES IN SOILS**

**M.Sc. Thesis by  
Zeynep ŞEKERER**

**Department : Civil Engineering**

**Programme : Soil Mechanics and Geotechnical  
Engineering**

**JUNE 2009**



**BEHAVIOUR OF LATERRALLY LOADED PILES IN SOILS**

**M.Sc. Thesis by  
Zeynep ŞEKERER  
(501051316)**

**Date of submission : 04 MAY 2009  
Date of defence examination: 01 JUNE 2009**

**Supervisor (Chairman) : Assist. Prof. Dr. Berrak TEYMÜR (ITU)  
Members of the Examining Committee : Assoc.Prof. Dr. İsmail Hakkı AKSOY  
(ITU)  
Assist. Prof. Dr. Kubilay KELEŞOĞLU  
(IU)**

**JUNE 2009**



**İSTANBUL TEKNİK ÜNİVERSİTESİ ★ FEN BİLİMLERİ ENSTİTÜSÜ**

**YANAL YÜKLÜ KAZIKLARIN ZEMİNLERDE DAVRANIŞI**

**YÜKSEK LİSANS TEZİ  
Zeynep ŞEKERER  
(501051316)**

**Tezin Enstitüye Verildiği Tarih : 04 Mayıs 2009**

**Tezin Savunulduğu Tarih : 01 Haziran 2009**

**Tez Danışmanı : Yrd. Doç. Dr. Berrek TEYMÜR (İTÜ)  
Diğer Jüri Üyeleri : Doç. Dr. İsmail Hakkı AKSOY (İTÜ)  
Yrd. Doç. Dr. Kubilay KELEŞOĞLU  
(İÜ)**

**JULY 2009**



## **FOREWORD**

I would like to express my deep appreciation and thanks for my supervisor, Assist. Prof. Dr. Berrak TEYMÜR. She has made this work possible in many ways by offering excellent guidance and support during this work. Without her understanding and friendly attitude, this study would not have been easy to handle.

I am grateful to Zetaş Zemin Teknolojisi A.Ş., for providing the test site, equipment and great literature. I am also grateful to Reinforced Earth İnşaat Proje ve Tic. A.Ş., for supporting to the thesis work.

I owe heartfelt gratitude to Murat Oşar for his affection, guidance and kind help during this study because he has always supported encouraged and motivated me.

Finally, I would like to thank my mother Filiz Şekerer, Metin Şekerer, Ufuk Şekerer and Selin Şekerer for their great patience, support and love during this study.



## TABLE OF CONTENTS

	<u>Page</u>
<b>LIST OF TABLES.....</b>	<b>ix</b>
<b>LIST OF FIGURES.....</b>	<b>xi</b>
<b>SUMMARY.....</b>	<b>xvii</b>
<b>1. INTRODUCTION.....</b>	<b>1</b>
<b>2. RESPONSE OF A PILE UNDER LOADINGS.....</b>	<b>3</b>
2.1    Classification of Piles.....	3
2.1.1    Timber Piles.....	3
2.1.2    Concrete piles.....	5
2.1.3    Steel pile.....	7
2.1.4    Cast-in-place pipe pile.....	7
2.2    Classification of Piles Loading.....	8
2.2.1    Static Loading.....	8
2.2.2    Cyclic Loading.....	9
2.2.3    Sustained Loading.....	13
2.2.4    Dynamic Loading.....	13
<b>3. LATERAL LOADING CAPACITY OF SINGLE PILES.....</b>	<b>15</b>
3.1    Load Transfer Mechanism for Laterally Loaded Piles.....	18
3.2    p-y Curves for Piles in Sand.....	18
3.3    p-u Curves for Piles in Clay.....	28
3.3.1    P-y Curve from Measured Strain Data.....	30
3.4    Centrifuge Modelling.....	34
3.5    Analysis Methods of Lateral Loaded Piles.....	36
3.6    Broms's Theory.....	37
3.7    Elasticity Theory.....	40
3.8    P-y Analysis Method.....	43
3.9    Winkler Foundation Model.....	48
<b>4. ANALYSIS OF PILE BEHAVIOR.....</b>	<b>49</b>
4.1    Pile Behaviour During Earthquake.....	52
4.1.1    Liquefaction.....	52
4.1.2    Cause of Pile Failures during Earthquakes.....	54
4.2    Lateral Behaviour of Pile Groups.....	60
<b>5. CASE HISTORY.....</b>	<b>63</b>
5.1    Example of the Showa Bridge.....	63
5.2    The 1964 M 7.5, Niigata, Japan Earthquake.....	65
<b>6. ANALYSIS AND NUMERICAL SIMULATION.....</b>	<b>67</b>
6.1    OpenSees.....	67
6.1.1    Comparison of Lpile and OpenseesPL.....	71
6.1.2    EGEGAZ Aliaga Terminal.....	78

6.1.3 OpeenseesPL result.....	82
<b>7. CONCLUSION.....</b>	<b>91</b>
<b>REFERENCES.....</b>	<b>98</b>
<b>APPENDICES.....</b>	<b>101</b>
<b>CURRICULUM VITA.....</b>	<b>129</b>

## LIST OF TABLES

	<u>Page</u>
<b>Table 3.1</b> : Representative Values of k (Mosher and Dawkins, 2000).....	20
<b>Table 3.2</b> : Relationships commonly used for elastic piles in flexion (U.S. Department of Transportation) .....	25
<b>Table 3.3</b> : Representative Values of $\varepsilon_{50}$ (Mosher and Dawkins, 2000). .....	29
<b>Table 6.1</b> : Representative set of basic material parameters (data based on Seed and Idriss (1970), Holtz and Kovacs (1981), Das (1983), and Das (1995)).....	70
<b>Table 6.2</b> : Predefined soil properties in OpenSeesPL.....	71
<b>Table 6.3</b> : Load cases for the study.....	72
<b>Table 6.4</b> : Lateral Loading Test loading/waiting stages .....	80
<b>Table 7.1</b> : Sandy soils deflection results.....	92
<b>Table 7.2</b> : Clayey soils deflection results .....	92
<b>Table 7.3</b> : Sandy soils rotation results from Openseespl program.....	92
<b>Table 7.4</b> : Clayey soils rotation results from Openseespl program .....	93
<b>Table A 1</b> : Aliaga test data.....	126



## LIST OF FIGURES

	<u>Page</u>
<b>Figure 2.1:</b> General view of the timber piles .....	4
<b>Figure 2.2 :</b> Protecting timber piles from decay (a) by precast concrete upper section above water level; (b) by extending pile cap below water level (Tomlinson, 1994) .....	5
<b>Figure 2.3 :</b> Example designs for precast concrete piles (Tomlinson, 1994).....	6
<b>Figure 2.4 :</b> Stages in installing a pile (a) Driving piling tube, (b) Placing concrete in piling tube, (c) Compacting concrete in shaft, (d) Completed pile (Tomlinson, 1994).....	6
<b>Figure 2.5:</b> H-Pile ( <a href="http://www.conklinsteel.com/Images/pilepoint1.gif">http://www.conklinsteel.com/Images/pilepoint1.gif</a> ) .....	7
<b>Figure 2.6 :</b> Common types of composite piles ( FHWA-HRT-04-043, 2006). .....	8
<b>Figure 2.7:</b> Typical p-y curve and resulting soil modulus (Reese and Van Impe, 2001).....	9
<b>Figure 2.8:</b> Simplified response of piles in clay due to cyclic loading (from Long 1984). ....	10
<b>Figure 2.9 :</b> Effect of number of cycles on the p-y behavior at very low cyclic strain loading. (Reese and Van Impe, 2001) .....	11
<b>Figure 2.10 :</b> p-y curves developed from static load test (Reese et al. 1975). .....	12
<b>Figure 2.11 :</b> p-y curves developed from cyclic load test (Reese et al. 1975). .....	12
<b>Figure 3.1:</b> Laterally loaded pile (Mosher and Dawkins, 2000) .....	16
<b>Figure 3.2 :</b> Elements of a characteristic p-y curve for sand based on recommendations by Reese et al. (1974) .....	20
<b>Figure 3.3 :</b> Model of a Laterally Loaded Pile (Reese, 1997).....	20
<b>Figure 3.4 :</b> Factors for calculation of ultimate soil resistance for laterally loaded pile in sand (Mosher and Dawkins, 2000). .....	21
<b>Figure 3.5 :</b> Nondimensional coefficient A or ultimate soil resistance versus depth (Mosher and Dawkins, 2000). .....	22
<b>Figure 3.6 :</b> Nondimensional coefficient B for soil resistance versus depth (Mosher and Dawkins, 2000).....	23
<b>Figure 3.7 :</b> p-y curves (Reese, Cox, and Koop, 1974).....	24
<b>Figure 3.8 :</b> Laterally loaded pile and typical profiles .....	26
<b>Figure 3.9:</b> The static p-y curve (Mosher and Dawkins, 2000). .....	30
<b>Figure 3.10:</b> Equilibrium of an Element of Pile (Gabr et al., 2002) .....	31
<b>Figure 3.11:</b> Typical stress–strain relationships obtained from shear box tests for dry sands (Brandenberg, et al, 2005). .....	35
<b>Figure 3.12 :</b> Scaling of physical models. ....	36
<b>Figure 3.13:</b> Assumed soil pressure distribution under lateral loads by different researchers ( Prasad and Chari, 1999).....	36
<b>Figure 3.14 :</b> Distribution of lateral resistance (Poulos and Davis, 1980) .....	38
<b>Figure 3.15 :</b> Effect of aspect ratio and adhesion ratio on lateral resistance for purely cohesive soil. ....	39
<b>Figure 3.16 :</b> Lateral resistance factors $K_c$ and $K_q$ (Brinch Hansen, 1961).....	39
<b>Figure 3.17 :</b> Lateral resistance factors at ground surface (0) and great depth ( $\infty$ )(Brinch Hansen, 1961).....	40
<b>Figure 3.18:</b> Displacement Influence Factor for Horizontal Load ( Poulos, 1971). .....	42
<b>Figure 3.19:</b> Displacement Influence Factor for Moment ( Poulos, 1971) .....	43
<b>Figure 3.20 :</b> Distribution of stresses against a pile before and after lateral loading (Reese and Van Impe 2001). .....	44

<b>Figure 3.21</b> : Typical p-y curve and resulting p-y modulus (Reese and Van Impe 2001). ...	45
<b>Figure 3.22</b> : Schematic showing the influence of shape of cross section of pile on the soil reaction $p$ ( Reese and Van Impe, 2001).....	46
<b>Figure 3.23</b> : Beam on Winkler foundation model for a single pile under lateral loading (J. Ramachandran, 2005 ). .....	48
<b>Figure 4.1</b> : Schematic of Pile Damage Mechanisms in Level Ground Areas (Tokimatsu et al. 1996) .....	53
<b>Figure 4.2</b> : Schematic of Pile Damage Mechanisms in Laterally Spreading Areas (Tokimatsu et al. 1996).....	53
<b>Figure 4.3</b> : Schematic of BNWF or “p-y” Model (Wilson et al. 2000). .....	54
<b>Figure 4.4</b> : Current understanding of pile failure, (Bhattacharya, 2003). .....	55
<b>Figure 4.5</b> : Surface observations of lateral spreading at (a) bridge site in 1995 Kobe earthquake (b): Navalakhi port in 2001 Bhuj earthquake, (Bhattacharya,2003) ....	55
<b>Figure 4.6</b> : The idealization for seismic design of bridge foundation (JRA, 1996).....	56
<b>Figure 4.7</b> : Failure of piles in NFCH building during the 1964 Niigata earthquake (Hamada 1992a). .....	56
<b>Figure 4.8</b> : Failure of piled buildings; (a) A collapsed building after the 1995 Kobe earthquake, showing the hinge formation after Tokimatsu et al. (1997); (b): Failure piles of the NHK building after Hamada (1992b).....	57
<b>Figure 4.9</b> : (a) Observed failure of a piled foundation (Kandla Port tower) in 2001 Bhuj earthquake, Madabhushi et al. (2001); (b): Pile (marked 3) failure in centrifuge test SB-02; (c): Excavated piles in a 3 storied building in 1995 Kobe earthquake, Tokimatsu et al., (1997). .....	57
<b>Figure 4.10</b> : Failure of Showa Bridge after NISEE, (Hamada, 1992). .....	58
<b>Figure 4.11</b> : Schematic diagram of the Fall-off of the girders in Showa bridge (Takata et al., 1965). .....	59
<b>Figure 4.12</b> : (a): Piled “Million Dollar” bridge after 1964 Alaska earthquake (USA); (b): Piled “Showa Bridge” after 1964 Niigata earthquake (JAPAN); (c): Piled tanks after 1995 Kobe earthquake (JAPAN), photo courtesy of NISEE.....	59
<b>Figure 4.13</b> : Schematic representation of pile group response to lateral loading ( Ghosh et al., 2004 ). .....	60
<b>Figure 5.1</b> : Piles of Showa Bridge; (a): Post earthquake recovery and deformation of the pile from Showa Bridge, (b): Schematic diagram of the pile and the soil profile. .	64
<b>Figure 5.2</b> : Schematic diagram showing the predicted loading based on JRA code.....	65
<b>Figure 6.1</b> : Conical yield surfaces for granular soils in principal stress space and deviatoric plane (Prevost, 1985; Yang et al., 2003).....	68
<b>Figure 6.2</b> : Shear stress-strain and effective stress path under undrained shear loading conditions (Yang et al., 2003).....	68
<b>Figure 6.3</b> : OpenSeesPL user interface with mesh showing a circular pile in level ground (view of ½ mesh employed due to symmetry for uni-directional lateral loading)..	69
<b>Figure 6.4</b> : Graph types available in the deformed mesh window. ....	70
<b>Figure 6.5</b> : Type of soil defined. ....	71
<b>Figure 6.6</b> : Finite element mesh employed in the study by Elgamal and Lu (2007).....	73
<b>Figure 6.7</b> : Comparison of pile deflection profiles for the fixed-head condition by Elgamal and Lu (2007).....	74
<b>Figure 6.8</b> : Comparison of pile rotation profiles for the fixed-head condition by Elgamal and Lu (2007). ....	74
<b>Figure 6.9</b> : Comparison of bending moment profiles for the fixed-head condition by Elgamal and Lu (2007). ....	75
<b>Figure 6.10</b> : Comparison of shear force profiles for the fixed-head condition by Elgamal and Lu (2007). ....	75
<b>Figure 6.11</b> : Comparison of pile deflection profiles for the free-head condition by Elgamal and Lu (2007).....	75
<b>Figure 6.12</b> : Comparison of pile rotation profiles for the free-head condition by Elgamal and Lu (2007). ....	76

<b>Figure 6.13:</b> Comparison of bending moment profiles for the free-head condition by Elgamal and Lu (2007).....	76
<b>Figure 6.14:</b> Copmarison of shear force profiles for the free-head condition by Elgamal and Lu (2007).....	76
<b>Figure 6.15 :</b> Stress ratio contour fill of the nonlinear run for the fixed-head condition (red color shows yielded soil elements) by Elgamal and Lu (2007).....	77
<b>Figure 6.16:</b> Stress ratio contour fill of the nonlinear run for the free-head condition (red color shows yielded soil elements) by Elgamal and Lu (2007).....	77
<b>Figure 6.17:</b> TP1 pile plan view and cross-section .....	80
<b>Figure 6.18:</b> TP1 Aliaga soil profile .....	81
<b>Figure 6.19:</b> Time- Deformation test graph .....	82
<b>Figure 6.20:</b> TP1 Load-Deformation test graph.....	82
<b>Figure 6.21:</b> Aliaga pile displacement result with openseespl program .....	83
<b>Figure 6.22:</b> Loose sandy soils L: 20.5m Openseespl result.....	84
<b>Figure 6.23:</b> Loose sandy soils L: 15m Openseespl result.....	85
<b>Figure 6.24:</b> Loose sandy soils L: 10m Openseespl result.....	85
<b>Figure 6.25:</b> Loose sandy soils L: 6m Openseespl result.....	85
<b>Figure 6.26:</b> Dense sandy soils L: 20.5m Openseespl result .....	86
<b>Figure 6.27:</b> Dense sandy soils L: 15m Openseespl result .....	86
<b>Figure 6.28:</b> Dense sandy soils L: 10m Openseespl result .....	87
<b>Figure 6.29:</b> Dense sandy soils L: 6m Openseespl result .....	87
<b>Figure 6.30:</b> Soft clay soils L: 20.5m Openseespl result .....	88
<b>Figure 6.31:</b> Soft clay soils L: 15m Openseespl result .....	88
<b>Figure 6.32:</b> Soft clay soils L: 10m Openseespl result .....	88
<b>Figure 6.33:</b> Soft clay soils L: 6m Openseespl result .....	89
<b>Figure 6.34:</b> Stiff clay soils L: 20.5m Openseespl result.....	89
<b>Figure 6.35:</b> Stiff clay soils L: 15m Openseespl result.....	90
<b>Figure 6.36:</b> Stiff clay soils L: 10m Openseespl result.....	90
<b>Figure 6.37:</b> Stiff clay soils L: 10m Openseespl result.....	90
<b>Figure A. 1:</b> Rotation of the pile in the soil Aliaga.....	100
<b>Figure A. 2 :</b> a)Displacement of the pile in the soil Aliaga, b) Bending Moment of the pile in the soil Aliaga.....	100
<b>Figure A. 3 :</b> a)Shear force of the pile in the soil Aliaga, b) Pressure of the pile in the soil Aliaga .....	101
<b>Figure A. 4 :</b> Rotation of the 20.5 m pile in loose sandy soil. ....	101
<b>Figure A. 5 :</b> a)Displacement of the 20.5 m pile in loose sandy soil., b) Bending moment of the 20.5 m pile in loose sandy soil.....	102
<b>Figure A. 6 :</b> a)Shear force of the 20.5 m pile in loose sandy soil., b) Pressure of the 20.5 m pile in loose sandy soil. ....	102
<b>Figure A. 7 :</b> Rotation of the 15 m pile in loose sandy soil. ....	103
<b>Figure A. 8 :</b> a) Displacement of the 15 m pile in loose sandy soil. b) Bending moment of the 15 m pile in loose sandy soil.....	103
<b>Figure A. 9 :</b> a)Shear force of the 15 m pile in loose sandy soil. b) Pressure of the 15 m pile in loose sandy soil. ....	104
<b>Figure A. 10 :</b> Rotation of the 10 m pile in loose sandy soil. ....	104
<b>Figure A. 11 :</b> a) Displacement of the 10 m pile in loose sandy soil.b) Bending moment of the 10 m pile in loose sandy soil.....	105
<b>Figure A. 12 :</b> a) Shear Force of the 10 m pile in loose sandy soil. b) Pressure of the 10 m pile in loose sandy soil. ....	105
<b>Figure A. 13 :</b> Rotation of the 6 m pile in loose sandy soil. ....	106
<b>Figure A. 14 :</b> a) Displacement of the 6 m pile in loose sandy soil.b) Bending moment of the 6 m pile in loose sandy soil. ....	106
<b>Figure A. 15 :</b> a) Shear Force of the 6 m pile in loose sandy soil. b) Pressure of the 6 m pile in loose sandy soil. ....	107
<b>Figure A. 16 :</b> Rotation of the 20.5 m pile in dense sandy soil.....	107

<b>Figure A. 17 :</b> a) Displacement of the 20.5 m pile in dense sandy soil.b) Bending moment of the 20.5 m pile in dense sandy soil. ....	108
<b>Figure A. 18 :</b> a) Shear Force of the 20.5 m pile in dense sandy soil. b) Pressure of the 20.5 m pile in dense sandy soil. ....	108
<b>Figure A. 19 :</b> Rotation of the 15 m pile in dense sandy soil. ....	109
<b>Figure A. 20 :</b> a) Displacement of the 15 m pile in dense sandy soil.b) Bending moment of the 15 m pile in dense sandy soil. ....	109
<b>Figure A. 21 :</b> a) Shear Force of the 15 m pile in dense sandy soil. b) Pressure of the 15 m pile in dense sandy soil. ....	110
<b>Figure A. 22 :</b> Rotation of the 10 m pile in dense sandy soil. ....	110
<b>Figure A. 23 :</b> a) Displacement of the 10 m pile in dense sandy soil.b) Bending moment of the 10 m pile in dense sandy soil. ....	111
<b>Figure A. 24 :</b> a) Shear Force of the 10 m pile in dense sandy soil. b) Pressure of the 10 m pile in dense sandy soil. ....	111
<b>Figure A. 25 :</b> Rotation of the 6 m pile in dense sandy soil. ....	112
<b>Figure A. 26 :</b> a) Displacement of the 6 m pile in dense sandy soil.b) Bending moment of the 6 m pile in dense sandy soil. ....	112
<b>Figure A. 27 :</b> a) Shear Force of the 6 m pile in dense sandy soil. b) Pressure of the 6 m pile in dense sandy soil. ....	113
<b>Figure A. 28 :</b> Rotation of the 20.5 m pile in soft clayey soil. ....	113
<b>Figure A. 29 :</b> a) Displacement of the 20.5 m pile in soft clayey soil.b) Bending moment of the 20.5 m pile in soft clayey soil. ....	114
<b>Figure A. 30 :</b> a) Shear Force of the 20.5 m pile in soft clayey soil. b) Pressure of the 20.5 m pile in soft clayey soil. ....	114
<b>Figure A. 31 :</b> Rotation of the 15 m pile in soft clayey soil. ....	115
<b>Figure A. 32 :</b> a) Displacement of the 15m pile in soft clayey soil.b) Bending moment of the 15 m pile in soft clayey soil. ....	115
<b>Figure A. 33 :</b> a) Shear Force of the 15 m pile in soft clayey soil. b) Pressure of the 15 m pile in soft clayey soil. ....	116
<b>Figure A. 34 :</b> Rotation of the 10 m pile in soft clayey soil. ....	116
<b>Figure A. 35 :</b> a) Displacement of the 10 m pile in soft clayey soil.b) Bending moment of the 10 m pile in soft clayey soil. ....	117
<b>Figure A. 36 :</b> a) Shear Force of the 10 m pile in soft clayey soil. b) Pressure of the 10 m pile in soft clayey soil. ....	117
<b>Figure A. 37 :</b> Rotation of the 6 m pile in soft clayey soil. ....	118
<b>Figure A. 38 :</b> a) Displacement of the 6 m pile in soft clayey soil.b) Bending moment of the 6 m pile in soft clayey soil. ....	118
<b>Figure A. 39 :</b> a) Shear Force of the 6 m pile in soft clayey soil. b) Pressure of the 6 m pile in soft clayey soil. ....	119
<b>Figure A. 40 :</b> Rotation of the 20.5 m pile in stiff clayey soil.....	119
<b>Figure A. 41 :</b> a) Displacement of the 20.5 m pile in stiff clayey soil.b) Bending moment of the 20.5 m pile in stiff clayey soil.....	120
<b>Figure A. 42 :</b> a) Shear Force of the 20.5 m pile in stiff clayey soil. b) Pressure of the 20.5 m pile in stiff clayey soil.....	120
<b>Figure A. 43 :</b> Rotation of the 15m pile in stiff clayey soil.....	121
<b>Figure A. 44 :</b> a) Displacement of the 15 m pile in stiff clayey soil.b) Bending moment of the 15 m pile in stiff clayey soil.....	121
<b>Figure A. 45 :</b> a) Shear Force of the 15 m pile in stiff clayey soil. b) Pressure of the 15 m pile in stiff clayey soil.....	122
<b>Figure A. 46 :</b> Rotation of the 10 m pile in stiff clayey soil.....	122
<b>Figure A. 47 :</b> a) Displacement of the 10 m pile in stiff clayey soil.b) Bending moment of the 10 m pile in stiff clayey soil.....	123
<b>Figure A. 48 :</b> a) Shear Force of the 10 m pile in stiff clayey soil. b) Pressure of the 10 m pile in stiff clayey soil.....	123
<b>Figure A. 49 :</b> Rotation of the 6 m pile in stiff clayey soil.....	124

**Figure A. 50 :** a) Displacement of the 6 m pile in stiff clayey soil.b) Bending moment of the 6 m pile in stiff clayey soil. ....124

**Figure A. 51:** a) Shear Force of the 6 m pile in stiff clayey soil. b) Pressure of the 6 m pile in stiff clayey soil. ....125



## **BEHAVIOUR OF LATERALLY LOADED PILES IN SOILS**

### **SUMMARY**

Piles or pile foundations are often exposed to lateral loads as well as axial loads. Although design methods due to axial loading are well known and used commonly, lateral loading cases have attracted more attention recently following reported case histories of damaged piles during earthquakes. Therefore, lateral analyses methods are known less especially among practicing engineers. In this thesis, pile design due to lateral loading in tuff soils is considered. Main goal was to introduce pile behaviour to the local civil engineering society to sample soil profiles in Izmir-Aliaga region. For this purpose pile deflections, bending moment, shear force and rotation was accounted with openseespl program. Engineers who are dealing with pile design in tuff soils of Aliaga area and soils that have similar characteristics should consider soil-pile interaction. One should also keep in mind that Izmir has been graded as a first-degree earthquake zone and lateral loads due to seismic events often govern pile design.

Results of the research study presented in this thesis are used to develop and validate a procedure for the analysis of laterally loaded bored piles embedded in a tuff soil. The procedure is based on the Openseespl program analysis in which the types of the soils are defined. The research used the computer program Openseespl to analyse the resistances encountered in a laterally loaded pile and the results of a full scale laterally loaded pile tests to develop and verify the displacement curves in tuff soils.



## YANAL YÜKLÜ KAZIKLARIN ZEMİNLERDE DAVRANIŞI

### ÖZET

Kazıklar veya kazıklı temeller eksenel yüklere maruz kaldıkları kadar sıklıkla yanal yüklere de maruz kalırlar. Tasarım yöntemleri eksenel yükleme nedeniyle iyi bilinmesine ve yaygın olarak kullanılmasına rağmen, son yıllarda deprem esnasında hasar gören yanal yüklü kazık hikayeleri dikkat çekmeye başlamıştır. Bu nedenle, yanal analiz yöntemleri özellikle uygulama mühendisleri arasında az bilinir. Nispeten kolay anlaşılır ve iyi kurulmuş yöntemler kullanılmıştır. Bu tezin kapsamı, yanal yüklü kazıkların tuf zeminler içindeki durumunu gözönünde bulundurmaktır. Tezin ana amacı İzmir/Aliağa bölgesinde bulunan zemin profilinde kazık davranışını mühendislere tanıtmaktır. Bu amaçla Openseespl programıyla kazık sapması, momenti, kesme kuvveti ve dönme durumları hesaplandı. Aliağa bölgesinde tuff zemin ve benzerleri içinde kazık dizayn edecek mühendisler zemin-kazık etkileşimini göz önünde bulundurmaları gerklidir. İzmir' in birinci derece deprem bölgesi olduğunu ve sismik olayların kazık üzerinde yanal etkiye sebep olduğu da unutmamalı ve belirleyici rol oynadığı bilinmelidir.

Bu tezin amacı tuf zeminler içine soketlenmiş yanal yüklü kazıkların analizini geliştirmek ve doğrulamaktır. Bu amaç ile Openseespl programında tanımlanan zemin tipleri kullanılmış ve ayrıca Aliağa profiline uygun program içinde zemin parametreleri belirlenerek program kullanılmıştır. Openseespl bilgisayar programı üç boyutlu analiz ile yanal yüklü kazıklarda meydana gelen dirençlerin belirlenmesi ve tuf zeminde yapılan yanal yüklü kazık deneyleri sonuçları kullanılarak kazıklarda meydana gelen yerdeğiştirme eğrisinin belirlenmesi ve doğrulanmasıdır.



## 1. INTRODUCTION

There are significant differences between the behavior of a pile under horizontal and vertical loads. Under axial load, the structural section of the pile is subjected to confined compression: the stress is generally much lower than the strength of the material (wood, steel, concrete) of the pile; the failure, if any, occurs at the interface between the pile and the soil and the structural section of the pile does not give rise to significant design problems. Under lateral load, on the contrary, the pile is subjected to bending moment and shear, and the behaviour of its section is a major component of the pile response. The behaviour of a vertically loaded pile, and in particular its bending capacity, depends essentially on the characteristics of the soil immediately adjacent to the shaft and below the base; in these zones the pile installation produced significant variations in the state of soil stresses and soil properties. Accordingly the behaviour of a vertically loaded pile, and particularly its bearing capacity, is affected by the installation procedures. Under horizontal load, the pile-soil interaction is confined to a volume of soil close to the surface; a major part of this volume is not influenced by the pile installation. Accordingly, the behaviour of the pile is usually considered not to be affected by the installation technique.

In the second chapter, types of piles (timber piles, concrete piles and steel piles) and types of loadings (static loadings, cyclic loadings, sustained loadings and dynamic loadings) are explained. In the following chapters, lateral loading capacities of single piles are explained. Case histories in the literature are briefly mentioned and using Aliaga region soil parameters pile deflection was determined with the Openseespl program. After that a lateral loaded pile were considered and its behaviour is compared in different soil types.

The aim of this research is to emphasize the pile behaviour in different soils and soil pile interaction. For this purpose, pile behaviour and pile soil interaction methods are provided in the following chapters. Applications of these methods are made and

compared with Openseespl program to illustrate the behaviour of laterally loaded piles in different soils. The result of laterally loaded pile in field at Aliaga (Izmir) was compared with the result obtained for the same test using Openseespl program. Results and comparisons show that pile response is as estimated by the Openseespl program.

## **2. RESPONSE OF A PILE UNDER LOADINGS**

### **2.1 Classification of Piles**

The British Standard Code of Practice for pile foundations are divided into three categories. These are large displacement piles, small displacement piles and replacement piles. The types of piles are explained below.

Large displacement piles comprise solid-section piles or hollow-section piles with a closed end, which are driven or jacked into the ground and thus displace the soil. All types of driven and cast-in-place piles come into this category. Timber (round or square section, jointed or continuous), Precast concrete (solid or tubular section in continuous or jointed units), Prestressed concrete (solid or tubular section), Steel tube (driven with closed end), Steel box (driven with closed end), Fluted and tapered steel tube, Jacked-down steel tube with closed end, Jacked-down solid concrete cylinder. Large displacement piles (driven and cast-in-place types) are Steel tube driven and withdrawn after placing concrete, Precast concrete shell filled with concrete, Thin-walled steel shell driven by withdrawable mandrel and then filled with concrete.

#### **2.1.1 Timber Piles**

The first pile type used is timber piles. Therefore, we can say that timber pile is the father of piles. Timber piles have successfully supported structures for more than 6000 years. Over the years, the methods that man has employed to extend the life of timber piling have evolved to the point that timber piles will last for over 100 years. Ancient civilizations used various animal, vegetable, and mineral oils to preserve timber. In Roman times, timbers were smeared with cedar oils and pitch, and then charred to extend their service life. Roman roads built on treated piles were still in good condition 1900 years later. A building built in Venice, Italy in 900 A.D. was rebuilt around 1900 on the same 1000 year old piles.( Timber Piling Council American Wood Preservers Institute, 2002). In addition, some palaces and mosques

foundations were timber piles in Istanbul. Although these buildings were near to the Bosphorus, they are still standing.

Tomlinson (1994) recommends, many aspects of timber are an ideal material for the pile foundation. It has a high strength to weight ratio, it is easy to handle, it is readily cut to length and trimmed after driving, and in favourable conditions of exposure durable species have an almost indefinite life. Timber piles used in their most economical form consist of round untrimmed logs which are driven. General view of a timber pile is shown in Figure 2.1. Timber piles, when situated wholly below ground-water level, are resistant to fungal decay and have an almost indefinite life. However, the portion above ground-water level in a structure on land is liable to decay. Although creosote or other preservatives extend the life of timber in damp or dry conditions they will not prolong its useful life indefinitely. Therefore it is the usual practice to cut off timber piles just below the lowest predicted ground-water level and to extend them above this level with concrete as shown Figure 2.2a. If the ground-water level is shallow, the pile cap can be taken down below the water level as shown in Figure 2.2b.



**Figure 2.1:** General view of the timber piles

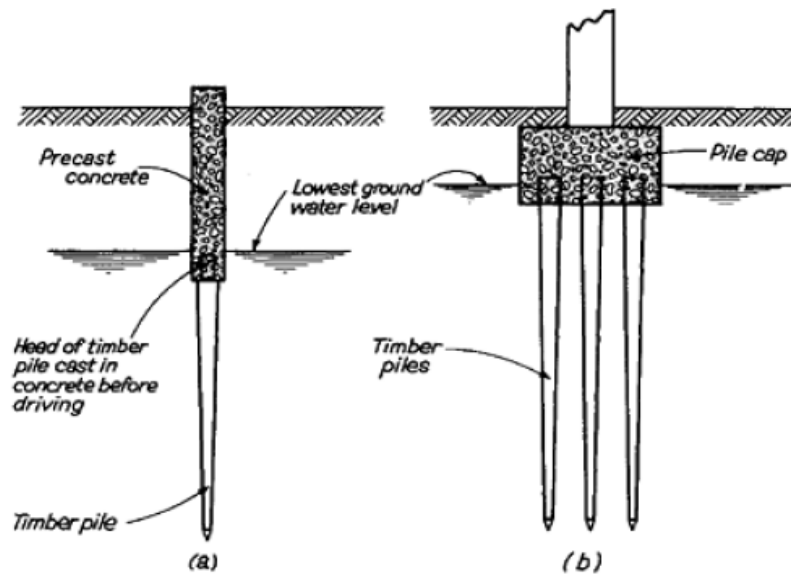


**Figure 2.2 :** Protecting timber piles from decay (a) by precast concrete upper section above water level; (b) by extending pile cap below water level (Tomlinson, 1994)

### 2.1.2 Concrete piles

Concrete piles come in precast, prestressed, cast-in-place, or composite construction form.

Precast piles are cast at a production site and shipped to the project site. The contractor should take special care when moving these piles as not to create tension cracks (Kansas Department of Transportation, 2007). Example of design of precast concrete pile is shown in Fig. 2.3.

Prestressed piles are produced in the same manner as a prestressed concrete beam. The advantage of prestressed piles is their ability to handle large loads while maintaining a relatively small cross section. Also a prestressed pile is less likely to develop tension cracks during handling (Kansas Department of Transportation, 2007).

Cast-in-place pressure grouted piles are constructed by drilling with a continuous-flight, hollow-shaft auger to the required depth. A non-shrinking mortar is then injected, under pressure, through the hollow shaft as the rotating auger is slowly withdrawn. A reinforcing steel cage is placed in the shaft immediately after the auger is withdrawn. When a shell or casing is used the contractor must make sure that the

inside of the casing is free of soil and debris before placing the concrete. This system is used when hammer noise or vibration could be detrimental to adjacent footings or structures (Kansas Department of Transportation, 2007). Piling procedure is shown in Figure 2.4.

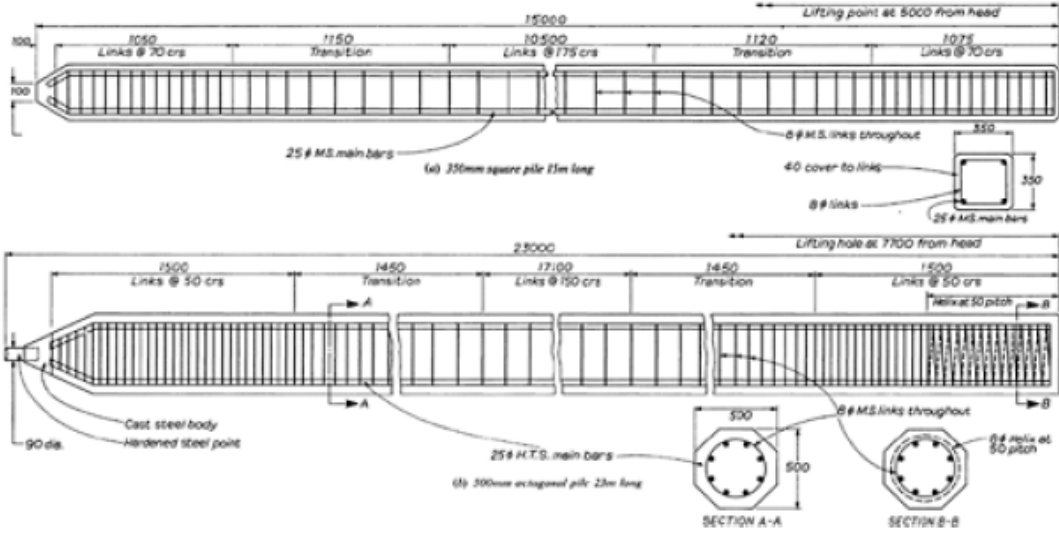


**Figure 2.3 :** Example designs for precast concrete piles (Tomlinson, 1994).

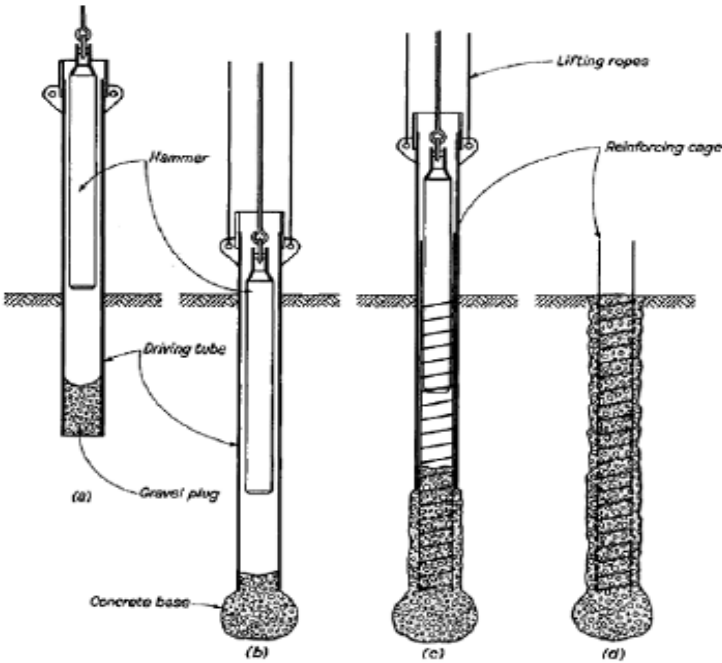


**Figure 2.4 :** Stages in installing a pile (a) Driving piling tube, (b) Placing concrete in piling tube, (c) Compacting concrete in shaft, (d) Completed pile (Tomlinson, 1994)

### 2.1.3 Steel pile

Steel piles are generally rolled H-pile used in point bearing. H-pile are available in many sizes, and are designated by the depth of the member and the mass (weight) per unit length. H-piles are well adapted to deep penetration and close spacing due to their relatively small point area and small volume displacement. They can be designed as small displacement piles, which is advantageous in situations where ground heave and lateral displacement must be avoided. They can be readily cut down and extended where the level of the bearing stratum varies; also the head of a pile which buckles during driving can be cut down and re-trimmed for further driving (Tomlinson, 1994). They can also be driven into dense soils, coarse gravel and soft rock without damage. In some foundation materials, it may be necessary to provide pile points to avoid damage to the pile. In some instances it may become necessary to increase the length of H-Pile by welding two pieces together as shown in Fig. 2.5.



**Figure 2.5:** H-Pile (<http://www.conklinsteel.com/Images/pilepoint1.gif>)

### 2.1.4 Cast-in-place pipe pile

Cast-in-place pipe piles are considered as displacement (friction) type pile. Closed-end pipe piles are formed by welding a watertight plate on the end to close the tip end of the pile. The shell is driven into the foundation material to the required depth and then filled with concrete. Thus both concrete and steel share in supporting the load. After the shell is driven and before filling with concrete, the shell is inspected internally its full length to assure that damage has not occurred during the driving operation. Pipe pile may be either spiral or longitudinally welded, or seamless steel.

Pipe piles are normally used in foundation footings. Their use for above ground pile bents is not recommended.

Several composite pile products are also available in the market today, such as steel pipe core piles, structurally reinforced plastic matrix piles, concrete-filled FRP pipe piles, fiberglass pultruded piles, and plastic lumber piles. Of these five pile types, the first three are considered to be better suited for load-bearing applications (Lampo, et al., 1998). These three pile types are shown in Figure 2.6. ( FHWA-HRT-04-043, 2006)

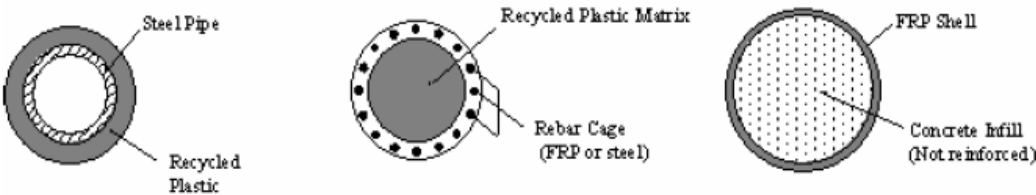


**Figure 2.6 :** Common types of composite piles ( FHWA-HRT-04-043, 2006).

## 2.2 Classification of Piles Loading

The nature of the loading and the kind of soil around the pile, are important in predicting the response of a single pile or a group of piles. With respect to active loadings at the pile head, four types can be identified: short term or static, cyclic, sustained and dynamic. In addition, passive loadings can occur along the length of a pile from moving soil, when a pile is used as an anchor. Another problem to be addressed is when existing piles are in the surrounding of pile driving or earth work. In this section, various loadings on the piles will be explained along with the response of a pile.

### 2.2.1 Static Loading

Reese and Van Impe (2001) define static loadings with the following graphs: the curve in Figure 2.7a represents the case for a particular value of z where a short term, monotonic loading was applied to a pile. This case is the static loading which is encountered in practice. However, static curves are useful because analytical procedures can be used to develop statements to correlate with some portions of the

curves. Also, the curves serve as a baseline for demonstrating the effects of other types of loading and the curves can be used for sustained loading for some clays and sands. The curves in Figure 2.10 resulted from static loading of the pile. In this figure, it is observed that the initial stiffness of the curves and the ultimate resistance increases with depth. The scatter in the curves show that errors are present in the analysis of the numerical results from measurements of bending moments with depth. These points demonstrate that analyses employing soil properties can be correlated with the experimental results, emphasizing the need to do static loading tests on piles.

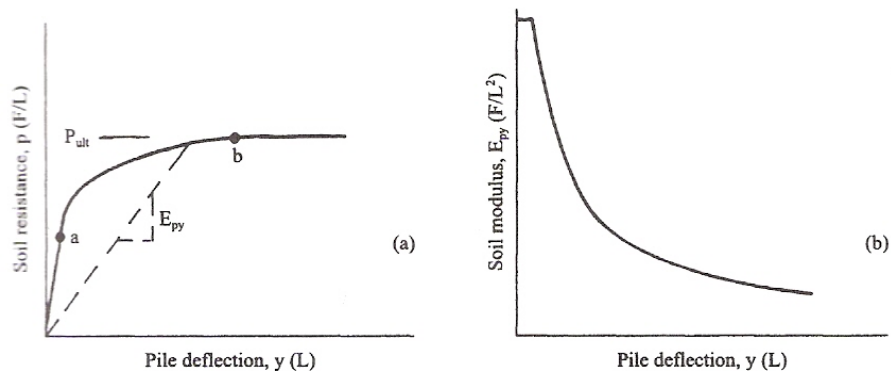


**Figure 2.7:** Typical p-y curve and resulting soil modulus (Reese and Van Impe, 2001).

### 2.2.2 Cyclic Loading

The cyclic loading of laterally loaded piles occurs with offshore structures, bridges, overhead signs and other structures. For stiff clays above the water table and for sands, the effect of cyclic loading is important. However saturated clays below water, which includes soft clays, the loss of resistance in comparison to that from static loading can be major. Experiments have shown that stiff clay distance from the pile near the ground surface when a pile deflects, such as shown in Fig. 2.8, where two-way cyclic loading was applied. The re-application of a load causes water to be forced from the opening at a velocity related to the frequency of loading. The usual consequence is that scour of the clay occurs with an additional loss of lateral resistance. In the full-scale experiments with stiff clay that have been performed, the scour of the soil during cyclic loading is readily observed by clouds of suspension

near the front and back faces of the pile (Reese et al. 1975). The gapping around a pile is not significant as in soft clay, as the clay is so weak to collapse when the cyclic loading is applied. The clouds of suspension were not observed during the testing of piles in soft to medium clays but the cycling caused a substantial loss in lateral resistance (Matlock, 1970).

As may be seen in Fig. 2.8, the soil resistance near the water table would be zero up to a given deflection. No failure of the soil has occurred because the resistance is transferred to the lower portion of the soil profile. There will be an increase in the bending moment in the pile, for a given value of lateral loading (Reese and Van Impe, 2001).

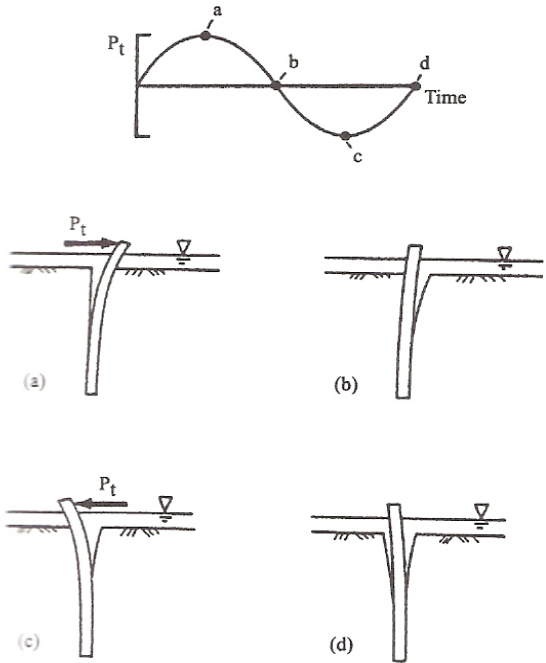


**Figure 2.8:** Simplified response of piles in clay due to cyclic loading (from Long 1984).

Figure 2.9a shows a typical p-y curve at a particular depth. Point b represents the value of  $p_{ult}$  for static loading and  $p_{ult}$  is assumed to remain constant for deflections larger than that for point b. The shaded portion of Figure 2.9a indicates the loss of resistance due to cyclic loading. For the case shown, the static and cyclic curves are identical through the initial straight-line portion to point a and to a small distance into the nonlinear portion at point c. With deflections larger than those for point c, the values of  $p$  decrease sharply due to cyclic loading to a value at point d. In some

experiments, the value of  $p$  remained constant beyond point d. The loss of resistance shown by the shaded area is, for a given soil, plainly a function of the number of cycles of loading. As may be seen, for a constant value of deflection, the value of  $E_{py}$  is lowered significantly even at relatively low strain levels, due to cyclic loading.

A comparison of the curves in Fig. 2.10 and 2.11 demonstrates the influence of cyclic loading, on a site where there is stiff clay of a given set of characteristics. At low magnitudes of deflection, the initial stiffnesses are only moderately affected. However, at large magnitudes of deflection, the  $p$ -values show spectacular decreases. The values of  $p_{ult}$  are also decreased. While the results of static loading of a pile may be correlated with soil properties, plainly the results of cyclic loading will not easily yield to analysis. The results are from carefully performed tests of full-sized piles under lateral loading in a variety of soils (Reese and Van Impe, 2001).

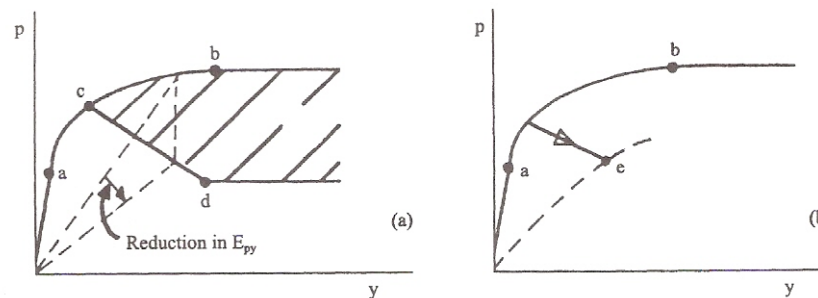


**Figure 2.9 :** Effect of number of cycles on the  $p$ - $y$  behavior at very low cyclic strain loading. (Reese and Van Impe, 2001)

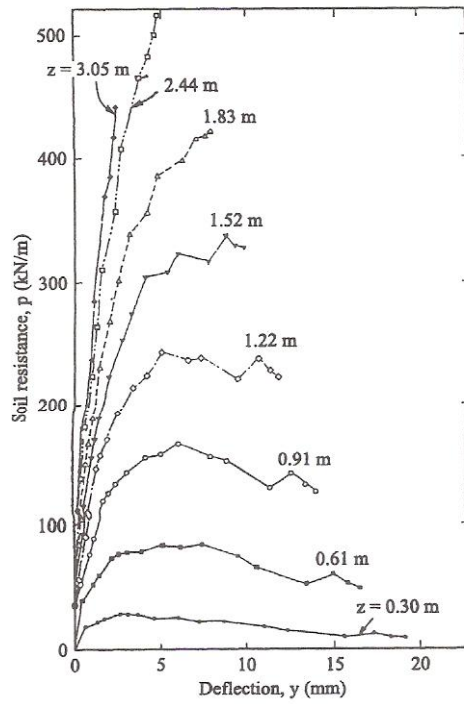


Figure 2.10 : p-y curves developed from static load test (Reese et al. 1975).

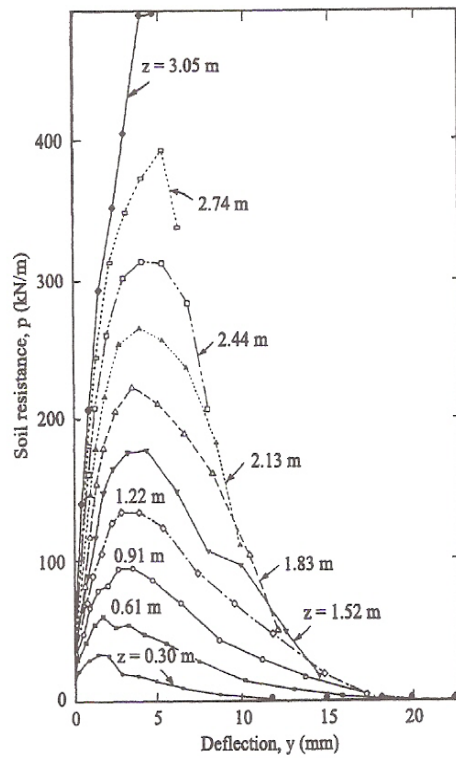


Figure 2.11 : p-y curves developed from cyclic load test (Reese et al. 1975).

### 2.2.3 Sustained Loading

Sustained loading of a pile in soft clay would likely result in a significant amount of time-related deflection. Analytical solutions can be made, using the three-dimensional theory of consolidation, but the formulation of the equations depends on a large number of parameters not clearly defined physically. The generalization of such a procedure is not yet available in the literature. Figure 2.9b shows an increasing deflection with sustained loading. The decreasing value of  $p$  implies the shifting of resistance to lower elements of soil. The effect of sustained loading is likely to be negligible for overconsolidated clays and for granular soils.

The influence of sustained loading, in some cases, can be solved with reasonable accuracy by experiment. At the site of the Pyramid Building in Memphis, Tennessee, a lateral load was applied to a testing pile with a diameter of 430 mm in silty clay with an average value of undrained shear strength over the top several diameters of the pile of 35 kPa. (Reuss et al, 1992). A load of 22 kN, corresponding approximately to the working load, was held for a period of 10 days, and deflection was measured. Some errors in the data occurred because the load was maintained by manual adjustment of the hydraulic pressure, rather than by a servo-mechanism. However, it was possible to analyze the data to show that soil-response curves could be stretched by increasing the deflection 20%, over that for static loading, to predict the behavior of the pile under sustained loading. At the Pyramid Building site, some thin strata of silt in the near-surface soils is believed to have promoted the dissipation of excess pore water pressure. (Reese and Van Impe, 2001)

### 2.2.4 Dynamic Loading

Pile-supported structures can be subjected to dynamic loads from machines, traffic, ocean waves, and earthquakes (Hadjian et al. 1992). The frequency of loading from traffic and waves is usually low enough that  $p$ - $y$  curves for static or cyclic loading can be used. Brief discussions are presented below about loadings from machinery and from earthquakes. In addition, some discussion is given to vibrations and perhaps permanent soil movement, as a result of the vibrations, due to installing piles in the vicinity of an existing pile-supported structure. With respect to dynamic loading, the greatest concern is that some event will cause liquefaction to occur in

the soil at the pile-supported structure. A discussion of liquefaction will not be presented beyond saying that liquefaction can occur in loose, granular soil below the water table. (Reese and Van Impe, 2001)

Soil resistance for static loadings can be related to the stress-strain characteristics of the soil; however, if the loading is dynamic, an inertia effect must be considered. Not only are the stress-strain characteristics necessary for formulating p-y curves for dynamic loading, but the mass of the soil must be taken into account. Use of the finite element method can be possible. However, if the finite element method is not proven completely successful for static loading cases, the application to the dynamic problem can be difficult. Thus, unproven assumptions must be made if the p-y method is applied directly to solving dynamic problems (Reese and Van Impe, 2001). If the loading is due to rotating machinery, the deflection is usually small, and a value of soil modulus may be used for analysis. Experimental techniques (Woods and Stokoe 1985, Woods 1978) have been developed for obtaining the soil parameters that are needed. Analytical techniques for solving the response of a pile-supported structure are presented by a number of researchers. Roesset (1988) and Kaynia & Kausel (1982) have developed techniques that are quite effective in dealing with machine-induced vibrations. If the loading is a result of a seismic event, the analysis of a pile-supported structure will be complex (Gazetas and Mylonakis 1998). If the soil movement is constant with depth, the piles will move with the soil without bending, p-y curves must be available with appropriate modification of the inertia effects. Many experimental data is available on which to base a method of computation.

### **3. LATERAL LOADING CAPACITY OF SINGLE PILES**

In the last decades, complicated analytical models as well as numerical processes were developed to analyze such as Opeenseespl, Lpile, Mpile and Plaxis. In this research, one site pile loading data and data from different researches will be used and compared. The design of piles for use against lateral loads is usually governed by the maximum tolerable deflection (Poulos and Davis 1990). Lateral deflections of single piles depend on the lateral load, the bending stiffness ( $EI$ ) of the pile, and the soil resistance to lateral movement (characterized by soil strength and stiffness)(FHWA, 2004). The effect of lateral load on piles has attracted attention in the last decade because of the increasing use of viaducts, offshore structures and high rise buildings. Designing these structures is very hard when wind load, braking vehicles or lateral spreading and horizontal ground movement occur. Under seismic forces, it is critical to analyze the behavior of the piles. Nevertheless, load-deflection responses of laterally loaded piles depend on many factors, such as pile dimensions, structural material properties, nearby soil conditions; lateral spreading, soil-structure interaction and type of loadings.

Usually designers consider axial loading of piles and most of the pile tests are done to determine load carrying capacity of piles. Unfortunately earthquakes cause catastrophic failures. Designers have to consider lateral loads. Axial loads produce displacement parallel to the axis of the pile in a one dimensional system. However lateral loads can produce deflection in any direction and situations. These situations are lateral displacements, bending moments and shears.

Mosher and Dawkins (2000) summarize that, the laterally loaded pile-soil system indicates a three-dimensional problem, if the pile cross section is not circular. Most of the research on the behavior of laterally loaded piles has been on piles of circular cross section in order to reduce the three-dimensional problem to two dimensions. Insufficient work has been done to search thoroughly the behavior of noncircular cross section piles under all kinds of loading. Most of the time, lateral load behavior

has been limited to vertical piles exposure to loads which cause displacements perpendicular to the axis of the pile. In the discussions which follow, it is assumed that the pile has a straight centroidal vertical axis. If the pile is nonprismatic and has a noncircular cross section, it is assumed that the principal axes of all cross sections along the pile fall in two mutually perpendicular planes and that the loads applied to the pile produce displacements in only one of the principal planes.

A laterally loaded pile is shown in Figure 3.1. The x-z plane is assumed to be a principal plane of the pile cross section. Due to the applied head shear,  $V_0$  and head moment  $M_0$ , each point on the pile undergoes a translation “u” in the x-direction and a rotation “ $\theta$ ” about the y-axis. Displacements and forces are positive if their senses are in a positive coordinate direction. The surrounding soil develops pressures denoted “p” in Figure 3.1, which resists the lateral displacements of the pile.

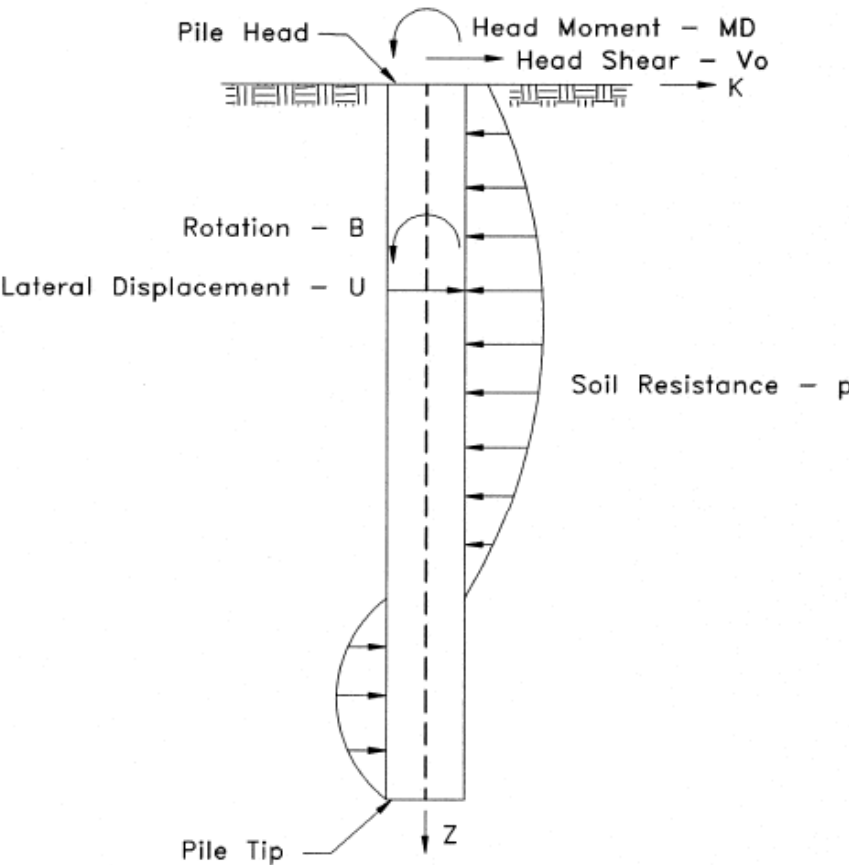


**Figure 3.1:** Laterally loaded pile (Mosher and Dawkins, 2000)

For laterally loaded “conventional” piles, it is common practice to analyze the load deflection response by using analytical methods such as the Winkler Method (subgrade reaction method), elastic continuum theory,  $p$ - $y$  method, and finite element-based methods. The principles of continuum mechanics and correlations with the results of tests of instrumented laterally loaded piles have been used to correlate the soil lateral resistance  $p$  at each point on the pile to the lateral displacement  $y$  at that  $u$  point (i.e. the Winkler assumption). The relationship between soil resistance and lateral displacement is presented as a nonlinear curve - the  $p$ - $y$  curve. Several methods are summarized in the following paragraphs for development of  $p$ - $y$  curves for laterally loaded piles in both sands and clays. In all of the methods, the primary  $p$ - $y$  curve is developed for monotonically increasing static loads. The static curve is then altered to account for the degradation effects produced by cyclic loads such as might be produced by ocean waves on offshore structures. Detailed descriptions of these methods can be found elsewhere (e.g., Reese 1984, Poulos and Davis 1990). All of these methods tend to model the pile as an elastic beam. However, for composite piles, this assumption may no longer be acceptable. Han (1997) and Han and Frost (1997) pointed out that to reasonably predict the load deflection response of a laterally loaded composite pile, the shear deformation effects should be taken into account. This issue arises due to the fact that composite materials have considerably lower shear modulus ( $G$ ) than conventional materials (Scott, et al., 1998). Therefore, the classical Bernoulli-Euler beam theory, which ignores shear deformation, is not applicable (Bank 1989, Han and Frost 1997). Han and Frost (1997) did a theoretical study that extended the existing elastic continuum solution to include shear deformation effects and pile-soil slip. Their solution, from the theoretical point of view, offers a reasonable design approach for composite piles. However, their model is quite complex and requires considerable computational effort. Also, their model has not yet been confirmed by model or full-scale tests of composite piles. Certainly more research is required in this area. Further research should aim not only to improve understanding of the load deflection response of composite piles, but also to develop reliable and easy to use design procedures that can be readily implemented by practitioners. (FHWA-HRT-04-043)

### 3.1 Load Transfer Mechanism for Laterally Loaded Piles

The load transfer mechanism for laterally loaded piles is much more complex than that for axially loaded piles. In an axially loaded pile the axial displacements and side friction resistances are unidirectional (i.e, a compressive axial head load produces downward displacements and upward side friction resistance at all points along the pile). Similarly, the ultimate side friction at the pile-soil interface depends primarily on the soil shear strength at each point along the pile. Because the laterally loaded pile is at least two-dimensional, the ultimate lateral resistance of the soil is dependent not only on the soil shear strength, but on a geometric failure mechanism. At points near the ground surface an ultimate condition is produced by a wedge type failure, while at lower positions failure is associated with plastic flow of the soil around the pile as displacements increase. In each methods which are described below, two alternative evaluations are made for the ultimate lateral resistances at each point on the pile, for wedge type failure and for plastic flow failure. The smaller values of the two is taken as the ultimate resistance (Mosher and Dawkins, 2000).

### 3.2 p-y Curves for Piles in Sand

A series of static and cyclic lateral load tests were performed on pipe piles driven in submerged sands (Cox, Reese, and Grubbs 1974; Reese, Cox, and Koop 1974; Reese and Sullivan 1980). Although the tests were conducted in submerged sands, Reese et al. (1980) have provided adjustments by which the p-y curve can be developed for either submerged sand or sand above the water table. The p-y curve for a point a distance  $z$  below the pile head extracted from the experimental results is shown in Figure 3.2. The curve consists of a linear segment from 0 to  $a$ , an exponential variation of  $p$  with  $y$  from  $a$  to  $b$ , a second linear range from  $b$  to  $c$ , and a constant resistance for displacements beyond  $c$ . Steps for constructing the p-y curve at a depth  $z$  below the ground surface are as follows (Mosher and Dawkins, 2000):

- Initial p-y modulus,  $E_{py-max}$ , that defines the initial portion of the curve up to point A,
- Ultimate soil resistance,  $p_{ult}$ , which defines the curve at point C and beyond,

— Transition zone between points A and C.

The coordinates of point C are  $y = 3b/80$  and  $p = p_{ult}$ , where  $b$  is the pile width. The transition zone consists of two parts: a parabolic section between points A and B, and a straight line portion between points B and C. The coordinates of point B are defined as:

$$y_B = \frac{b}{60}, \quad p_B = \frac{B_s}{A_s} \cdot p_{ult} \quad (3.1)$$

Where  $A_s$  and  $B_s$  are coefficients obtained from charts provided by Reese et al. 1974. The equation of the parabola is obtained knowing that it passes through point B and that it must be tangent to the straight line between points B and C. The coordinates of point A are obtained by finding the intersection point of the initial straight portion, with slope  $E_{py-max}$ , and the parabola (U.S. Department of Transportation, 2002).

u is y

The slope of the initial linear portion of the curve can be determined from,

where

( $k_p$  : initial slope of the unit tip reaction (q-w) curve in tsf/in.) and

$$k_p = kz \quad (3.2)$$

soil stiffness ( $k$ ) is obtained from Table 3.1 for either submerged sand or sand above the water table.

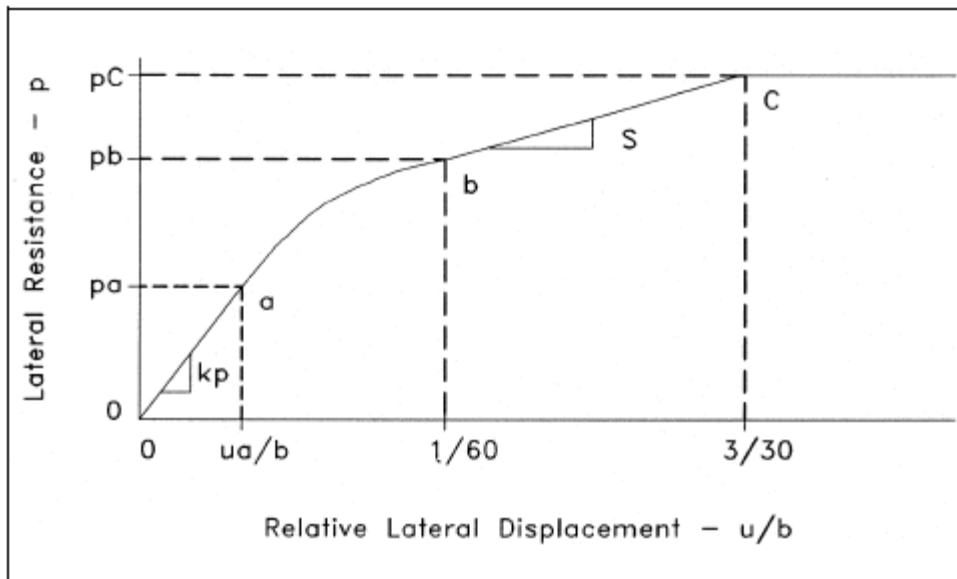


**Figure 3.2 :** Elements of a characteristic p-y curve for sand based on recommendations by Reese et al. (1974)

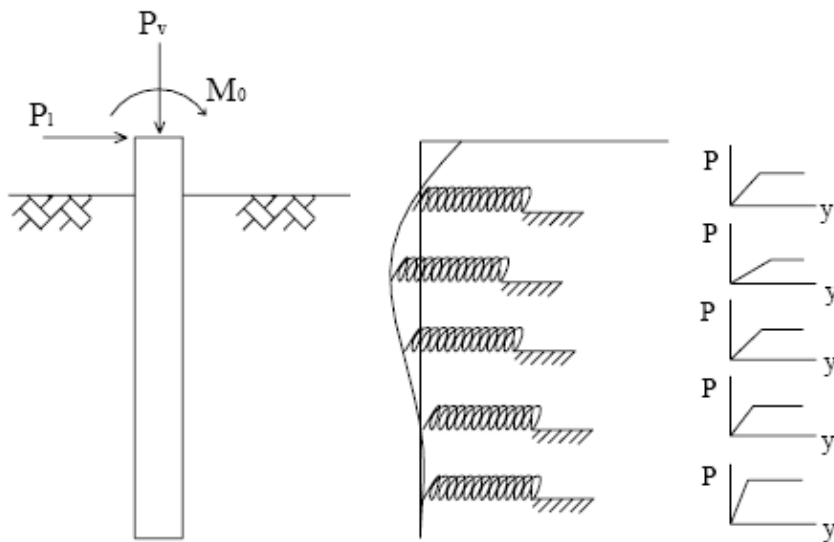


**Figure 3.3 :** Model of a Laterally Loaded Pile (Reese, 1997)

**Table 3.1 :** Representative Values of k (Mosher and Dawkins, 2000)

Sand	Relative Density		
	Loose	Medium	Dense
Submerged(pci)	20	60	125
Above water table (pci)	25	90	225

The ultimate lateral resistance can be computed as the smaller of,

$$p_s = (C_1 z + C_2 b) \gamma' z \quad (3.3)$$

for a wedge failure near the ground surface; or

$$p_s = C_3 b \gamma' z \quad (3.4)$$

Where,

$\gamma$  : effective unit weight of the sand

u: “y” deflection of lateral load pile

z: depth below ground surface

$\phi$  : angle of internal friction

$\beta$  :  $45 + \phi/2$

b: width of the pile perpendicular to the direction of loading

Values of  $C_1$ ,  $C_2$ ,  $C_3$  and the depth  $z_{cr}$  at which the transition from wedge failure to flow failure occurs are shown in Figure 3.4.

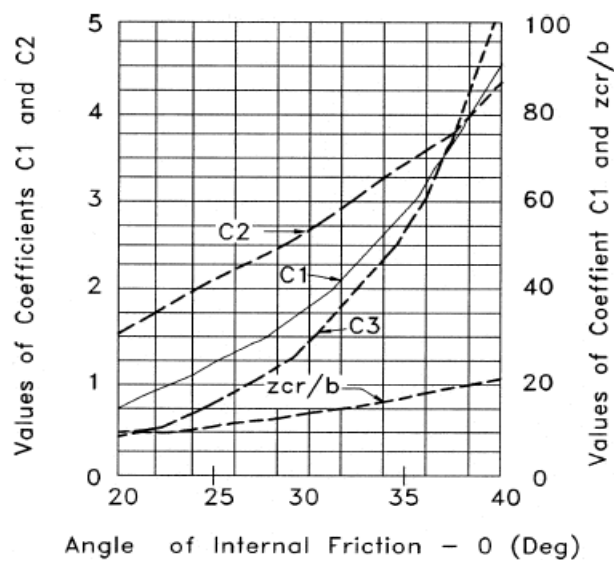


**Figure 3.4** : Factors for calculation of ultimate soil resistance for laterally loaded pile in sand (Mosher and Dawkins, 2000).

where A and B are reduction coefficients found from Figures 3.5 and 3.6, respectively, for the appropriate static or cyclic loading condition. The second straight line segment of the curve, from b to c, is established by the resistances  $p_b$  and  $p_c$  and the prescribed displacements of  $y = b/60$  and  $y = 3b/80$  as shown in Figure 3.7. The slope of this segment is given by;

$$s = \left( \frac{40(p_c - p_b)}{b} \right) \tag{3.5}$$

The exponential section of the curve, from a to b, is of the form

$$p = Cy^{1/n} \tag{3.6}$$

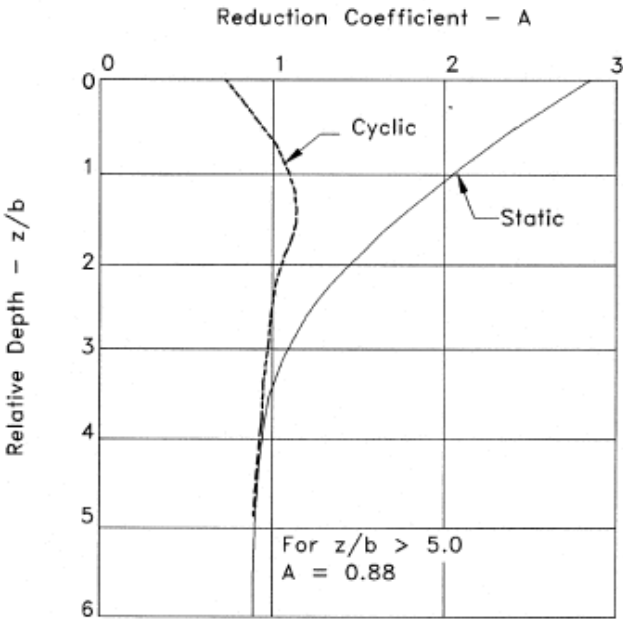


**Figure 3.5 :** Nondimensional coefficient A or ultimate soil resistance versus depth (Mosher and Dawkins, 2000).

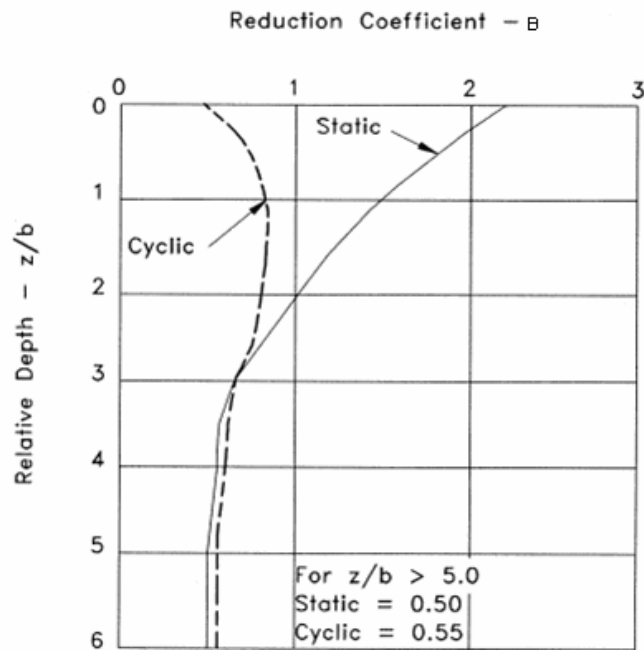


**Figure 3.6 :** Nondimensional coefficient B for soil resistance versus depth (Mosher and Dawkins, 2000).

where the parameters C, n and the terminus of the initial linear portion  $p_a$  and  $y_a$  are obtained by forcing the exponential function in Equation 3.6 to pass through  $p_b$  and  $y_b$  with the same slope s as segment  $p_c$  and to have the slope  $k_p$  at the terminus of the initial straight line segment at a. These results in;

$$n = \frac{p_b}{s y_b} \tag{3.7}$$

$$C = \frac{p_b}{y_b^{\frac{1}{n}}} \tag{3.8}$$

$$y_a = \left( \frac{C}{k_p} \right)^{\frac{n}{n-1}} \tag{3.9}$$

$$p_a = k_p y_a \quad (3.10)$$

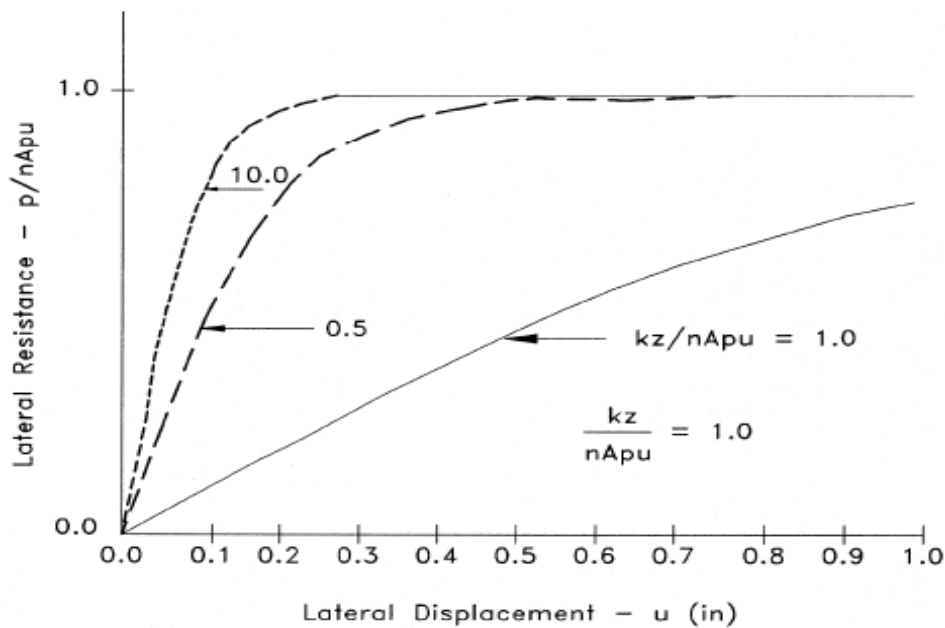


**Figure 3.7 :** p-y curves (Reese, Cox, and Koop,1974)

A laterally loaded single pile is a soil-structure interaction problem. The behavior of pile foundations under dynamic, such as earthquake loading is an important factor affecting the performance of many essential structures (Wilson, 1998). The potential significance of liquefaction-related damage to piles was clearly demonstrated during the 1999 İzmit earthquake. The soil reaction is dependent of the pile movement, and the pile movement is dependent of the soil reaction. The solution must satisfy a nonlinear differential equation and equilibrium and compatibility conditions. The solution usually requires several iterations. Elastic beam relationships that are commonly used in analysis of laterally loaded piles are summarized in Table 3.2. These quantities are obtained from differentiating deflection  $y$  with respect to the distance along the pile,  $x$ . (U.S. Department of Transportation, 2004)

**Table 3.2 :** Relationships commonly used for elastic piles in flexion (U.S. Department of Transportation)

Variable	Formula	Units
Distance along the length of the pile (measured from the pile head)	$x$	[L]
Distance to neutral axis within pile cross section	$z$	[L]
Deflection	$y$	[L]
Slope or rotation of pile section	$\theta = \frac{dy}{dx}$	[Dimensionless]
Curvature	$\kappa = \frac{d^2 y}{dx^2}$	[Radians/L]
Bending Moment	$M = E_p I_p \cdot \frac{d^2 y}{dx^2} = E_p I_p \cdot \kappa$	[FxL]
Shear force	$V = E_p I_p \cdot \frac{d^3 y}{dx^3}$	[F]
Axial load	$Q$	[F]
Soil reaction(or load intensity)	$p = E_p I_p \cdot \frac{d^4 y}{dx^4}$	[F]

Notes:  $E_p I_p$  = flexural stiffness of pile, where  $E_p$  is the elastic modulus of pile material, and  $I_p$  is the moment of

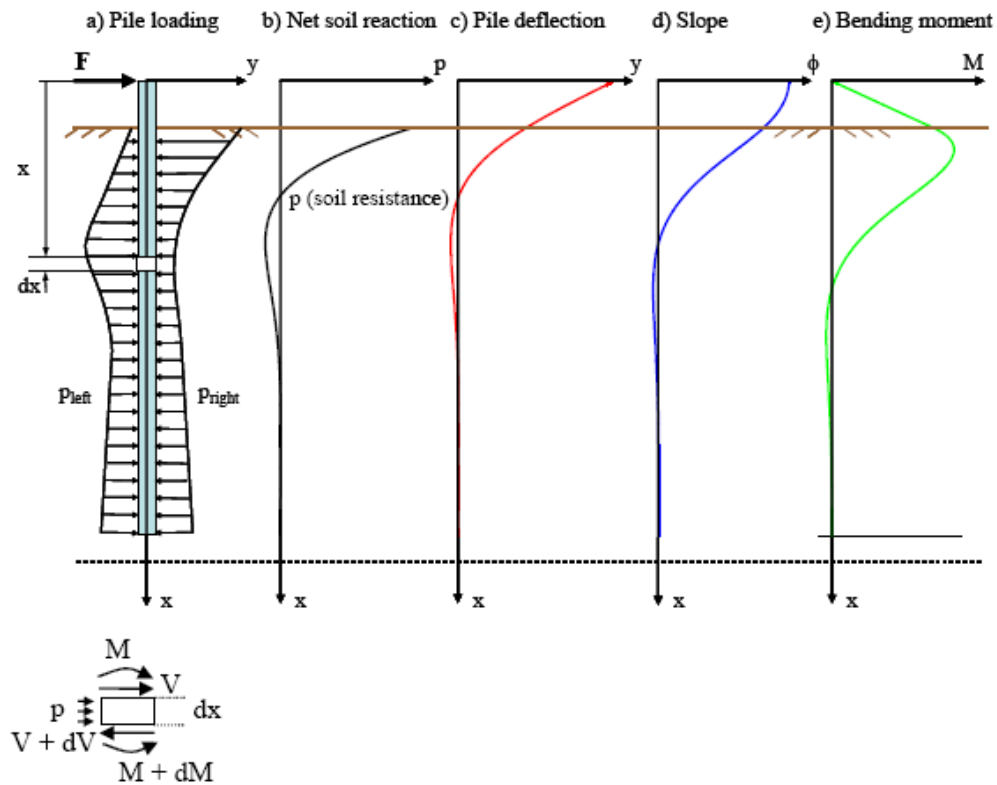
inertia of pile cross section with respect to the neutral axis.

Figure 3.8 shows a loaded pile and typical profiles of net soil reaction, deflection, slope, and moment. The governing differential equation for the problem of a laterally loaded pile was derived by Hetenyi (1946). The differential equation can be obtained by considering moment equilibrium of the infinitesimal element of length,  $dx$ , as shown in 3.11:

$$\sum M = (M + dM) - M - Vdx + Q.dy(p.dx) \cdot \frac{dx}{2} = 0 \quad (3.11)$$

neglecting quadratic terms, and differentiating twice with respect to  $x$ , we obtain:

$$\frac{d^2M}{dx^2} + Q \cdot \frac{d^2y}{dx^2} - \frac{dV}{dx} = 0 \quad (3.12)$$



**Figure 3.8 :** Laterally loaded pile and typical profiles

The term involving the axial load,  $Q$  can be ignored for the test piles investigated in this research since the vertical load present during testing was mainly from self weight and can be considered negligible. The magnitude of the bending moment acting at a given section of a pile can be calculated by integrating the normal stresses,  $\sigma(z)$  acting within the cross section of area,  $A$ , as follows in Equation 3.13:

$$M = \int_A \sigma(z) \cdot z \cdot dA. \quad (3.13)$$

If we assume that plane sections of the pile remain plane after loading, we can calculate the strains across the pile cross section if we know the rotation of the section,  $\theta = \frac{dx}{dy}$ , and the position of the neutral axis. For a given rotation,  $\theta$ , we

have the following:

$$y(x, z) = \theta \cdot z = \frac{dy}{dx} \cdot z \quad (3.14)$$

$$\varepsilon(z) = \frac{dy}{dx} = \frac{d^2 y}{dx^2} \cdot z = \kappa \cdot z \quad (3.15)$$

$$\sigma(z) = E_p \cdot \varepsilon(z) = E_p \cdot \kappa \cdot z \quad (3.16)$$

$y(x, z)$  = is the displacement in the x-direction across the pile cross section,

$\varepsilon(z)$  = strains in the x-direction across the pile cross section,

$z$  = distance to the neutral plane.

If the pile material is linear elastic with a constant young modulus,  $E_p$ , we obtain;

$$E_p I_p \frac{d^4 y}{dx^4} - \frac{dV}{dx} = 0 \quad (3.17)$$

From consideration of the horizontal force equilibrium of the infinitesimal element of the

pile shown in Figure 3.8 we obtain:

$$\frac{dV}{dx} = p(x) \quad (3.18)$$

$$E_p I_p \frac{d^4 y}{dx^4} - p(x) = 0 \quad (3.19)$$

The variable,  $p(x)$  in Equation 3.17, corresponds to the resultant soil resistance force per unit length of pile that occurs when the unit length of pile is displaced a lateral distance,  $y$ , into the soil. A crucial point for solution of the above differential equation is adequate representation of the soil reaction,  $p$ . If the soil reaction,  $p$ , has a linear relationship with lateral pile deflection,  $y$ , the above equation has a closed-form solution. However, the relationship between the soil reaction  $p$  and the pile

deflection  $y$  is non-linear and also varies along the pile depth. In practice it is common to solve the above differential equation using numerical methods such as the finite difference method, and by modeling the soil reaction using nonlinear  $p$ - $y$  curves. The analyses presented in this chapter were carried out using this approach. (U.S. Department of Transportation, 2004)

The behavior of piles has been studied extensively using both laboratory tests and theoretical studies. A comprehensive review of such research can be found in Stewart et al. (1994). Both the finite difference and finite element methods have been used in the analysis of soil pile interaction. In presence of single piles, the system is usually analyzed as a Winkler foundation in which the soil is represented by either elastic springs (Broms et al., 1987) or a series of nonlinear springs (Byrne et al., 1984 and Rajashree et al., 2001).

### 3.3 $p$ - $u$ Curves for Piles in Clay

Matlock (1970) used a series of lateral load tests on instrumented piles in clay to produce the  $p$ - $y$  relationship for piles in soft to medium clays subjected to static lateral loads as follows;

$$\frac{p}{p_u} = 0.5 \left( \frac{y}{y_c} \right) \quad (3.20)$$

$p_u$  where is the ultimate lateral resistance, given by the smaller of

$$p_u = \left( 3 + \frac{\gamma'}{s_u} z + \frac{J}{b} z \right) s_u b \quad (3.21)$$

for a wedge failure near the ground surface, or

$$p_u = 9s_u b \quad (3.22)$$

for flow failure at depth; and  $y_c$ , the lateral displacement at one-half of the ultimate resistance is given by

$$y_c = 2.5\varepsilon_{50}b \quad (3.23)$$

where

$\gamma'$  is effective unit weight of the soil

$s_u$  is shear strength of the soil

$J$  is 0.5 for a soft clay or 0.25 for a medium clay

$\varepsilon_{50}$  is strain at 50 percent of the ultimate strength from a laboratory stress strain curve

$y$  is illustrated as “u”

Typical values of  $\varepsilon_{50}$  are given in Table 3.3. The depth at which failure transitions from wedge equation 3.17 to flow equation 3.18 is

**Table 3.3:** Representative Values of  $\varepsilon_{50}$  (Mosher and Dawkins, 2000).

Shear Strength (psf)	Percent
250-500	0.02
500-1000	0.01
1000-2000	0.007
2000-4000	0.005
4000-8000	0.004

The static p-u curve is shown in Figure 3.9a.

For cyclic loads, the basic p-u curve for static loads is altered as shown in Figure 3.9b. The exponential curve of Equation 50 is terminated at a relative displacement  $y/y_c = 3.0$  at which the resistance diminishes with increasing displacement for  $z < z_{cr}$  or remains constant for  $z > z_{cr}$ .

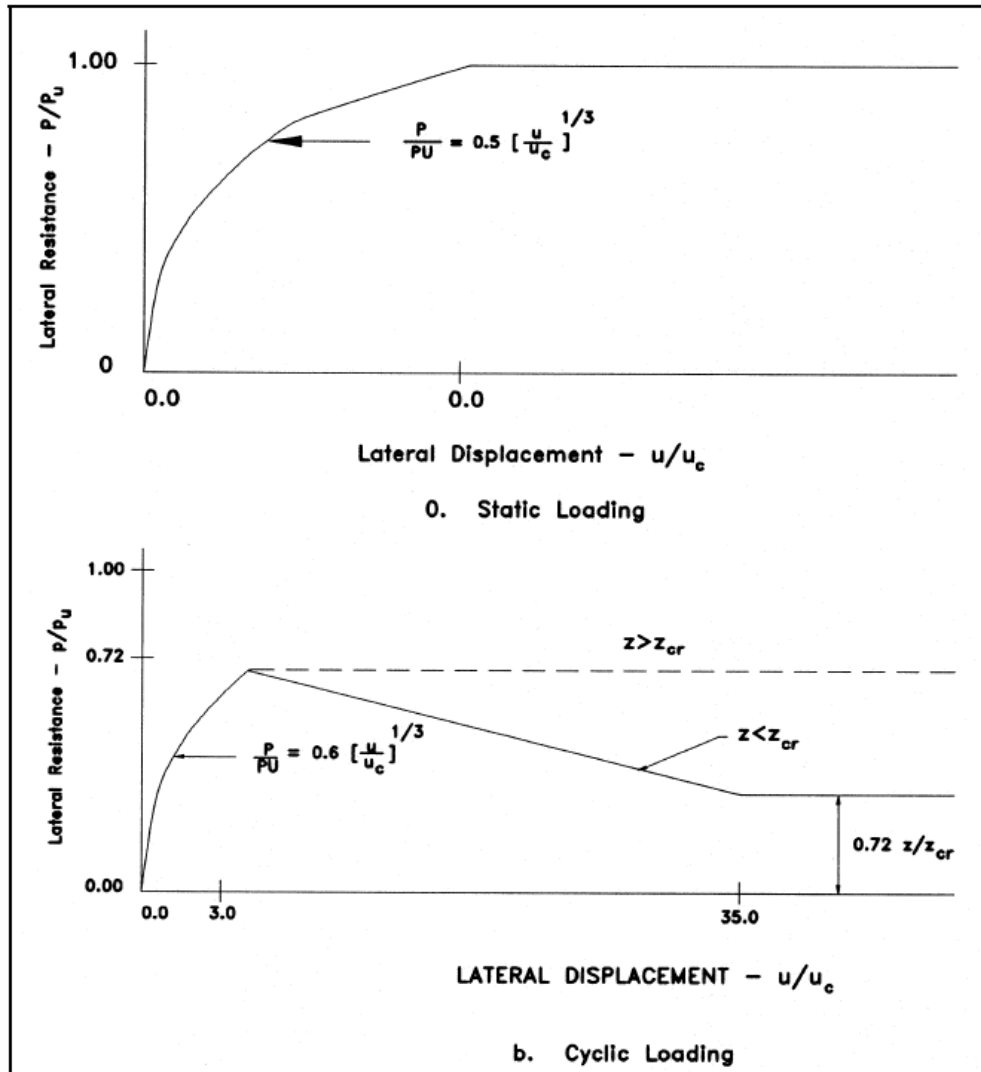


Figure 3.9: The static p-y curve (Mosher and Dawkins, 2000).

### 3.3.1 P-y Curve from Measured Strain Data

P-y curves from measured data can be evaluated using principles of statics. Two sets of equations are used to establish the governing differential equation based on geometry and structural element: the constitutive equation for the pile and the equilibrium equations for the pile element, as shown in Figure 3.10. The constitutive equation for the pile is defined as:

$$M = EI\phi = EI \frac{d^2 y}{dz} \quad (3.24)$$

where,  $M$  is the bending moment at depth,  $z$ ;

$E$  is modulus of elasticity of the pile;

$I$  is moment of inertia of the pile around the centroidal axis of the pile section;

$\phi$  is pile curvature;

$y$  is pile lateral displacement and

$z$  is depth.

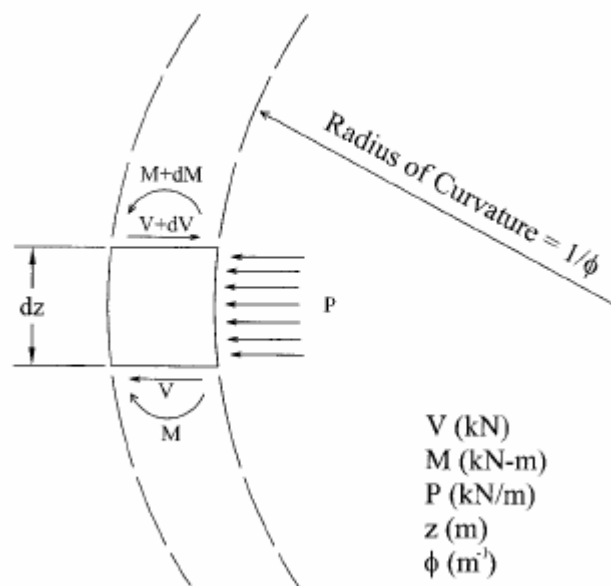


**Figure 3.10:** Equilibrium of an Element of Pile (Gabr et al., 2002)

Note that the moment of inertia is taken around the centroidal axis of the pile cross section. In the case of concrete piles which may crack, the pile cross section is reduced to account for cracking. In this case, it is necessary to first find the neutral axis of the section, under moments and axial loads, in order to evaluate the part of section that remains uncracked. Then the centroidal axis of the uncracked section is

found and moment of inertia is calculated around that axis. The horizontal force equilibrium equation for an element of pile is given as Figure 3.10:

$$dV = Pdz \quad (3.25)$$

The moment equilibrium equation for the pile element is given as:

$$dM = Vdz \quad (3.26)$$

Equations 3.22, 3.23, and 3.24 are combined and lead to the commonly used governing differential equation (Reese and Welch, 1975):

$$EI \frac{d^4 y}{dz^4} + V \frac{d^2 y}{dz^2} - P = 0 \quad (3.27)$$

For pile load tests commonly performed in the field, the major data measured are strains. Stresses acting normal to the cross section of the pile are determined from the normal strain,  $\varepsilon_x$ , which is defined as follows:

$$\varepsilon_x = -\frac{y}{\rho} = -\kappa y \quad (3.28)$$

Where,

$y$  is distance to the neutral axis;

$\rho$  is radius of curvature; and,

$\phi$  is curvature of the beam.

Assuming the pile material to be linearly elastic within a given loading range, Hooke's Law for uniaxial stress ( $\sigma = E\varepsilon$ ) can be substituted in to equation 3.26 to obtain equation 3.27.

$$\sigma_x = E\varepsilon_x = -\frac{Ey}{\rho} = -E\kappa y \quad (3.29)$$

Where,

$\sigma_x$  is stress along the x axis; and,

E is Young's Modulus of the material.

This equation shows that the normal stresses acting along the cross section vary linearly with the distance (y) from the neutral axis. For a circular cross section, the neutral axis is located along the centerline of the pile. Given that the moment resultant of the normal stresses is acting over the entire cross section, this resultant can be estimated as follows:

$$M_o = -\int \sigma_x y dA \quad (3.30)$$

Noting that  $-M_o$  is equal to the bending moment, M, and substituting for  $\sigma_x$  from equation 3.28, the bending moment can be expressed by equation 3.29 as:

$$M = -\kappa EI \quad (3.31)$$

Where,

$$I = \int y^2 dA \quad (3.32)$$

This equation can be rearranged as follows:

$$\kappa = \frac{1}{\rho} = \frac{M}{EI} \quad (3.33)$$

This equation is known as the moment-curvature equation and demonstrates that the curvature is directly proportional to the bending moment and inversely proportional to  $EI$ , where  $EI$  is the flexural stiffness of the pile. During a load test, collected strain-evaluated moment data are used to curve fit the function plotted with depth from the point of load application (Gabr et al., 2002).

### **3.4 Centrifuge Modelling**

Extensive damage to pile-supported bridges and other structures in areas of liquefaction and lateral spreading has been observed in many earthquakes around the world (JGS 1996, 1998). Centrifuge test is one of the rare experiment to understand soil-pile-soil interaction. Many important lessons and insights have been learned from case histories, physical model tests, and numerical studies in recent years, but numerous questions still remain regarding the basic mechanisms of soil-pile interaction in liquefiable soil and laterally spreading ground (Brandenberg, et al, 2005).

Wilson et al. (1998, 2000) presented the first dynamic characterization of  $p$ - $y$  behaviour in liquefiable level ground from centrifuge model tests. Ashford and Rollins (2002) developed cyclic  $p$ - $y$  relations from lateral load tests of piles in blast-induced liquefied soil. Tokimatsu et al. (2004) characterized  $p$ - $y$  relations in liquefiable soil during full-scale shaking table tests. Peak subgrade reaction values in liquefiable sand were estimated from centrifuge tests by Abdoun et al. (2003) and Dobry et al. (2003). Differences in the subgrade reaction behavior observed in the above studies are consistent with the effects of relative density, pile stiffness, dynamic shaking characteristics, and site response (Brandenberg, et al, 2005). For example, relatively small subgrade reaction loads were observed in loose sand, while larger loads were observed in medium dense sand.

Testing of scaled models is common in many disciplines of civil engineering. For example, hydraulic flow underneath dams or in open channels is modelled using scaled models. Similarly the airflow around a structure is modelled in wind tunnels. In geotechnical engineering testing of reduced scale models poses a fundamental difficulty. Soil is a nonlinear material and the stress-strain relationship of this

material can be determined by conducting direct shear box experiments. Typical stress–strain relationship for soils is as shown in Figure 3.11. As a result, if small-scale models are tested, the corresponding stresses and strains will be quite small and therefore incorrect stiffness of the soil is assumed (Brandenberg, et al, 2005).

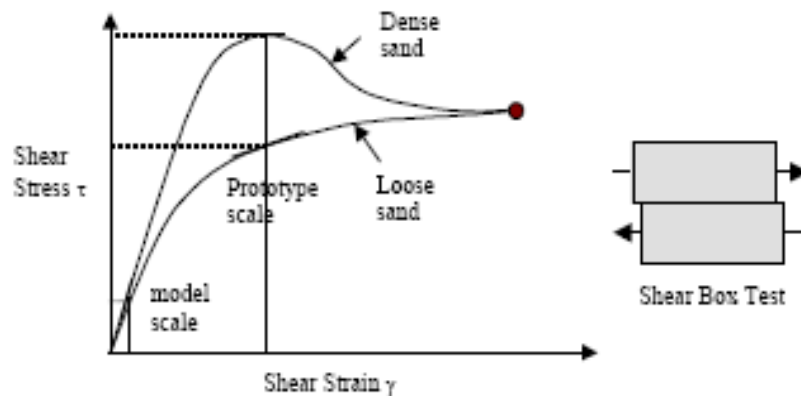


**Figure 3.11:** Typical stress–strain relationships obtained from shear box tests for dry sands (Brandenberg, et al, 2005).

In Figure 3.12 it can be seen that under prototype stresses and strains generated under a field structure the stiffness induced in either dense or loose sands could be much smaller than the stiffness generated in small-scale models in which the stresses and strains generated will be small. For example, a concrete dam 40 m high can generate a vertical stress of 960 kPa (assuming the unit weight of concrete to be 24 kN/m<sup>3</sup>). A 1/40th scale model of this dam that is only 1 m high in a laboratory will generate a vertical stress of 24 kPa. Obviously the soil underneath the model dam will have higher stiffness. Therefore, under this low vertical stress compared to the soil below the real dam, which is under much higher vertical stresses. The physical parameters obtained from smallscale model tests can have errors. For instance, the settlement of the dam predicted based on small scale tests will be much smaller as the stiffness is higher in these tests. The real dam will suffer much larger settlement, as the stiffness mobilized under prototype stresses inflicted by the real dam is much smaller. Clearly seen in the example, it is important that prototype stresses and strains need to be generated in small-scale models so that the correct stiffness of the soil is mobilized.

This can be achieved by centrifuge modelling. Centrifuge modelling contains testing of reduced scale models in the advanced gravity field of a geotechnical centrifuge. The gravity field is enhanced by subjecting the models to centrifugal acceleration as they are spun around in the centrifuge (Madabhushi, 2004).

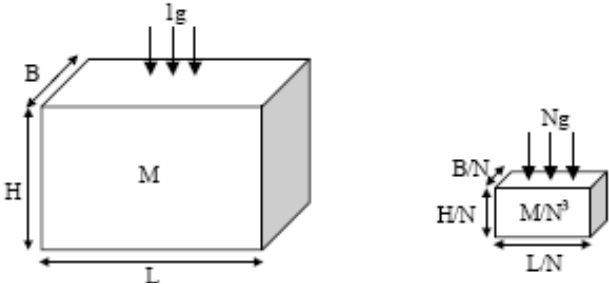


Figure 3.12 : Scaling of physical models.

3.5 Analysis Methods of Lateral Loaded Piles

There are a lot of factors that may impose lateral forces on foundation piles. In land structures, earth pressure, wind, earthquake, or vehicles may impose lateral forces. On the other hands, in marine structures, lateral forces are caused by impact of berthing ships, pull from mooring ropes, and pressure of winds, currents, waves and floating ice. Fig. 3.13 shows soil pressure distribution under lateral loads from different researches.

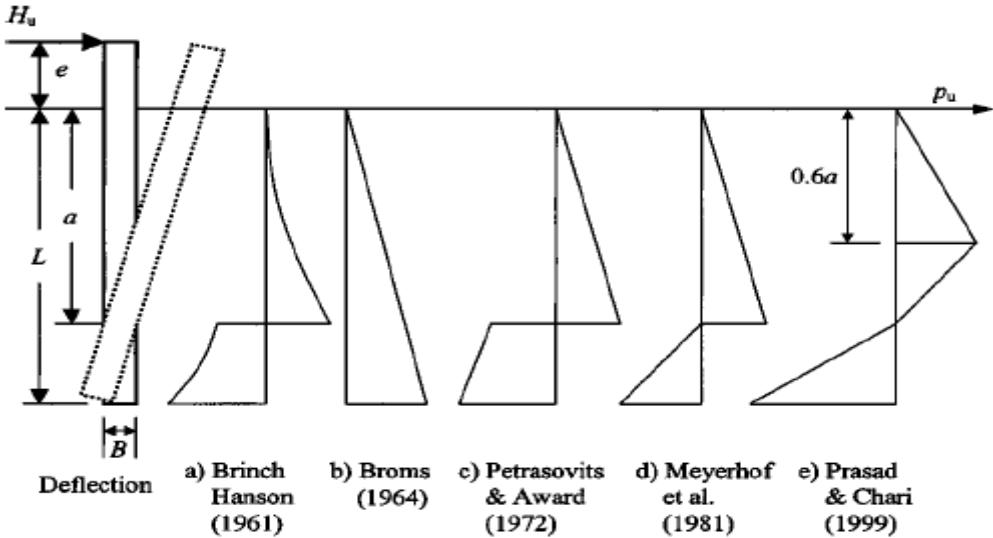
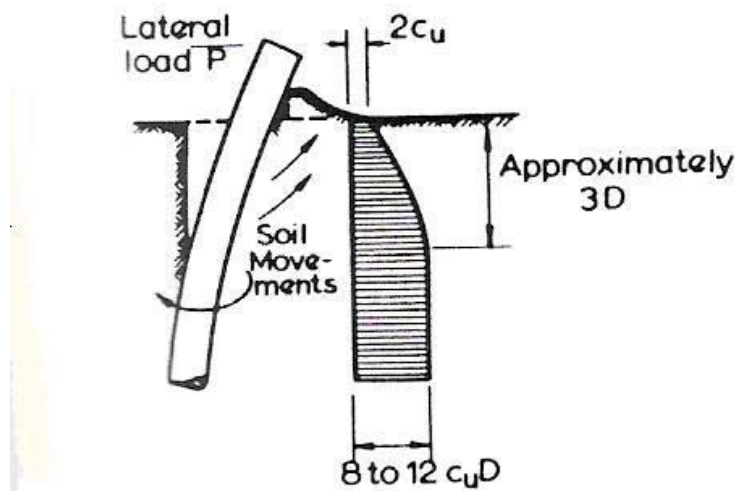


Figure 3.13: Assumed soil pressure distribution under lateral loads by different researchers ( Prasad and Chari, 1999)

### 3.6 Broms's Theory

Broms theory simlifies the ultimate soil resistance. Ultimate lateral soil resistance  $p_u$  increases from the surface down to the depth of about three piles diameters and remains constant for greater depth. This is shown in Fig. 3.14. When  $p_u$  becomes constant, lateral failer involves plastic flow of the soil around the pile in the horizontal plane only and the value of  $p_u$  can be determined by plasticity theory. The value of the lateral resistance factor  $K_c$  ( $p_u = K_c C$ ) depends on the ratio of piles adhesion to cohesion  $\frac{c_a}{c}$  and on the shape of the pile section, the most significant property of the shape being the aspect ratio d to b. The influence of the aspect ratio on the value of  $K_c$  is shown in Fig. 2.10 for  $\frac{c_a}{c} = 1$  and  $\frac{c_a}{c} = 0$ , and, to sufficient accuracy, the solution for any intermediate value of  $\frac{c_a}{c}$  can be obtained by linear interpolation. The curves in Fig. 3.15 have been obtained by plasticity theory using limit analysis. ( The upper bound obtained in this analysis generally only exceed the lower bound by 10 to 15% and the curves are for the average of the two bounds). The analysis assumed the pile section to be a round and may be slightly conservative for other convex shapes of the same aspect ratio. The lateral resistance at depth in purely cohesive soil is usually taken as  $9c$ , whatever the shape of the pile and value of  $\frac{c_a}{c}$ , as in the Broms' approach to ultimate pile capacity (Poulos and Davis, 1980).



(a) Deflection (b) Probable Distribution of Soil Reactions

**Figure 3.14 :** Distribution of lateral resistance (Poulos and Davis, 1980)

For the more general case of a  $c - \phi$  soil, an alternative derivation of the ultimate lateral soil resistance, based essentially on earth-pressure theory, has been given by Brinch Hassen (1961), who also consider the variation of resistance with depth along the pile. The ultimate resistance at any depth,  $z$ , below the surface is expressed as:

$$p_u = qK_q + cK_c \quad (3.34)$$

Where,

$q$ : vertical overburden pressure

$c$ : cohesion

$K_c, K_q$  : factors that are a function of  $\phi$  and  $z/d$

$K_c$  and  $K_q$  are plotted in Fig. 4.13, while the limiting values for the ground surface and for infinite depth are plotted in Fig. 4.14.

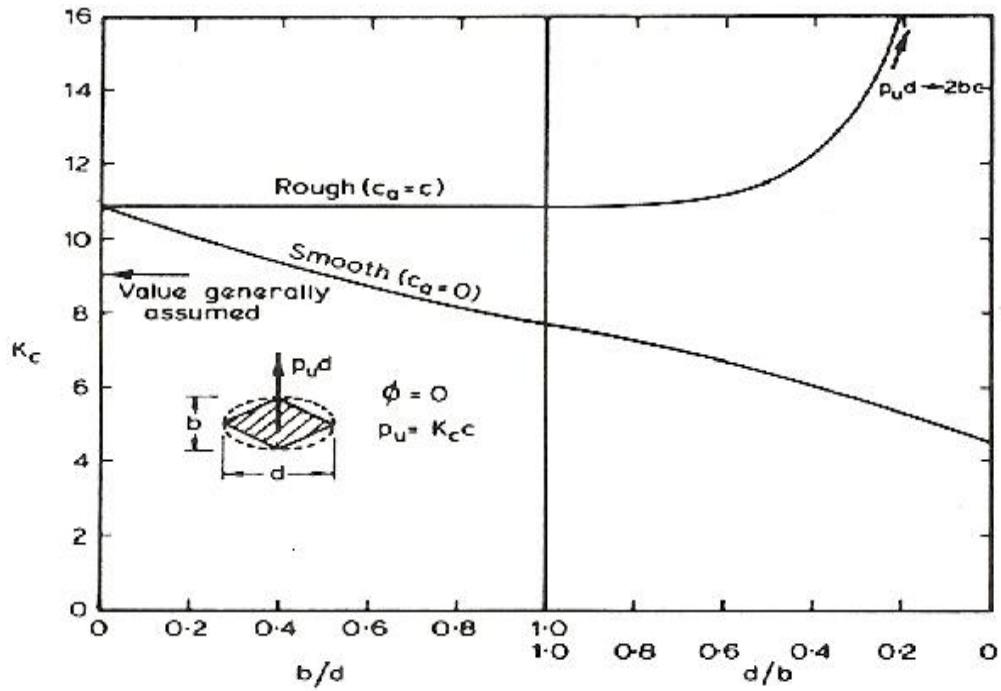


Figure 3.15 : Effect of aspect ratio and adhesion ratio on lateral resistance for purely cohesive soil.

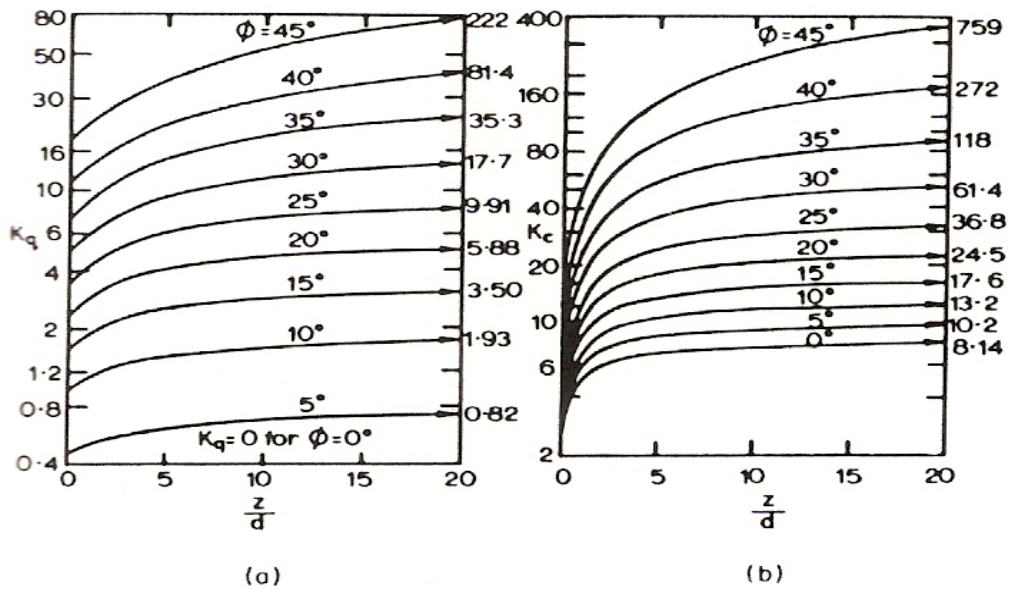
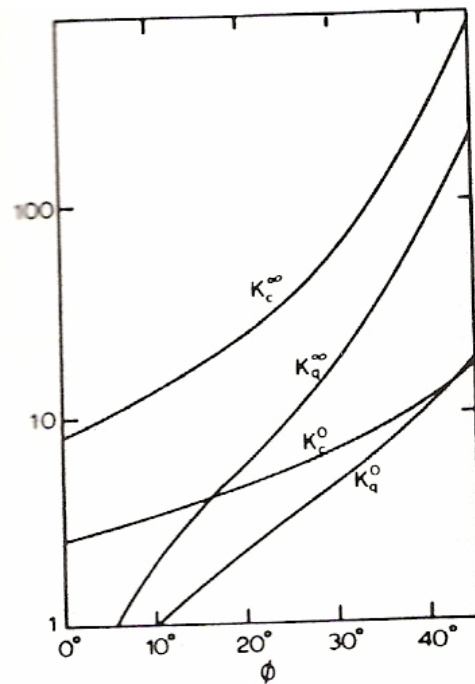


Figure 3.16 : Lateral resistance factors  $K_c$  and  $K_q$  (Brinch Hansen, 1961)



**Figure 3.17 :** Lateral resistance factors at ground surface (0) and great depth ( $\infty$ )(Brinch Hansen, 1961)

The theory developed by Broms (1964a and b) is fundamentally the same as that described except that simplification are made to the ultimate soil resistance distribution along the pile and also that full consideration is given to restrained or fixed-head piles as wellll as unrestrained or free head piles.

### 3.7 Elasticity Theory

The theory of elasticity is often used to estimate lateral movement of piles in a variety of geomaterial types. One approach, based on the theory of elasticity, was suggested by Poulos (1971). As presented by Poulos (1971), the lateral behavior of a given pile was generally influenced by the length-to-diameter ratio,  $L/d$ , stiffness of the pile, soil strength and stiffness properties. The soil in this case was assumed as an ideal, elastic, homogeneous, isotropic medium, having elastic parameters of  $E_s$  and  $I_s$  with depth. The pile was assumed to be a thin rectangular vertical strip of width ( $d$ ), Length ( $L$ ), and constant flexibility ( $E_p I_p$ ). In order to apply the analysis to a circular pile, the width ( $d$ ) can be taken as the diameter of the pile. To simplify the analysis, horizontal shear stresses, that develop between the soil and the sides of the pile, were not taken into account.

A dimensionless factor  $K_R$  describing the relative stiffness of the pile/soil material is defined as follows (Poulos, 1971):

$$K_R = \frac{E_p I_p}{E_s L^4} \quad (3.35)$$

Where,  $E_p$  : modulus of elasticity of pile;

$I_p$  : moment of inertia of pile;

$E_s$  : modulus of elasticity of soil; and,

$L$  : length of pile.

$K_R$  has limiting values of  $\infty$  for an infinitely rigid pile and zero for a pile of infinite length but with no stiffness. The displacement of the pile at the ground surface was presented using equation 3.35 and Figures 3.18 and 3.19 as follows (Poulos, 1971):

$$\rho = I_{\rho H} \frac{H}{E_s L} + I_{\rho M} \frac{M}{E_s L^2} \quad (3.36)$$

Where,  $H$  : applied horizontal load;

$M$  : applied moment;

$I_{\rho H}$  : the displacement influence factor for horizontal load only, acting on ground surface (Figure 3.18); and,

$I_{\rho M}$  : the displacement influence factor for moment only, acting on ground surface (Figure 3.19).

The theory of elasticity approach provides a means to estimate the behavior of drilled shaft based on mathematical derivation. However, in reality, soils and weathered rock are highly inelastic materials especially under relatively large deformations.

Accordingly, predicted shaft deflections commonly match field deflections at low loads (20~30% of total capacity). At higher load levels, the predicted deflections are too small (DiGioia and Rojas-Gonzalez, 1993).

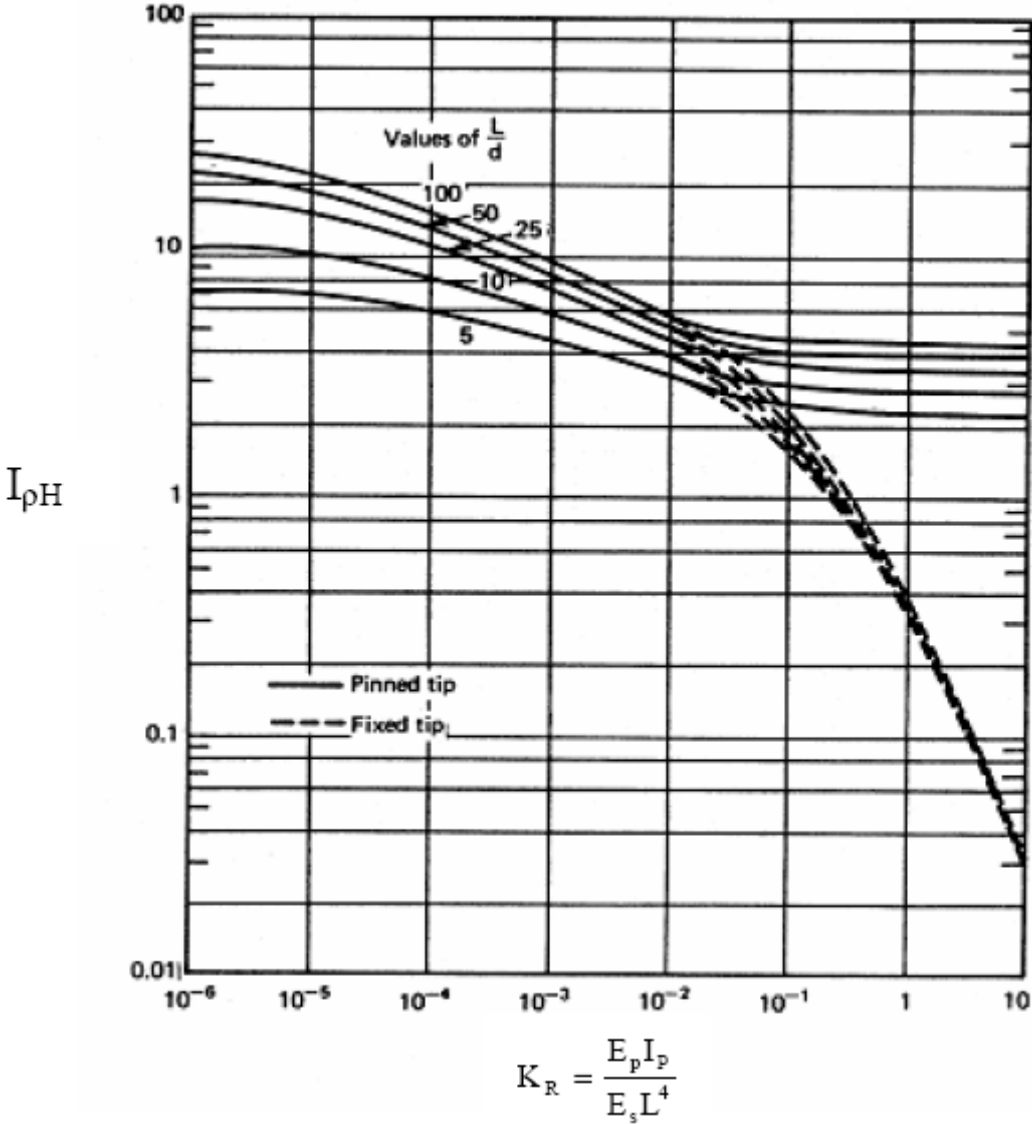


**Figure 3.18:** Displacement Influence Factor for Horizontal Load ( Poulos, 1971).

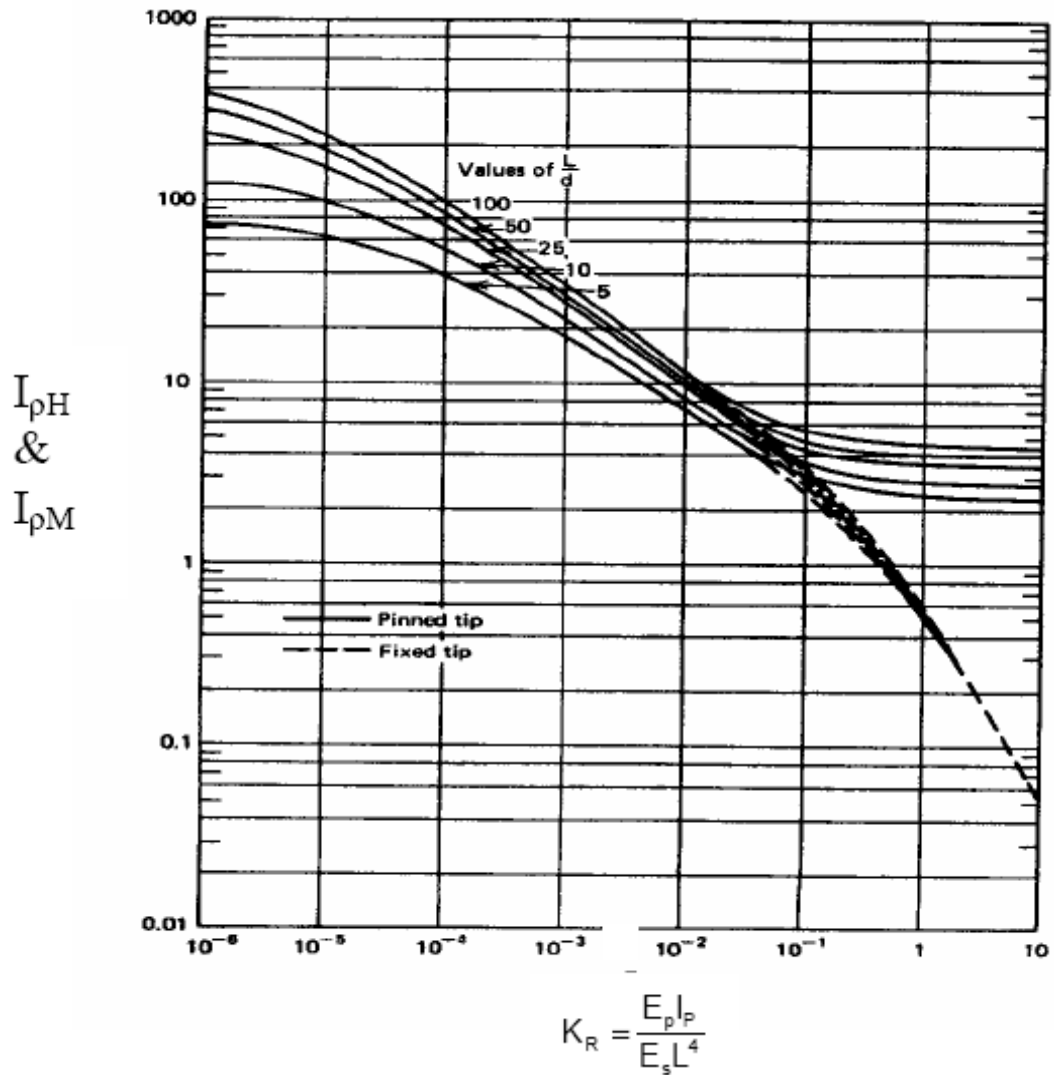


**Figure 3.19:** Displacement Influence Factor for Moment ( Poulos, 1971)

### 3.8 P-y Analysis Method

The p-y method is widely used for design of laterally loaded piles. This method replaces the soil reaction with a series of independent nonlinear springs as shown Fig. 3.20. The p-y curves represent the nonlinear behavior of the soil by relating the soil reaction and pile deflection at points along the pile length.

The prediction of the soil resistance at any point along the pile as a function of pile deflection is perhaps one of the most critical factors in solving the problem of a laterally loaded pile. The distribution of stresses against a cylindrical pile before installation is shown in the sketch in Figure 4.17a. The stresses, at a given depth, will

be uniform and normal to the pile wall (assuming the pile is installed vertical and without inducing bending) (Reese and Van Impe, 2001). Once the pile is subjected to lateral loading the pile will deflect and the soil stresses acting on the pile would have a distribution similar to the one shown in Figure 4.17b. It is important to point out that some of the stresses will not be perpendicular to the pile wall due to development of shear stresses at the interface between the pile and the soil. The net soil reaction,  $p(x)$ , is obtained by integrating the stresses around the pile cross section. The units of  $p(x)$  are force per unit length (U.S. Department of Transportation, 2002).

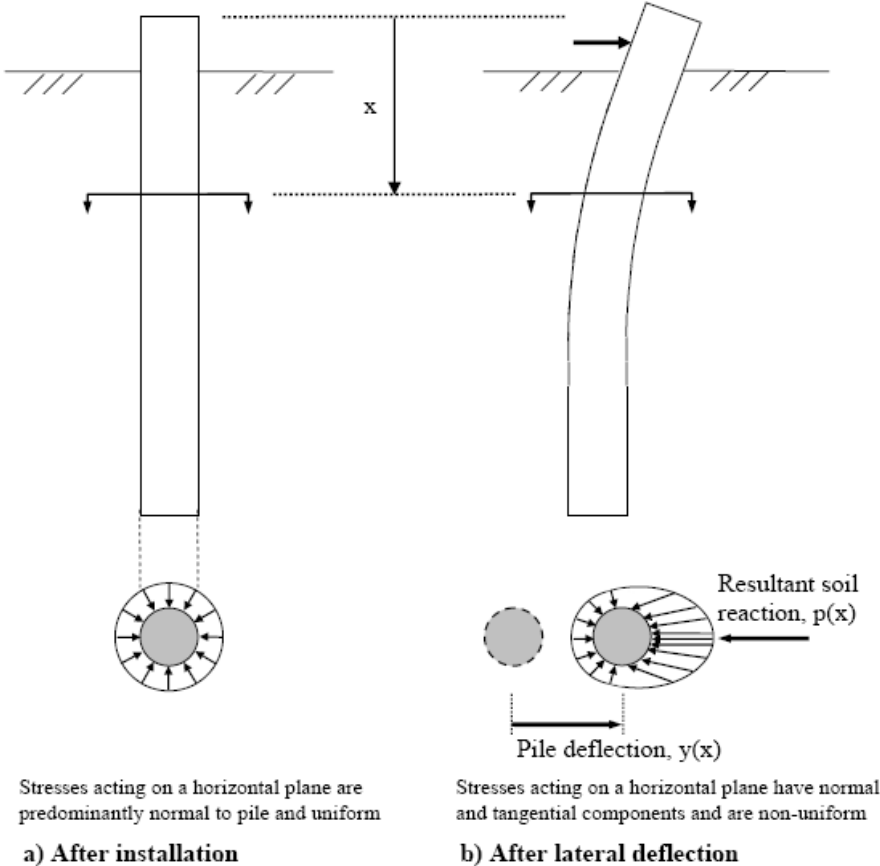


**Figure 3.20 :** Distribution of stresses against a pile before and after lateral loading (Reese and Van Impe 2001).

In general,  $p$ - $y$  curves are nonlinear and they are a function of depth, soil type, and pile dimensions and properties. A typical  $p$ - $y$  curve is shown in Figure 4.18.

Important elements of the  $p$ - $y$  curve include the initial slope,  $E_{py-max}$ , and the ultimate soil resistance value,  $P_{ult}$ .

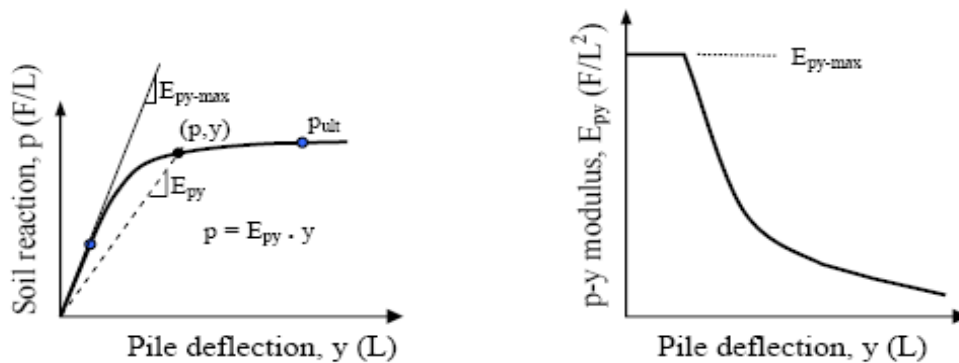


**Figure 3.21** : Typical  $p$ - $y$  curve and resulting  $p$ - $y$  modulus (Reese and Van Impe 2001).

At any point of the  $p$ - $y$  curve the soil reaction,  $p$ , is related to the pile deflection,  $y$  through the  $p$ - $y$  modulus,  $E_{py}$  (Reese and Van Impe, 2001). The  $p$ - $y$  modulus is also known as the reaction modulus and it has units of force/length<sup>2</sup>. Reese and Van Impe (2001) propose using the above nomenclature instead of the modulus of subgrade reaction which was originally developed for settlement of footings and it relates the footing pressure (units of force/length<sup>2</sup>) to the footing settlement (units of length). Point out at the Route 351 Bridge that although the subgrade modulus and  $E_{py}$  are related to the values of the young modulus of the soil,  $E_s$ , they are not only a function of the soil, but rather a result of the soil-structure interaction process between the soil and the footing and pile, respectively.

Ideally  $p$ - $y$  curves should be generated from full-scale lateral load tests on instrumented test piles. In the absence of experimentally derived  $p$ - $y$  curves it is possible to use empirical  $p$ - $y$  formulations that have been proposed in the literature for different types of soils.

The  $p$ - $y$  curves are not uniquely defined by soil characteristics (Ashour and Norris 2000). In addition to the properties of the soil surrounding the pile, the  $p$ - $y$  curves are influenced by several other factors, such as the shape of the pile cross-sectional shape and dimensions, interface friction angle between soil and pile, pile bending stiffness, pile head conditions (Ashour and Norris 2000, Reese and Van Impe, 2001).

Ashour and Norris (2000) used the strain wedge model to study analytically the influence of some of these factors on  $p$ - $y$  curves. They found that for uniform sand deposits a stiffer pile results in stiffer  $p$ - $y$  curves. They also found that two piles of the same width, but one with a circular cross-section, and another with a square cross section, resulted in different  $p$ - $y$  curves. The square pile in sand showed a soil-pile resistance higher than the circular pile. The findings from Ashour and Norris are based on analytical studies and to the best of our knowledge no full-scale experiments have been reported to confirm their findings. Reese and Van Impe (2001) also pointed out the influence of the shape of the pile cross-section on the soil resistance,  $p$  as illustrated in Figure 3.22 (U.S. Department of Transportation, 2002).

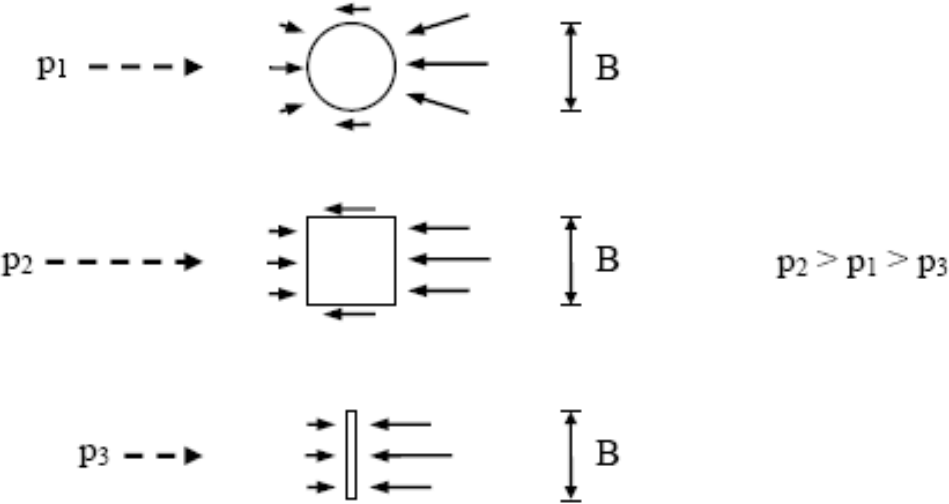


**Figure 3.22 :** Schematic showing the influence of shape of cross section of pile on the soil reaction  $p$  ( Reese and Van Impe, 2001)

The majority of the methods consider only the influence of the soil properties and the pile width. If it is desired to take into account other factors such as pile shape and surface texture,  $p$ - $y$  curves should be obtained experimentally based on full-scale tests.

The  $p$ - $y$  analyses carried out in this research used published recommendations for  $p$ - $y$  curves. The recommendations by Reese et al. (1974) were used for the sandy soils at the test site. A brief description of these recommendations is provided below.

Based on the subgrade reaction approach, the soil pressure,  $p_{(kN/m^2)}$  is correlated to the lateral deformation as follows (Matlock, 1970):

$$p = k_{ho} y \quad (3.37)$$

Where,  $k_{ho}$  :the coefficient of subgrade reaction that is normally defined on the basis of Winkler foundation ( $kN/m^3$ ); and,

$y$  = the lateral displacement of the pile (m).

Mltiplying the soil pressure,  $p_{(kN/m^2)}$ , by the pile width,  $b$  (m) (or diameter, if circular), the force per unit length,  $P(kN/m)$ , is obtained. Accordingly, the soil reaction  $P$  is expressed as follows:

$$p = k_h y \quad (3.38)$$

Where,  $P_{(kN/m)}$  is the soil reaction in force per unit length;

$k_h$  subgrade modulus  $k_{ho} b$  ;

$k_{ho}$  coefficient of subgrade reaction and

$y$  (m) is the pile displacement.

In the subgrade reaction approach for analysis of laterally loaded piles and shafts, the soil is replaced by a series of springs attached to an element of foundation, as shown in Figure 3.21. P-y curves are defined at various depth, as a function of soil type and geometry.

According to Mattlock (1970), the proper form of a P-y relation is influenced by many factors, including: (i) natural variation of soil properties with depth, (ii) the general form of the pile deflection, (iii) the corresponding state of stress and strain throughout the affected soil zone, and (iv) the rate sequence and history of load cycles. In order to perform an analysis for a given design, the complex pile-soil interaction is reduced at each depth to a simple  $p$ - $y$  curve.

### 3.9 Winkler Foundation Model

Winkler Foundation model is generally used on single piles. The Winkler approach is easily performed in the analysis of non-linear pile-soil systems using most standard 1-D finite element programs. In this approach, the pile is modelled as a beam and the surrounding soil is modelled using distributed continuous springs and dashpots. Pile nonlinearity could be considered in the analysis using an appropriate nonlinear material model (Ramachandran, 2005 ). Pile head deflection and variation of pile deformation and bending moment with depth using Winkler model can be solved. Figure 3.23 shows the discretised form of the Winkler model for the analysis of a single pile under dynamic (including seismic) lateral loading. A similar model may be used for the analysis of single piles under static lateral loads. However, under static loads, the dashpots would be irrelevant. ( Ramachandran, 2005 )

Nonlinear soil-pile interaction can be taken into consideration in this method. General theoretical considerations on this approach are summarized.

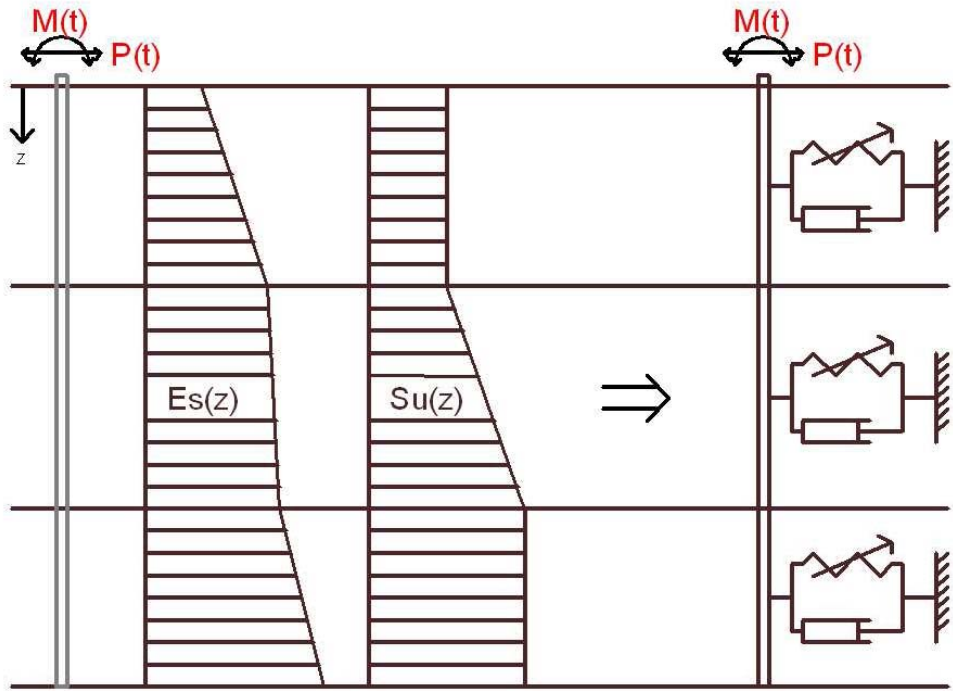


**Figure 3.23:** Beam on Winkler foundation model for a single pile under lateral loading (J. Ramachandran, 2005 ).

#### 4. ANALYSIS OF PILE BEHAVIOR

The purpose of a pile foundation is to transmit the loads of a superstructure to the underlying soil while preventing excessive structural deformations. The capacity of the pile foundation is dependent on the material and geometry of each individual pile, the pile spacing (pile group effect), the strength and type of the surrounding soil, the method of pile installation, and the direction of applied loading (axial tension or compression, lateral shear and moment, or combinations). Except in unusual conditions, the effects of axial and lateral loads may be treated independently. (Mosher and Dawkins, 2000)

Predicting the behavior of pile foundations in soft clay or liquefied ground under earthquake loading is a complex problem involving consideration of design motions, freefield site response, superstructure response, and soil-pile-superstructure interaction (Wilson, 1998).

The pile may be treated as a laterally loaded elastic beam for which the differential equation from conventional theory is

$$EI \frac{d^4 y}{dx^4} = p(x) \quad (4.1)$$

Where,

y: lateral displacement

x: length along pile

p: soil reaction

The soil reaction  $p_m$  for a finite element of the beam m can be written:

$$P_m = -E_s y_m = EI \left( \frac{t}{L} \right)^4 (y_{m-2} - 4y_{m-1} + 6y_m - 4y_{m+1} + y_{m+2}) \quad (4.2)$$

where the pile length,  $L$  is divided into  $t$  equal lengths and  $E_s$  is the modulus of the soil reaction and by definition the ratio between soil reaction at any point and the pile deflection at that point.

The corresponding pile slope  $S_m$ , moment  $M_m$  and shear  $V_m$  can be expressed by the following equations 4.3, 4.4 and 4.5:

$$S_m = \left( \frac{t}{L} \right) (y_{m-1} - y_m) \quad (4.3)$$

$$-M_m = EI \left( \frac{t}{L} \right)^2 (y_{m+1} - 2y_m + y_{m-1}) \quad (4.4)$$

$$-V = \frac{1}{2} EI \left( \frac{t}{L} \right)^3 (-y_{m+2} + 2y_{m+1} - 2y_{m-1} + y_{m-2}) \quad (4.5)$$

Insertion of the experimental data into these equations showed the differentiation by finite difference equations to be extremely sensitive to errors in pile deflection measurements. It has been pointed out by Matlock, 1956 that “attempts to obtain soil reaction values from deflection values or slope measurements alone are certain to fail because the attainment of reasonable accuracy and resolution (with respect to depth) in soil resistance value would require impossible precision in the original measurements”. This is due to the progressive loss in accuracy arising during the three of four differentiations. Even the technique of measuring the moments by strain gauge instrumentation suffers from the fact that measured moment values must be differentiated twice to yield soil resistance values. There would be no similar difficulty in obtaining accurate values of deflection from known moment values as the integration tends to smooth out the effects of the small experimental errors (Sağlamer and Parry, 1977).

As an alternative approach to the finite difference method, a linear variation in subgrade modulus  $k$  with depth was assumed. By this assumption it is possible to

determine the magnitude of the coefficient of subgrade modulus,  $k$  on the basis of the observed load-deflection relationship at the sand surface 4.2, 4.3, 4.4, 4.5 and 4.6. The pile deflection at the ground surface is related to the moment and shear acting on the pile at the ground surface by Eq. 4.2.

$$y_t = A_y \left( \frac{P_t T^3}{EI} \right) + B_y \left( \frac{M_t T^2}{EI} \right) \quad (4.6)$$

Where,

$y_t$  : Lateral deflection of the pile at the ground surface, in metres

$A_y$ ,  $B_y$  : Non-dimensional coefficients that depend on the ratio,  $L/T$ . Values of  $A_y$  and  $B_y$  are listed in Table 4.1 for “long” piles where  $L/T > 4$ ,

$P_t$  : Lateral load at the ground surface, in Newtons,

$M_t$  : Moment acting on the pile at the ground surface, in Newton-metres,

$EI$  : Flexural stiffness of the pile, in  $Nm^2$ .

The relative stiffness term  $T$  is defined by Eq. (4.7), and has the dimension of length

$$T = \left( \frac{EI}{k} \right)^{\frac{1}{5}} \quad (4.7)$$

Where,

$k$ : Coefficient of horizontal subgrade reaction in  $\left( \frac{N}{m^3} \right)$ , which is assumed to increase linearly with depth.

## **4.1 Pile Behaviour During Earthquake**

### **4.1.1 Liquefaction**

Pile foundations in liquefiable soils are very difficult problems to solve. Therefore, seismic design and seismic analysis of piles are complex to solve. In the last severe earthquake in Duzce, Turkey in 1999, serious damage on pile foundations and structures due to liquefaction and lateral spreading was observed. Although in the last decades research was done to better explain the liquefaction of soils, soil-pile interaction in liquefiable soils are not well understood yet. Figure 4.1 shows the damage on pile foundation after earthquake. For level ground areas and Fig.4.2 shows damage mechanisms of piles in lateral spreading areas.

Simplified design procedures for pile foundation in laterally spreading ground include limit equilibrium methods and beam on nonlinear Winkler foundation (BNWF) methods (Branderberg, et al 2001). The former approach applies lateral pressures against the pile which are independent of the free-field displacement. This approach is reasonable when the free-field displacements are large enough for the lateral soil pressures to reach their limiting values. In the latter approach, the free-field site response (e.g., dynamic or permanent deformations) are estimated separately, and then input to the BNWF model as illustrated in Fig. 4.3. Applying this approach to liquefaction problems is complicated as how liquefaction affects the “p-y” behavior of the liquefied soil or an overlying crust ( they are usually uncoupled to simplified analyses) and the uncertainty in modeling the free-field response of liquefied deposits are unknown (Branderberg, 2001).

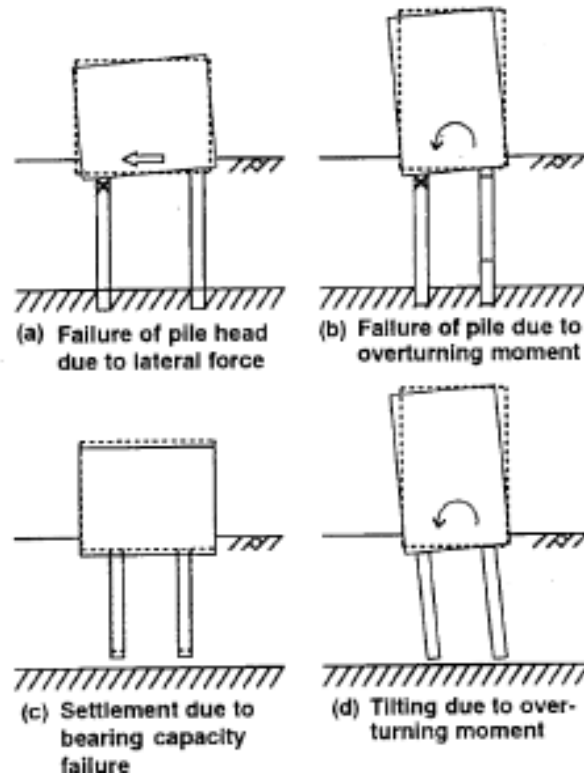


**Figure 4.1 :** Schematic of Pile Damage Mechanisms in Level Ground Areas (Tokimatsu et al. 1996)

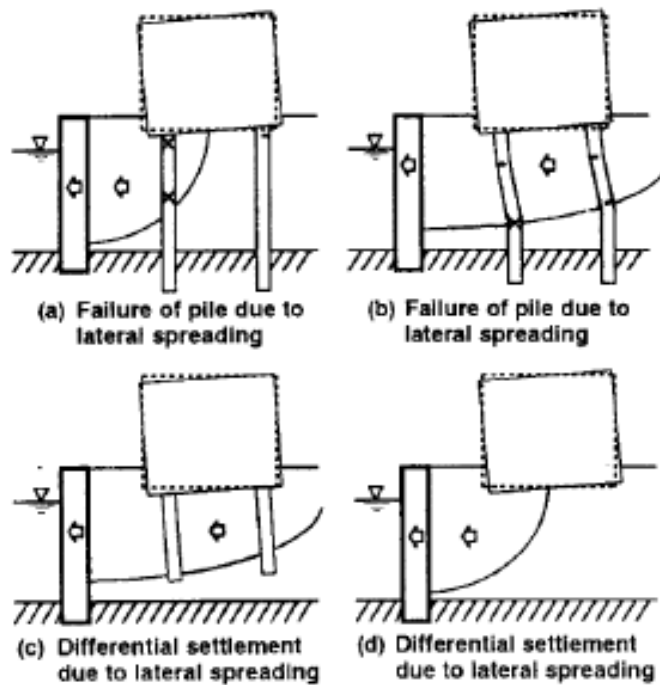


**Figure 4.2:** Schematic of Pile Damage Mechanisms in Laterally Spreading Areas (Tokimatsu et al. 1996)

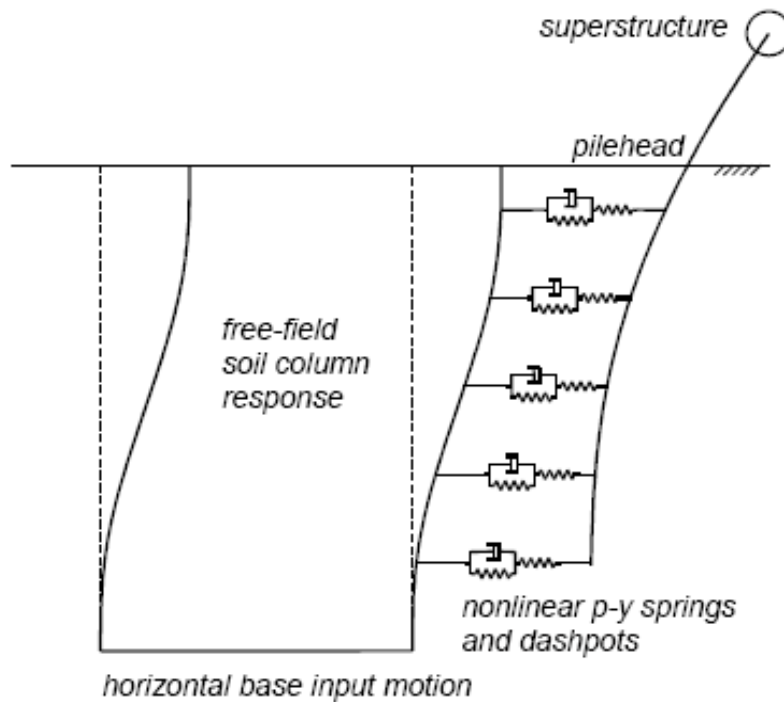


**Figure 4.3:** Schematic of BNWF or “p-y” Model (Wilson et al. 2000).

#### 4.1.2 Cause of Pile Failures during Earthquakes

In the previous strong earthquakes, pile foundation has collapsed in the liquefied soils. Piles behave as a beam element throughout an earthquake. Therefore, lateral spreading cause bending failure of the pile. Pile failure during earthquakes can be summarised as the soil liquefies, it loses its shear strength, causing it to flow and withdraw with it any overlying non-liquefied crust. Liquefied soil layers drag the pile with them, causing a bending failure as shown in Figure 4.4. This is often referred to as failure due to lateral spreading. In soil pile interaction, failure mechanism assumes that the soil pushes the pile. The deformation of the ground surface close to piled foundations often indicates mechanism. Figure 4.5 shows surface observations of lateral spreading observed after earthquakes.

The Japanese highway code of practice (JRA, 1996) has incorporated this understanding of pile failure as shown in Figure 4.6. The code advises practicing engineers to design piles against bending failure supposing that non-liquefied crust offers passive earth pressure to the pile while the liquefied soil itself offers a drag equal to 30% of total overburden pressure. Other codes such as the USA code

(NEHRP, 2000) and Eurocode 8, part 5 (1998) also focus on the bending strength of the pile.

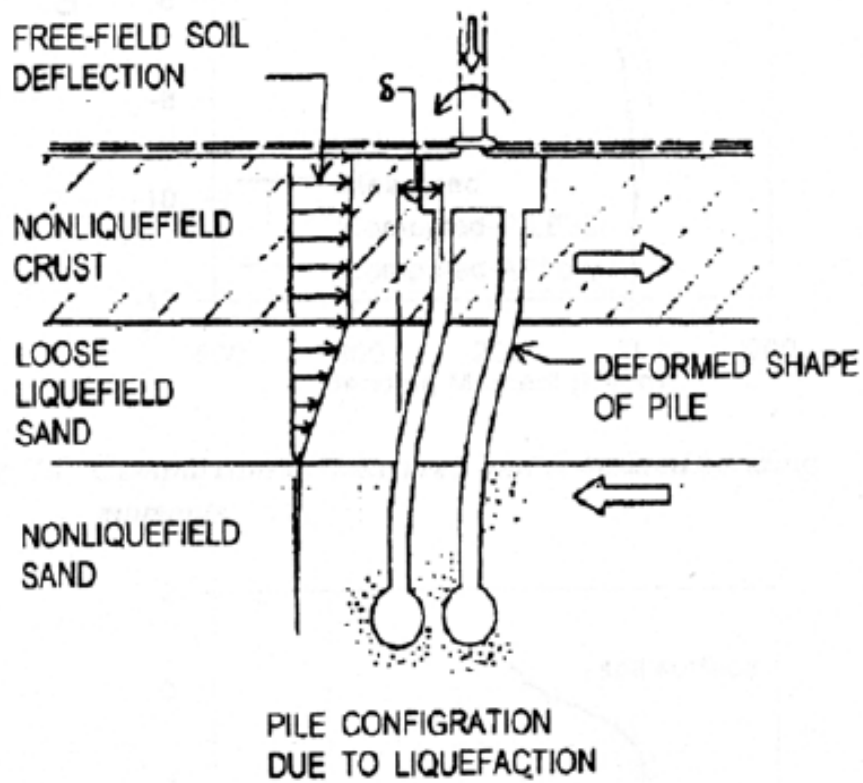


**Figure 4.4:** Current understanding of pile failure, (Bhattacharya, 2003).



**Figure 4.5 :** Surface observations of lateral spreading at (a) bridge site in 1995 Kobe earthquake (b): Navalakhi port in 2001 Bhuj earthquake, (Bhattacharya,2003)

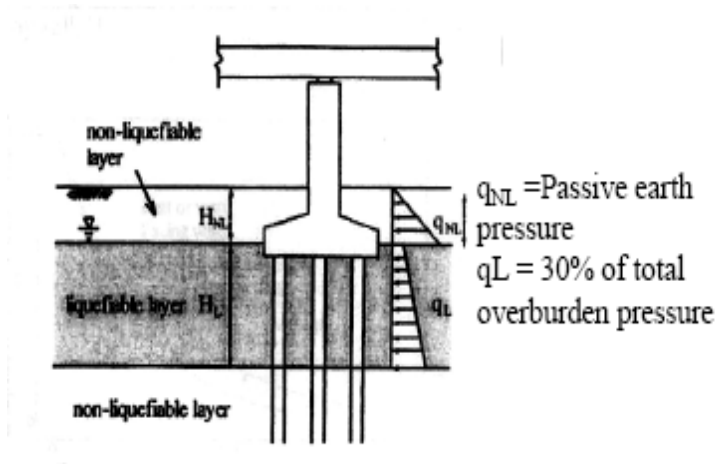


**Figure 4.6:** The idealization for seismic design of bridge foundation (JRA, 1996)

In many recent strong earthquakes structural failure of piles passing through liquefiable soils has been observed by the formation of plastic hinges as shown in Fig 4.7, 4.8 and 4.9. Example from a case of plastic yielding of a pile in the Niigata earthquake in 1964 (Hamada 1992a) is shown in Fig.4.7. This proposes that the bending moment or shear forces that are experienced by the piles exceed those predicted by the Japanese Code of Practice or design methods and in some cases exceed the “Plastic Moment Capacity of the section ( $M_p$ )” ( Bhattacharya and Bolton, 2004). Although high safety factors are used in current design codes, pile failures occur in seismic liquefaction zones. Design materials do not cause the failure. Consequently design methods may not be the design material failure. In other way, lateral spreading failure is not enough to solve by current understanding.

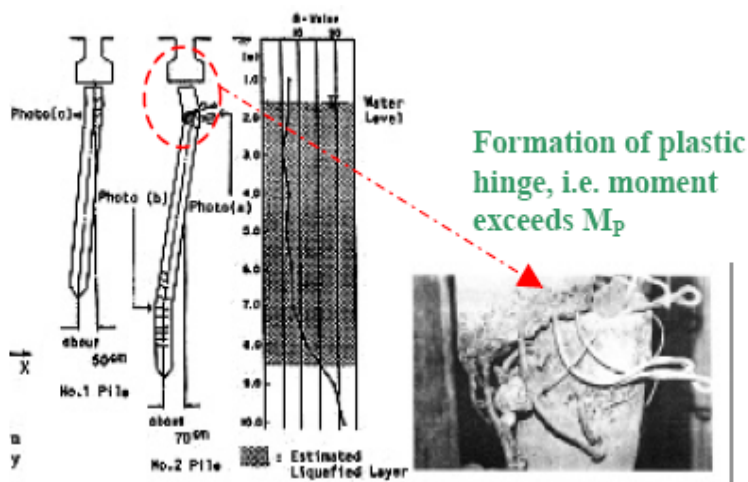


**Figure 4.7 :** Failure of piles in NFCH building during the 1964 Niigata earthquake (Hamada 1992a).

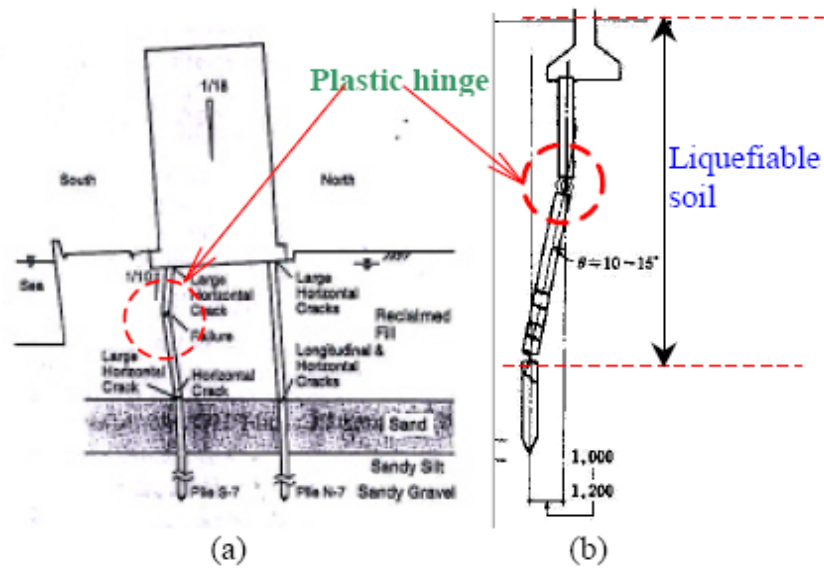


**Figure 4.8 :** Failure of piled buildings; (a) A collapsed building after the 1995 Kobe earthquake, showing the hinge formation after Tokimatsu et al. (1997); (b): Failure piles of the NHK building after Hamada (1992b).

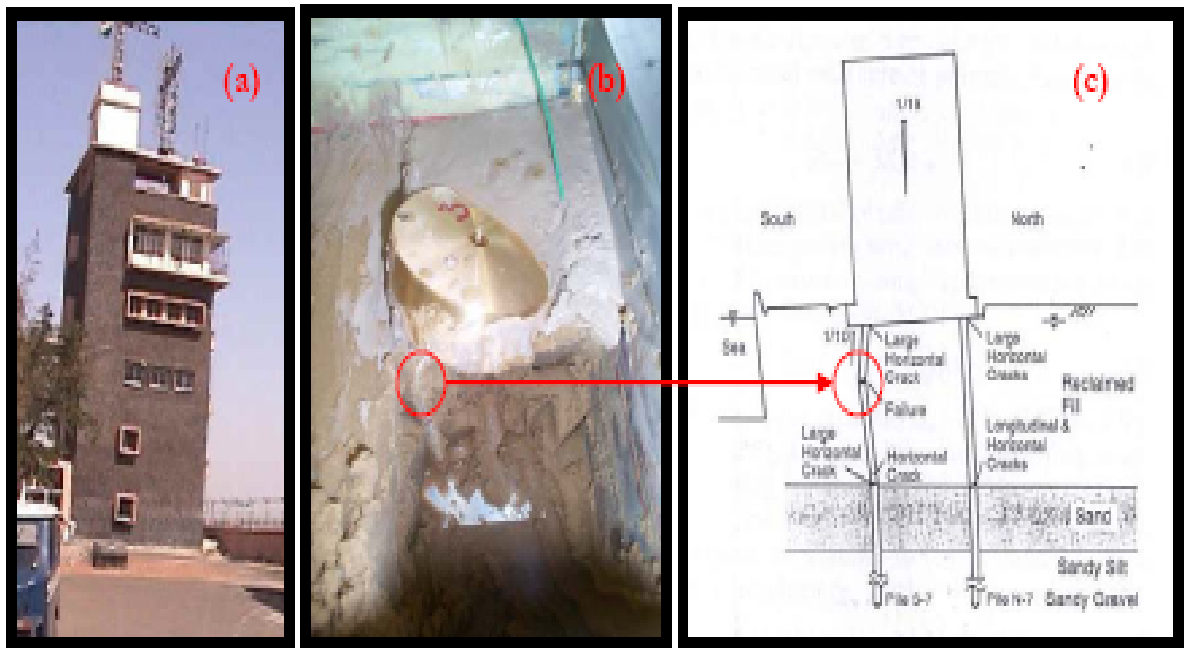


**Figure 4.9:** (a) Observed failure of a piled foundation (Kandla Port tower) in 2001 Bhuj earthquake, Madabhushi et al. (2001); (b): Pile (marked 3) failure in centrifuge test SB-02; (c): Excavated piles in a 3 storied building in 1995 Kobe earthquake, Tokimatsu et al., (1997).

After the detailed investigation of the failure of piles during 1995 Kobe earthquake, Tokimatsu and Asaka (1998) report that:

*“In the liquefied level ground, most PC piles (Prestressed Concrete pile used before 1980’s) and PHC piles (Prestressed High Strength Concrete piles used after 1980’s) bearing on firm strata below liquefied layers suffered severe damage accompanied by settlement and/or tilting of their superstructure, .....”.*

Lateral loading, due to slope movement (lateral spreading), inertia, or out-of-straightness, will increase lateral deflections. Lateral deflection in turn can cause plastic hinges to form, reducing the buckling load, and auxiliary more rapid collapse.

Understanding of pile failure is in the light of a well-documented case history of Showa Bridge during the 1964 Niigata earthquake. As shown in the Figures 4.10 and 4.11 the failure of the bridge is widely agree as being due to lateral spreading of the surrounding soil: see, for example, Hamada (1992a) and Ishihara (1993).



**Figure 4.10:** Failure of Showa Bridge after NISEE, (Hamada, 1992).

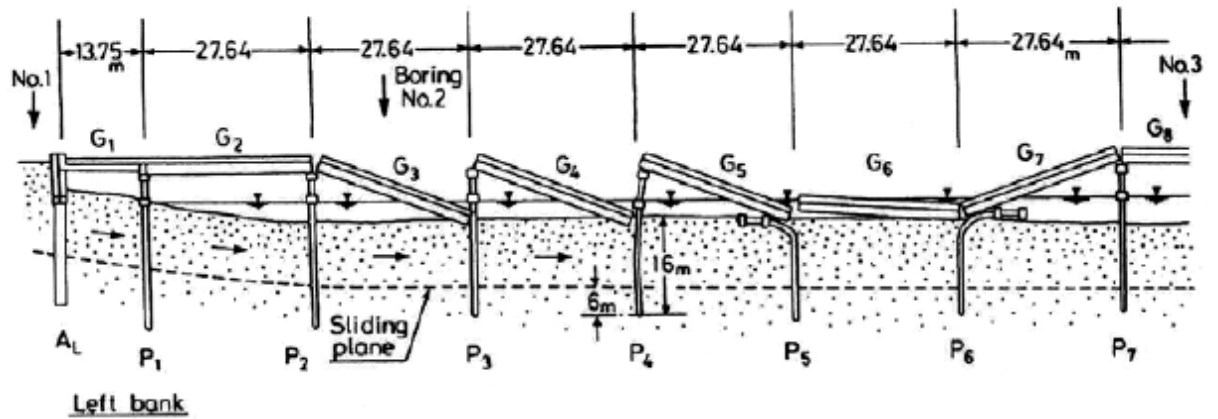


**Figure 4.11** : Schematic diagram of the Fall-off of the girders in Showa bridge (Takata et al., 1965).

Figure 4.12 Shows the Showa bridge, piles under pier no. P5 which has deformed towards the left and the piles of pier P6 deformed towards the right (Bhattacharya, 2003). The cause of pile failure was due to lateral spreading and the piers should have deformed identically in the direction of the slope. In addition, the piers close to the riverbanks did not fail, whereas the lateral spread is seen to be severe at these places.

Bhattacharya (2003) reported that the location of a plastic hinge due to lateral spreading is expected to occur at the interface of the liquefiable and non-liquefiable layer as this section experiences the highest bending moment. It is often seen, however, that hinge formation also occurs within the top third of the pile as seen in Figures 4.12 (b) and 4.11.



**Figure 4.12:** (a): Piled “Million Dollar” bridge after 1964 Alaska earthquake (USA); (b): Piled “Showa Bridge” after 1964 Niigata earthquake (JAPAN); (c): Piled tanks after 1995 Kobe earthquake (JAPAN), photo courtesy of NISEE.

## 4.2 Lateral Behaviour of Pile Groups

In general piles are subjected to the lateral forces which increase due to earthquakes, wind, earth pressure and heavy vehicles. The excessive lateral loads can cause serviceability problems. In the last decades, analytical and in numerical methods timely from finite element, elastic limit element and non-linear subgrade reaction methods are developed. Experimental work were also used to improve these methods. Current practice for analyzing non-linear soil response is to use the subgrade reaction method (Winkler, 1867) where the pile-soil interaction is represented by a series of non-linear subgrade reaction or ‘p-y’ curves which relate the pile pressure (p) to the pile displacement (y) at a particular depth ( Matlock and Reese 1960, API 1987, DNV 1992). Although methods are available to predict the response of single piles under static loads, there is limited information available in the design of closely spaced pile groups under lateral loading. As closely spaced piles move laterally, the deformation zone of the piles overlap resulting generally in the decrease of their lateral resistance for a given displacement. This is called group interaction or pile-soil-pile interaction and methods must be chosen to reduce the stiffness of the p-y curves used in design accordingly ( Ghosh et al., 2004 ). The pile group geometry and the loading condition investigated are shown in Figure 4.13.

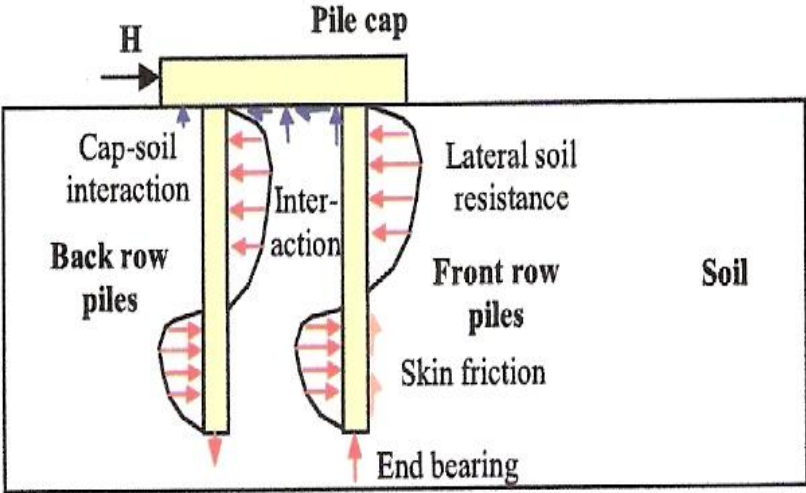


**Figure 4.13 :** Schematic representation of pile group response to lateral loading ( Ghosh et al., 2004 ).

Most of the pile foundations are groups of piles rather than single piles. Different numerical and analytical methods have been developed for the analysis of single

piles and pile groups. Most popular methods of analysis of group piles are 3D finite element analysis methods which are performed under static and dynamic conditions. Winkler model is usually used to analyse single piles. The resistance provided by the group under vertical and lateral loading is generally not equal to the sum of the resistance of the individual piles. Most often, group resistance is less than the sum of the individual pile resistance and is a function of the pile group configuration as well as pile spacing. This 3D method is applicable to pile groups in elastic soils under static loading conditions ( Ramachandran, 2005). A method of analysis for pile groups using interaction factors and based on the theory of elasticity was proposed by Poulos and Davis.



## **5. CASE HISTORY**

In this chapter, two case histories of behaviour of piled structures during earthquakes will be explained. This section highlights the shortcomings of the current understanding of pile failure in the light of a well-documented case history of Showa Bridge during the 1964 Niigata earthquake. The failure of the bridge is widely accepted as being due to lateral spreading of the surrounding soil.

### **5.1 Example of the Showa Bridge**

Hamada (1992) presents aerial photographs, taken before and after the 1964 earthquake, of the stretch of river from the Showa Bridge to the Bandai Bridge, together with a diagram showing the loss of river width following the earthquake. The narrowing is particularly severe, at 23 m, at the Bandai Bridge, where displacement occurred on both banks of the river. The offset of the riverbank is especially noticeable at the bridge, a rigid arch structure, which presumably did not shorten. Other bridges suffered less dramatic, but nevertheless important damage has occurred. Lateral spreading also caused severe damage to embankments and to railway yards.

At the Showa Bridge, lateral displacement of the piers caused five simply supported spans to fall as shown in Fig.5.1. The bridge was founded on nine 600 mm diameter vertical steel piles driven through a 10 m layer of loose medium sand 6 m into an underlying layer of dense fine sand. The 10 m layer is believed to have liquefied from the level of the riverbed to its full depth. The deformed shape of an extracted pile and predicted loading are shown in Fig.5.1 and 5.2. From the s-shape of the deformed pile it is clear that movement of the liquefied sand layer towards the centre of the river caused the deformation of the pile, not forces transmitted through the superstructure from the abutments, which themselves were displaced by movement

of the riverbank. Note the regions of high curvature (and thus bending moment) both at the base and near the top of the liquefied layer.

It is interesting to note that collapse of the bridge apparently did not occur until a minute or two after the shaking has stopped. Hamada (1992) cites reliable eyewitnesses which to the delayed failure of the structure, and infers that the collapse was thus due to liquefaction rather than inertia forces generated in the superstructure by the shaking.

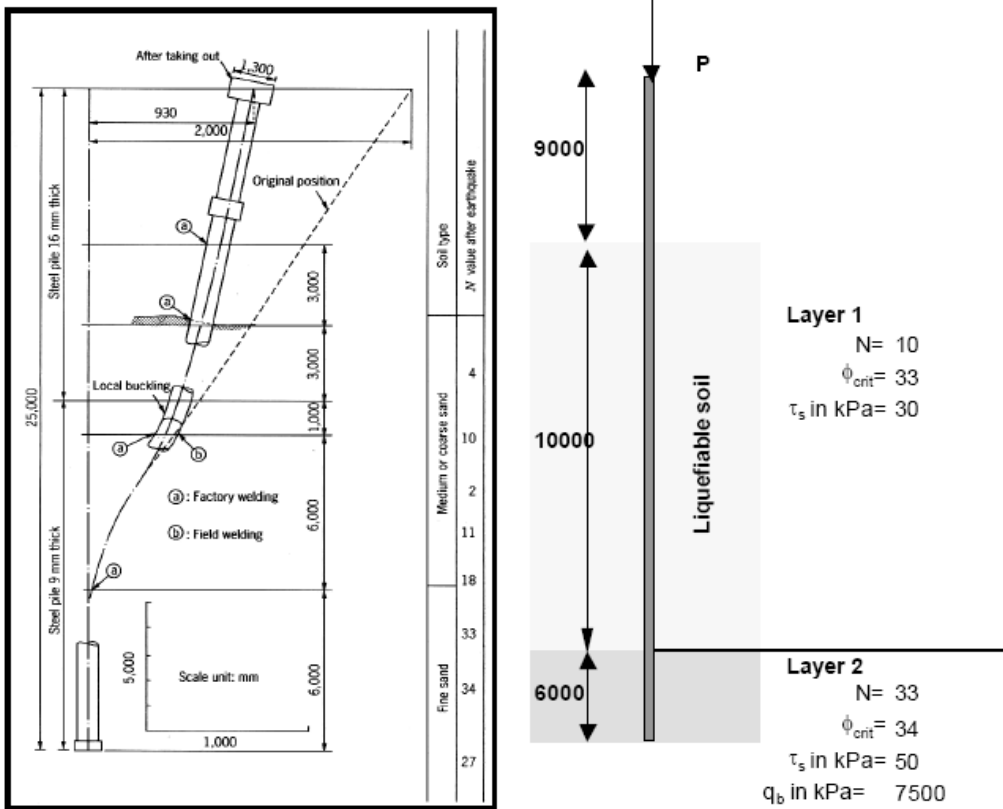


**Figure 5.1 :** Piles of Showa Bridge; (a): Post earthquake recovery and deformation of the pile from Showa Bridge, (b): Schematic diagram of the pile and the soil profile.

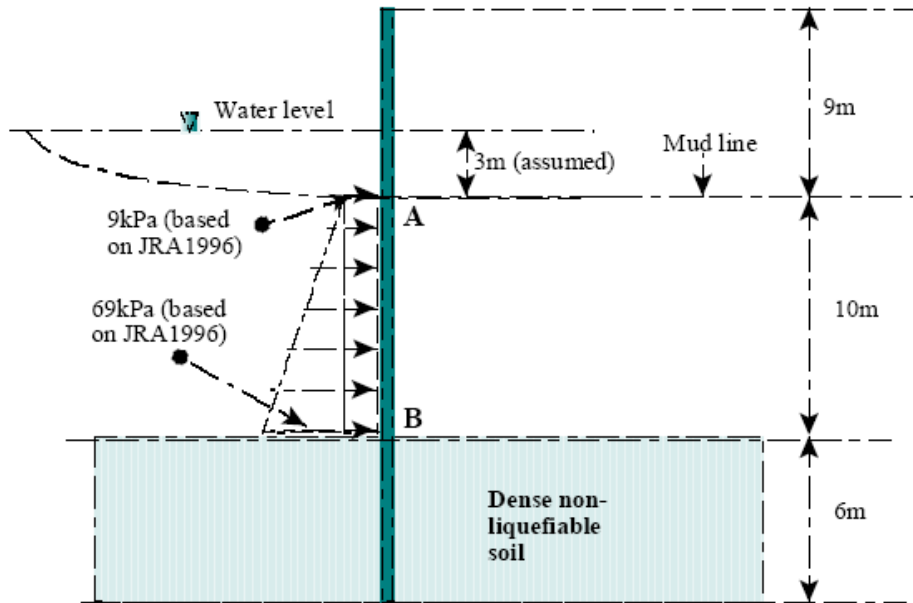


**Figure 5.2:** Schematic diagram showing the predicted loading based on JRA code.

## 5.2 The 1964 M 7.5, Niigata, Japan Earthquake

Niigata city is located on the west coast of Honshu, Japan. The city has difficult and variable foundation soils typical of coastal alluvial plains, especially those associated with active rivers. They are characterised by 10-20 m of mostly loose Holocene soils comprising both loose fluvial sediments, deposited rapidly as sea level rose in the post glacial period, together with usually denser dune sand. These conditions are seen at Niigata, where the city is founded partly on esturine soils, partly on alluvial sand, deposited by the river, loose manmade fill, and partly on dune sand. M7.5 earthquake of 16 June, with epicenter about 50 km offshore to the north and with a focal depth of 40 km, generated quite modest ground acceleration of up to 0.25 g at Niigata (Hamada, 1992). Liquefaction has occurred in loose sands extensively. Especially low-lying sand fill and in river channel material of the most recently abandoned meanders along the lower reaches of the Shinano River, damaging buildings, houses, tanks, bridges, roads, railways, river dikes and buried pipes. Little or no liquefaction damage was seen in the dune sands (Fukuoka, 1996), essentially of the same origin as the river sands, but deposited in a denser state.

Damage included the settlement and tilting of buildings, with some structures settling by a metre or more and tilting several degrees off vertical. In one well-known case, an apartment building at Kawagishi-cho tilted almost to the horizontal as soil beneath its foundation has liquefied. Lateral spreading on shallow slopes of just a few degrees caused widespread damage to buried services, roads and railways, riverside retaining walls and to bridge and building foundations. Light-weight buried structures floated upwards in liquefied sands. Settlement of the ground surface also resulted in inundation of already low-lying areas. The ejected sand itself proved to be a great nuisance, clogging pipes and hindering recovery operations.

A first lesson to be made from Niigata is a geological one; namely, that it was the recent fill and fluvial soils that has liquefied. In general, dune sands, compacted by sea-wave energy, are denser than similar river-lain soils and therefore less liable to liquefaction. However, they are not immune from liquefaction; there are several instances, for example from the 1968, Inangahua, New Zealand earthquake (Berrill et al., 1987), of beach sands liquefying. However, they generally require stronger shaking to do so than their fluvial counterparts.

## **6. ANALYSIS AND NUMERICAL SIMULATION**

Mazzonet et al. (2006) has calibrated a nonlinear elasto-plastic computational model, within the Pacific Earthquake Engineering Research (PEER) Center OpenSees Framework (developed under the leadership of Professor Gregory Fenves of UC Berkeley) with the available centrifuge test data. OpenSees is a software framework for developing applications to simulate the performance of structural and geotechnical systems subjected to earthquakes. In this chapter, this program will be explained briefly and the results of analysis done on laterally loaded piles in different soil types will be presented.

### **6.1 OpenSees**

The soil constitutive model (Parra, 1996; Yang and Elgamal, 2002; Elgamal et al., 2003) implemented in OpenSees was developed based on the original multi-surface-plasticity theory for frictional cohesionless soils (Prevost, 1985). This model shown in Figures 6.1 and 6.2 was developed with emphasis on simulating the liquefaction-induced shear strain accumulation mechanism in clean medium-dense sands (Yang and Elgamal, 2002; Elgamal et al., 2003). Special attention was given to the deviatoric volumetric strain coupling (dilatancy) under cyclic loading, which causes increased shear stiffness and strength at large cyclic shear strain excursions (i.e., cyclic mobility).

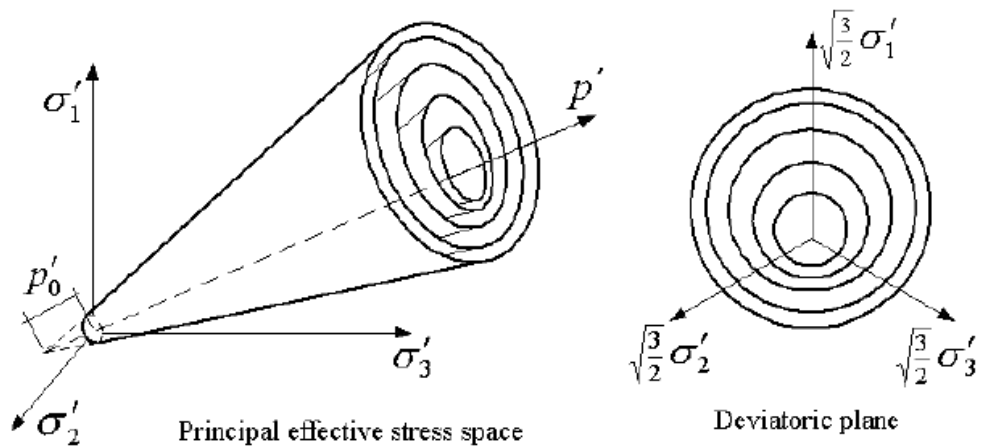


**Figure 6.1** : Conical yield surfaces for granular soils in principal stress space and deviatoric plane (Prevost, 1985; Yang et al., 2003).

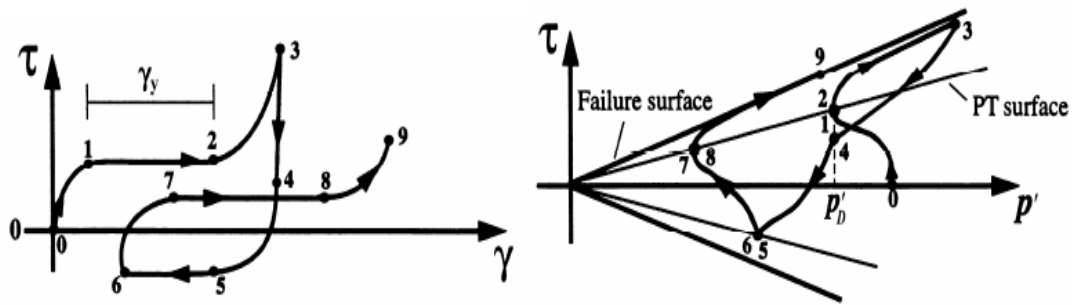


**Figure 6.2** : Shear stress-strain and effective stress path under undrained shear loading conditions (Yang et al., 2003).

A user interface for “OpenSeesPL” can be seen in Figure 6.3, to allow for the execution of single pile simulations under seismic excitation scenarios as well as for pushover studies (Lu et al., 2006). The finite element analysis engine for this interface is the OpenSees framework (Mazzoni et al., 2006).

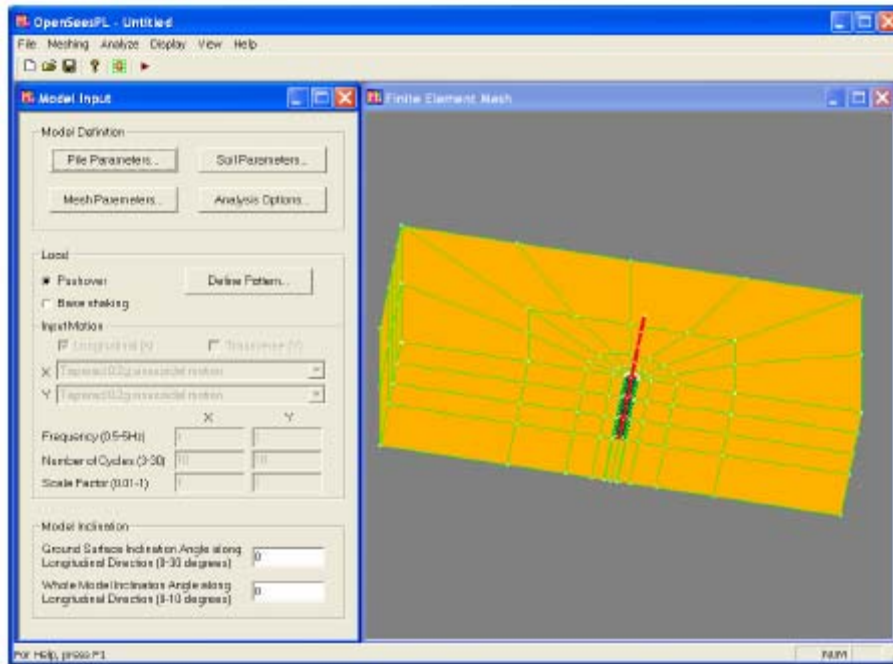


**Figure 6.3 :** OpenSeesPL user interface with mesh showing a circular pile in level ground (view of  $\frac{1}{2}$  mesh employed due to symmetry for uni-directional lateral loading).

OpenSeesPL includes a pre-processor for: 1) definition of the pile geometry (circular or square pile) and material properties (linear or nonlinear), 2) definition of the 3D spatial soil domain (with uniform soil properties for each layer laterally), 3) definition of the boundary conditions and input excitation or push-over analysis parameters, and 4) selection of soil materials from an available menu of cohesionless and cohesive soil materials in Table 6.1. The menu of materials in Table 6.1 includes a complementary set of modeling parameters representing loose, medium and dense cohesionless soils (with silt, sand or gravel), and soft, medium and stiff clay (J2 plasticity cyclic response model). Representative soil properties are pre-defined for each of these soils in Table 6.1.

OpenSeesPL allows convenient pre-processing and graphical visualization of the analysis results including the deformed mesh shown in Figure 6.4, ground response time histories and pile responses. This interface is designed for simplicity, and is intended to be intuitive and self-explanatory. OpenSeesPL makes it possible for geotechnical and structural engineers/researchers to build a model, run the finite element analysis and evaluate performance of the pile-ground system (Lu et al., 2006).

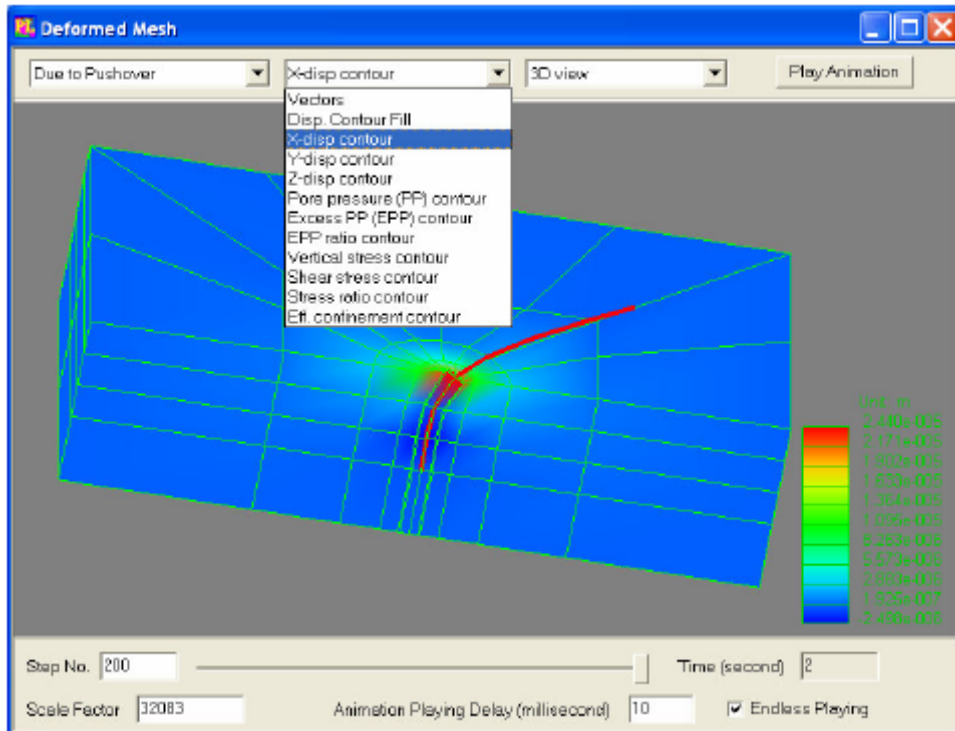


**Figure 6.4 :** Graph types available in the deformed mesh window.

**Table 6.1:** Representative set of basic material parameters (data based on Seed and Idriss (1970), Holtz and Kovacs (1981), Das (1983), and Das (1995)).

Cohesionless Soils	Shear wave velocity* at 10m depth (m/s)	Friction angle (degrees)	Possion's ratio	Mass density (kg/m <sup>3</sup> )
Loose	185	29	0.4	1.7x10 <sup>3</sup>
Medium	205	31.5	0.4	1.9x10 <sup>3</sup>
Medium-dense	225	35	0.4	2.0x10 <sup>3</sup>
Dense	255	40	0.4	2.1x10 <sup>3</sup>
Cohesive Soils	Shear wave velocity (m/s)	Undrained shear strength (kPa)	Possion's ratio	Mass density (kg/m <sup>3</sup> )
Soft clay	100	18.0	0.4	1.3x10 <sup>3</sup>
Medium clay	200	37.0	0.4	1.5x10 <sup>3</sup>
Stiff clay	300	75.0	0.4	1.8x10 <sup>3</sup>

\* Shear wave velocity of cohesionless soils in proportion to  $(p_m)^{1/4}$  where  $p_m$  is effective mean confinement.

There are 18 predefined materials in OpenSeesPL as shown in Table 6.2. Basic model parameter values for these materials are listed in Figure 6.5. The cohesionless very loose soil is same as the cohesionless loose soil except the user is allowed to specify the residual shear strength for the very loose one. Otherwise 0.2 kPa is defined by default. In addition, user-defined cohesionless and cohesive soil materials (U-Sand1, U-Sand2, UClay1 and U-Clay2) are also available to choose.

1: Cohesionless very loose, silt permeability
2: Cohesionless very loose, sand permeability
3: Cohesionless very loose, gravel permeability
4: Cohesionless loose, silt permeability
5: Cohesionless loose, sand permeability
6: Cohesionless loose, gravel permeability
7: Cohesionless medium, silt permeability
8: Cohesionless medium, sand permeability
9: Cohesionless medium, gravel permeability
10: Cohesionless medium-dense, silt permeability
11: Cohesionless medium-dense, sand permeability
12: Cohesionless medium-dense, gravel permeability
13: Cohesionless dense, silt permeability
14: Cohesionless dense, sand permeability
15: Cohesionless dense, gravel permeability
16: Cohesive soft
17: Cohesive medium
18: Cohesive stiff
19: U-Sand1...
20: U-Sand2...
21: U-Clay1...
22: U-Clay2...

**Figure 6.5:** Type of soil defined.

**Table 6.2 :** Predefined soil properties in OpenSeesPL

Cohesionless Soil	Reference shear modulus $G_r$ (kPa, at $p'_r=80$ kPa) <sup>1</sup>	Reference bulk modulus $B_r$ (kPa, at $p'_r=80$ kPa)	Friction angle $\phi$ (degrees) <sup>2</sup>	Permeability coeff. <sup>3</sup> (m/s)	Mass density <sup>4</sup> (ton/m <sup>3</sup> )
Very loose, silt permeability	5.5E+04	1.5E+05	29	1.0E-07	1.7
Very loose, sand permeability	5.5E+04	1.5E+05	29	6.6E-05	1.7
Very loose, gravel permeability	5.5E+04	1.5E+05	29	1.0E-02	1.7
Loose, silt permeability	5.5E+04	1.5E+05	29	1.0E-07	1.7
Loose, sand permeability	5.5E+04	1.5E+05	29	6.6E-05	1.7
Loose, gravel permeability	5.5E+04	1.5E+05	29	1.0E-02	1.7
Medium, silt permeability	7.5E+04	2.0E+05	33	1.0E-07	1.9
Medium, sand permeability	7.5E+04	2.0E+05	33	6.6E-05	1.9
Medium, gravel permeability	7.5E+04	2.0E+05	33	1.0E-02	1.9
Medium-dense, silt permeability	1.0E+05	3.0E+05	37	1.0E-07	2.0
Medium-dense, sand permeability	1.0E+05	3.0E+05	37	6.6E-05	2.0
Medium-dense, gravel permeability	1.0E+05	3.0E+05	37	1.0E-02	2.0
Dense, silt permeability	1.3E+05	3.9E+05	40	1.0E-07	2.1
Dense, sand permeability	1.3E+05	3.9E+05	40	6.6E-05	2.1
Dense, gravel permeability	1.3E+05	3.9E+05	40	1.0E-02	2.1
Cohesive Soil	Shear modulus $G$ (kPa)	Bulk modulus $B$ (kPa)	Cohesion $c$ (kPa) <sup>5</sup>	Permeability coeff. <sup>3</sup> (m/s)	Mass density <sup>4</sup> (ton/m <sup>3</sup> )
Soft	1.3E+04	6.5E+04	18.0	1.0E-09	1.3
Medium	6.0E+04	3.0E+05	37.0	1.0E-09	1.5
Stiff	1.5E+05	7.5E+05	75.0	1.0E-09	1.8

### 6.1.1 Comparison of Lpile and OpenseesPL

Elgamal and Lu (2007) conducted a finite element simulation of a CalTrans 42" CIDH pile using the 3D OpenSeesPL interface. The simulated pile responses were

also compared with LPILE results. The geometric and elastic material properties of the pipe pile are listed below:

Diameter  $D = 42''$  or radius  $a = 21''$

Wall thickness  $h = 0.75''$

Pile length,  $l = 35 \text{ ft}$

Moment of Inertia of Pile  $I = \pi a^3 h = 21,821 \text{ in}^4$

Young's Modulus of Pile  $E_s = 29,000 \text{ ksi}$

In their initial study, the pile was modeled to remain linear (also in view of the applied load levels) and linear and nonlinear soil responses were investigated. The medium relative-density granular soil type (Lu et al. 2006) were selected in the analyses. The material properties of the soil are the reference confinement of 80 kPa (or 11.6 psi), the shear modulus of soil  $G_s$  is 10.88 ksi and the bulk modulus of soil  $B$  is 29 ksi (i.e., Poisson's ratio = 0.33) (Lu et al. 2006). Unit weight of the soil is 110 pcf. For nonlinear analysis, the friction angle  $\phi$  is  $33^\circ$  and the peak shear stress occurs at a shear strain  $\gamma_{max}$  is 10% (at the 11.6 psi confinement). The parameter  $\gamma_{max}$  along with the shear modulus define the nonlinear soil stress-strain curve. A total of six load cases (Table 6.3) were studied and the loads were applied at the pile head.

**Table 6.3:** Load cases for the study

	Pile Head Condition	Shear(kips)	Moment (kip-ft)
Load case 1	Fixed head	64	0
Load case 2	Fixed head	128	0
Load case 3	Fixed head	256	0
Load case 4	Free head	64	0
Load case 5	Free head	128	0
Load case 6	Free head	256	0

In view of symmetry, a half-mesh (2,900 8-node brick elements, 19 beam-column elements and 180 rigid beam-column elements in total) was studied as shown in Figure 6.6. Length of the mesh in the longitudinal direction is 1360 ft, with 680 ft transversally (in this half-mesh configuration, resulting in a 1360 ft x 1360 soil domain in plan view). Layer thickness is 60 ft (the bottom of the soil domain is 25 ft

below the pile tip, so as to mimic the analytical half-space solution). The floating pile was modeled by beam-column elements (Mazzoni et al. 2006), and rigid beam-column elements are used to model the pile size (diameter). The following boundary conditions were enforced: i) The bottom of the domain is fixed in the longitudinal (x), transverse (y), and vertical (z) directions. ii) Left, right and back planes of the mesh are fixed in x and y directions (the lateral directions) and free in z direction. iii) Plane of symmetry is fixed in y direction and free in z and x direction (to model the full-mesh 3D solution). The lateral load was applied at the pile head (ground level) in x (longitudinal) direction.

The above simulations were performed using OpenSeesPL (Lu et al. 2006).

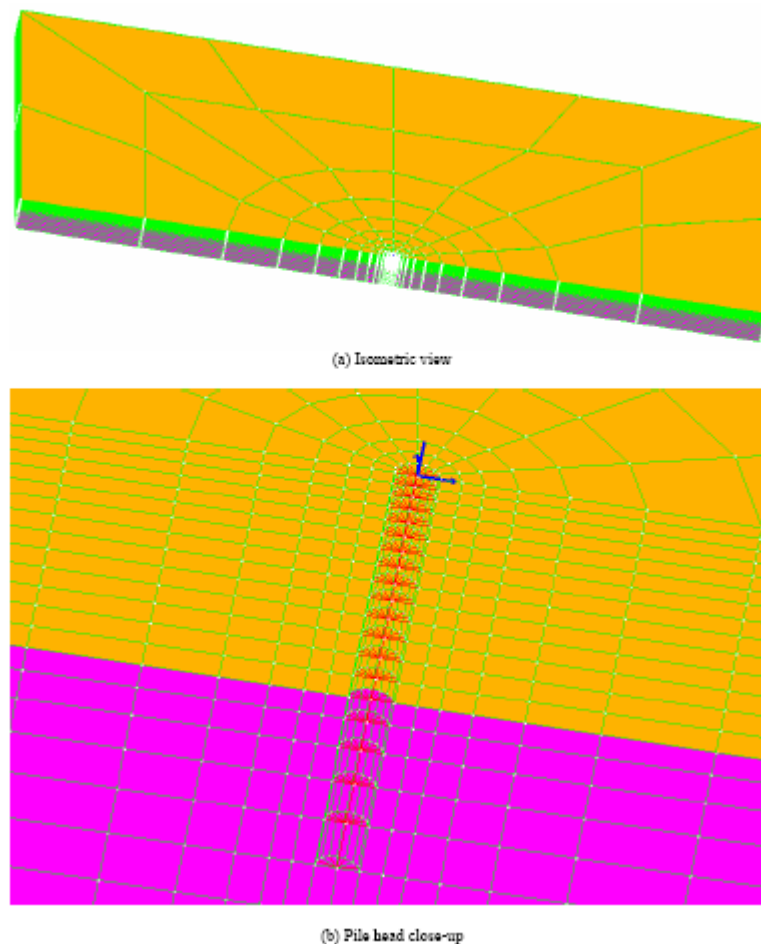


**Figure 6.6 :** Finite element mesh employed in the study by Elgamal and Lu (2007).

Figures 6.7, 6.8 and 6.9 show comparisons of the pile deflection, rotation, bending moment and shear force profiles, respectively, for the fixed-head condition (load

cases 1, 2 and 3), along with LPILE results for comparison. Figures 6.10–6.14 show comparisons of the pile deflection, rotation, bending moment and shear force profiles, respectively, for the free-head condition (load cases 4, 5 and 6), also along with LPILE results for comparison. The stress ratio contour fill of the nonlinear runs for the fixed and free head conditions are displayed in Figures 6.15 and 6.16.

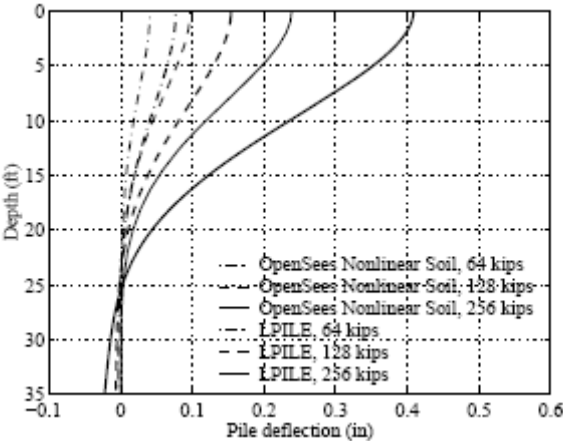


**Figure 6.7 :** Comparison of pile deflection profiles for the fixed-head condition by Elgamal and Lu (2007).

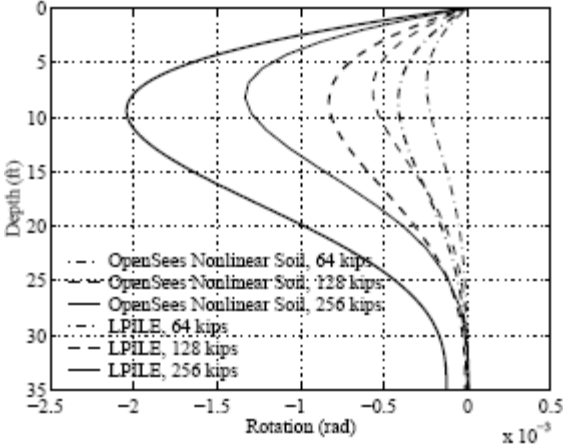


**Figure 6.8:** Comparison of pile rotation profiles for the fixed-head condition by Elgamal and Lu (2007).

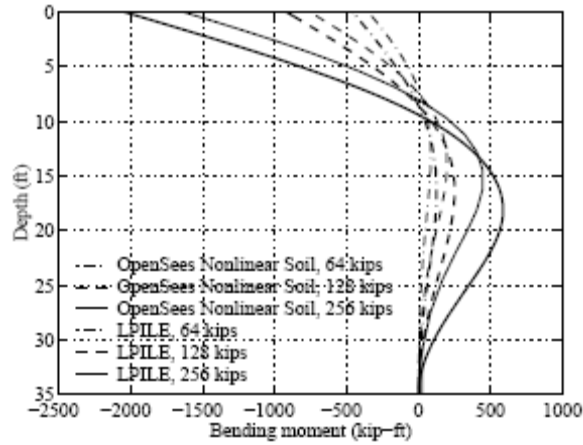


**Figure 6.9 :** Comparison of bending moment profiles for the fixed-head condition by Elgamal and Lu (2007).

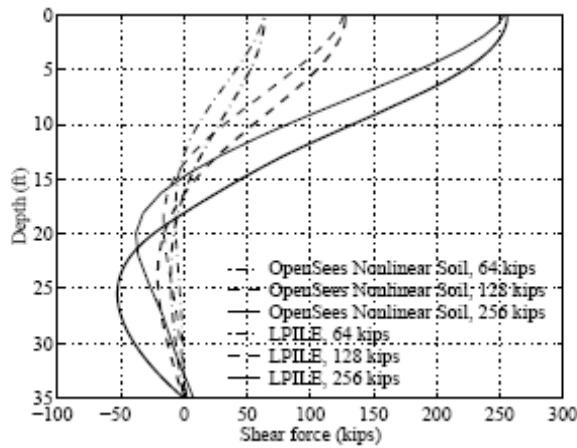


**Figure 6.10:** Comparison of shear force profiles for the fixed-head condition by Elgamal and Lu (2007).

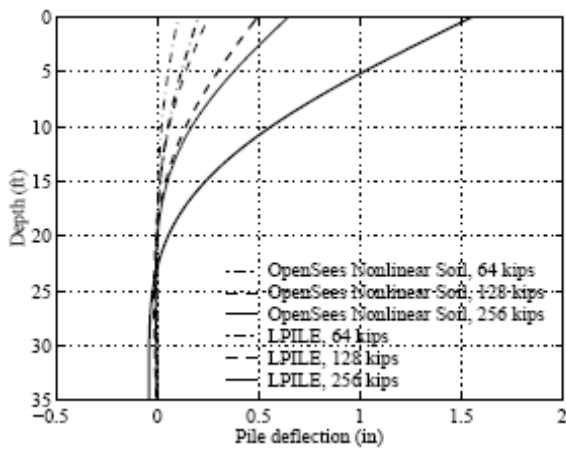


**Figure 6.11:** Comparison of pile deflection profiles for the free-head condition by Elgamal and Lu (2007).

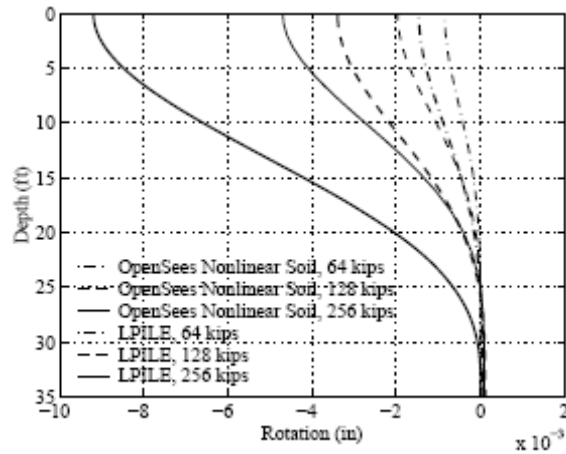


**Figure 6.12:** Comparison of pile rotation profiles for the free-head condition by Elgamal and Lu (2007).

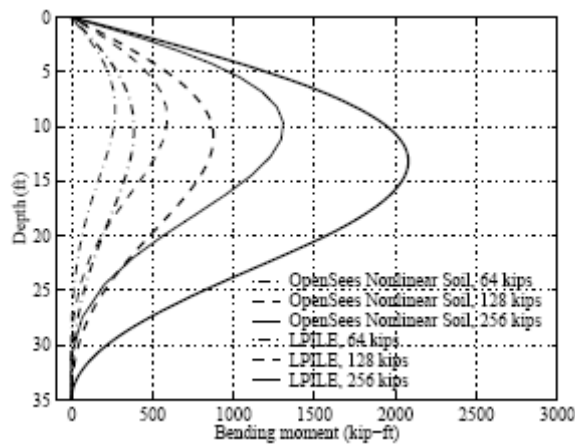


**Figure 6.13:** Comparison of bending moment profiles for the free-head condition by Elgamal and Lu (2007).

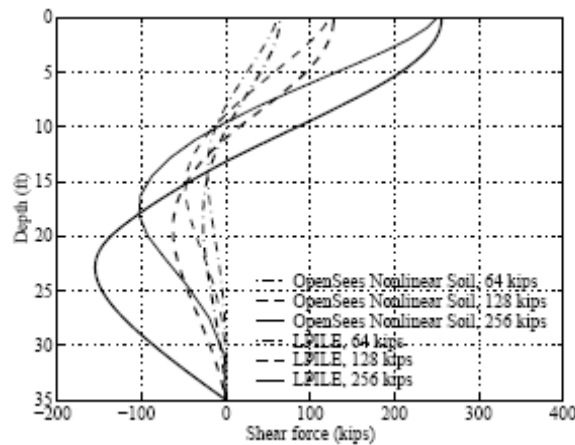


**Figure 6.14:** Comparison of shear force profiles for the free-head condition by Elgamal and Lu (2007).

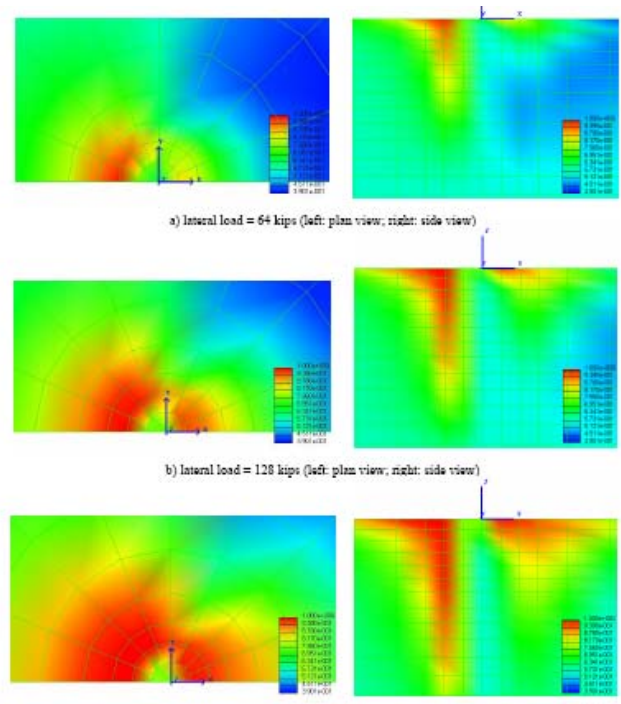


**Figure 6.15 :** Stress ratio contour fill of the nonlinear run for the fixed-head condition (red color shows yielded soil elements) by Elgamal and Lu (2007)..

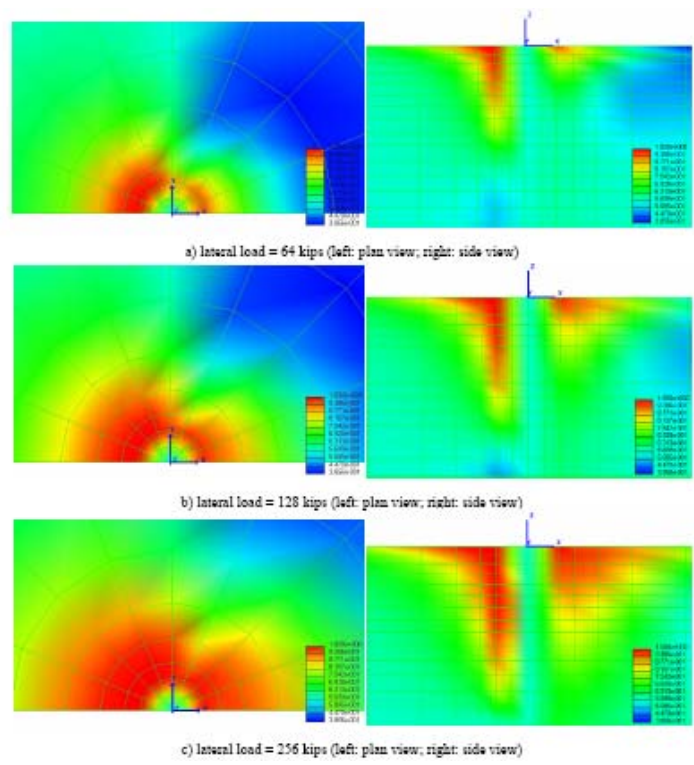


**Figure 6.16:** Stress ratio contour fill of the nonlinear run for the free-head condition (red color shows yielded soil elements) by Elgamal and Lu (2007).

### 6.1.2 EGEGAZ Aliaga Terminal

It was planned to construct a 140000 m<sup>3</sup> capacity tank named “T103” at the EGEGAZ LNG Terminal in Aliaga, Izmir in 2001. Axial and lateral loading tests were conducted on the 120cm diameter bored piles proposed for use in supporting tank T-103 in order to verify the assumed design loads.

The soil investigation done by Ege Jeoteknik Company consisted of four boreholes. two boreholes were drilled during the first exploration investigation in the sea in 1998-1999, boreholes 3/0 to 3/3 were drilled in July 1999 in the sea and boreholes 3/4 to 3/10 were drilled in 2001 after the tank site was filled. The soil profile is as follows:

- o Fill having a thickness of 7.5-9.0m  $N_{30}=8-50$
- o Organic Mud (silt+sand) having a thickness 2.5-4.0m  $N_{30}=1-2$  (before the construction of fill)  $N_{30}=4-16$  (under the fill load)
- o Tuff bedrock having a thickness exceeding 40m (highly fractured tuff layer is weathered near the rockhead down to several meters depth (1.0-3.0m) and interbedded with clay layers. The Core Recovery ratio and RQD values are found to be low.

As the elevations varied between +5.35 and +6.25, bored piles were decided to be constructed. The tuff bedrock elevations at these points are approximately -5.95m.

Pile installation at two test points (Type 1 pile having 120 cm diameters) is completed one month prior to load testing. The works done during the load tests could be grouped into four general sections : Bored pile installation, pile axial compression load tests, pile lateral load tests and pile integrity testing (CHSL). Type 1 pile test pile is located north of the site and next to the tank foundation area. It's drilled with casing down to tuff formation and no groundwater encountered during drilling. The pile is drilled through fill material and completed after pile was socketed 5.2m in tuff.

Lateral pile loading tests were performed on TP1 test piles on 14/08/2002. Two tension piles of 65cm diameter were used as reaction piles during the test. A hydraulic jack of 250 tons capacity is utilized for the test load. Lateral displacements are measured from 3 points from the pile cap in plane of the jack, parallel to the direction of loading, from the sides and the middle. A fourth dial gauge is installed in order to monitor the possible rotations due to the eccentric loading of the adjacent perpendicular sides. The maximum load applied is 80 tons DVL (design verification load). In TP1, the lateral load is applied at the working platform level and displacements are measured.

Lateral load tests at two different locations were performed on previously constructed  $\phi$  120cm diameter piles. The test performed on piles minimum 30 days after the completion of test pile and reaction piles. Lateral load tests were conducted in accordance with ASTM D3966. Reaction was provided by means of two pile of  $\phi$  65 cm diameter. The layout plan, section of piles and the reinforcement calculations for piles are given in Figure 6.6. The maximum load applied was 80 tons DVL. Total test load were applied by means of a hydraulic jack with 250 ton capacity.

Deformations were measured by means of dial gauges with 0.01 mm sensitivity, at three different points from a reference beam. The calibration certificates of dial gauges were done prior to test. The displacement of the pile relative to ground were measured by means of dial gauges to be mounted on a rigid reference beam supported sufficiently away from the test pile, and the average of the measurements considered. In addition, rotation of pile cap was controlled by means of a fourth dial gauge.

Loading was in stages of 12.5% of DVL. At each loading stage readings were taken at 0, 5, 10 and 20 minutes. The waiting time at each loading stage (excluding max. load) was 20 minutes. At the loading stage DVL=80 ton, waiting time was 1 hour and at this stage readings were taken at 0, 5, 15, 25, 45 and 60 minutes. Unloading was performed in stages of 25% of the DVL, and readings were taken at 0, 5 and 10 minutes. At the load stage of 0\*DVL a final reading 30 minutes after the loading stage was reached was made. Loading/waiting stages for lateral loading test is given in Table 6.4 below. General plan view and cross-section are as shown in Fig. 6.17.

Soil profile shown in Fig. 6.18 Total test duration was 5 hours. Test result are shown in Fig. 6.19 and Fig. 6.20.

**Table 6.4:** Lateral Loading Test loading/waiting stages

LOAD	TIME
0.125 DVL (10 t)	20 minutes
0.250 DVL (20 t)	20 minutes
0.375 DVL (30 t)	20 minutes
0.500 DVL (40 t)	20 minutes
0.625 DVL (50 t)	20 minutes
0.750 DVL (60 t)	20 minutes
0.850 DVL (68 t)	20 minutes
0.900 DVL (72 t)	20 minutes
0.950 DVL (76 t)	20 minutes
1.000 DVL (80 t)	1 hour
0.750 DVL (60 t)	10 minutes
0.500 DVL (40 t)	10 minutes
0.250 DVL (20 t)	10 minutes
0.000 DVL (0)	30 minutes

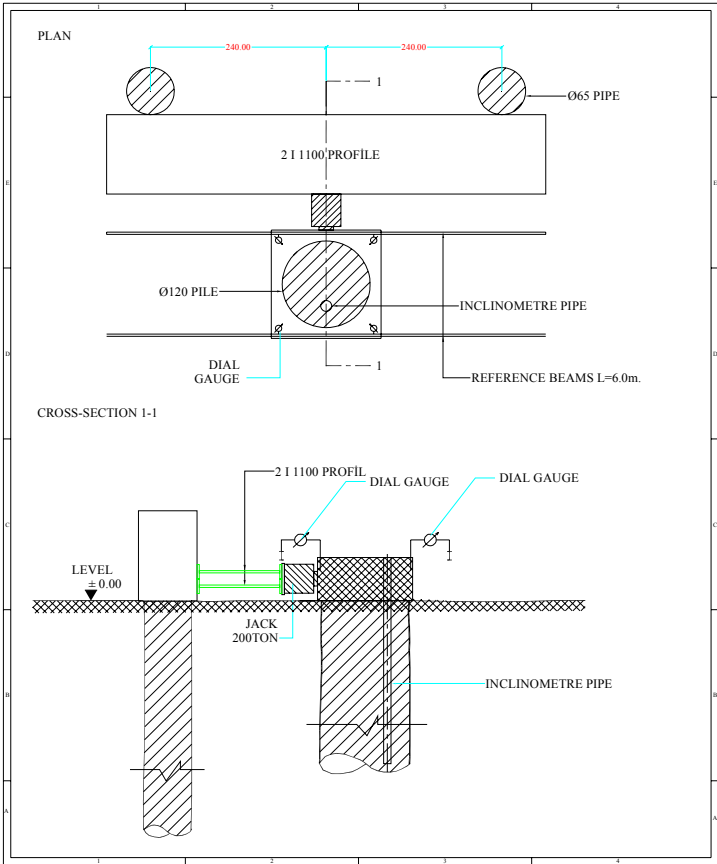
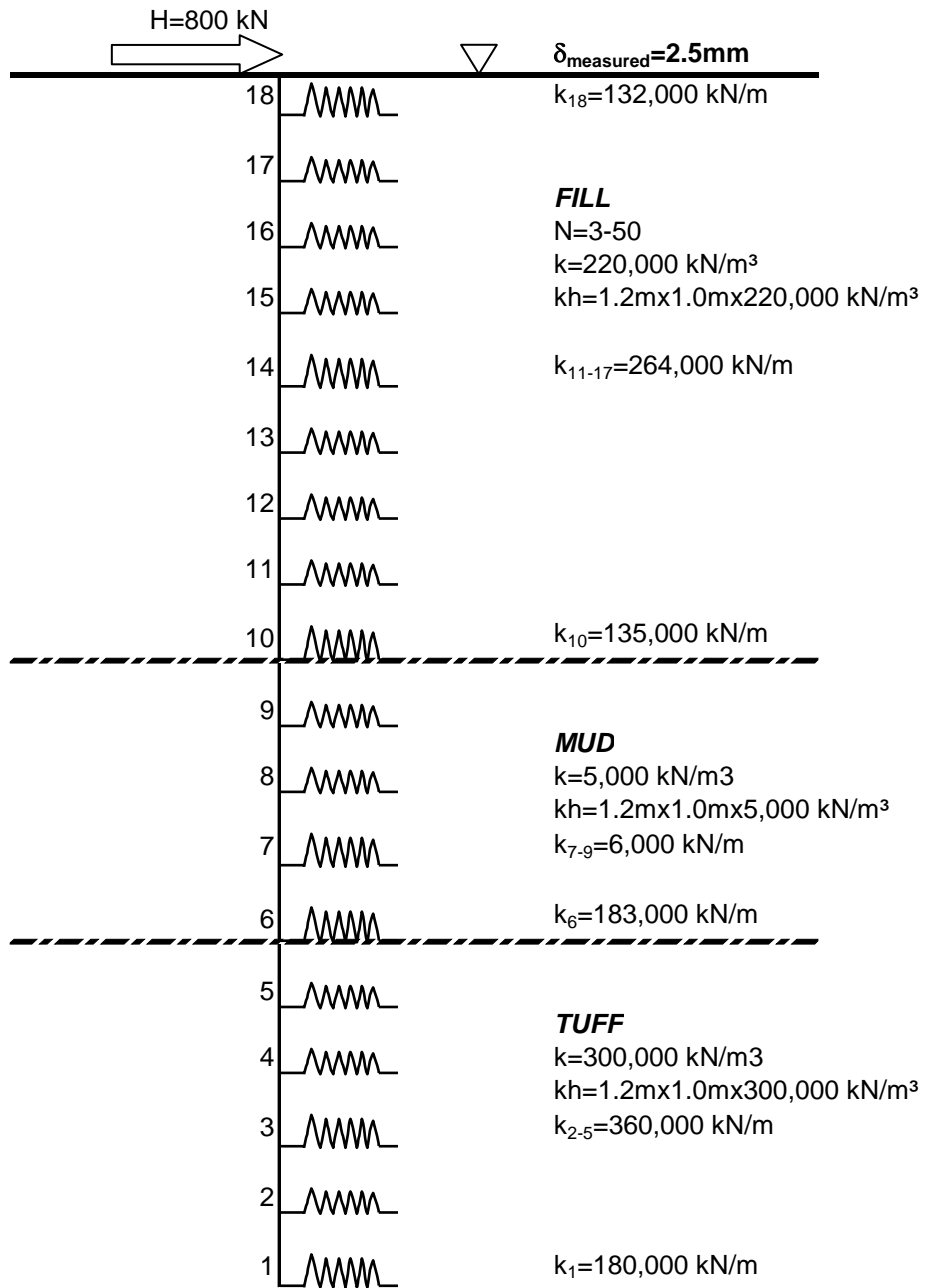


**Figure 6.17:** TP1 pile plan view and cross-section

# TP1



BS30  
 $E_s=31,800,0000 \text{ kN/m}^2$

**Figure 6.18:** TP1 Aliaga soil profile

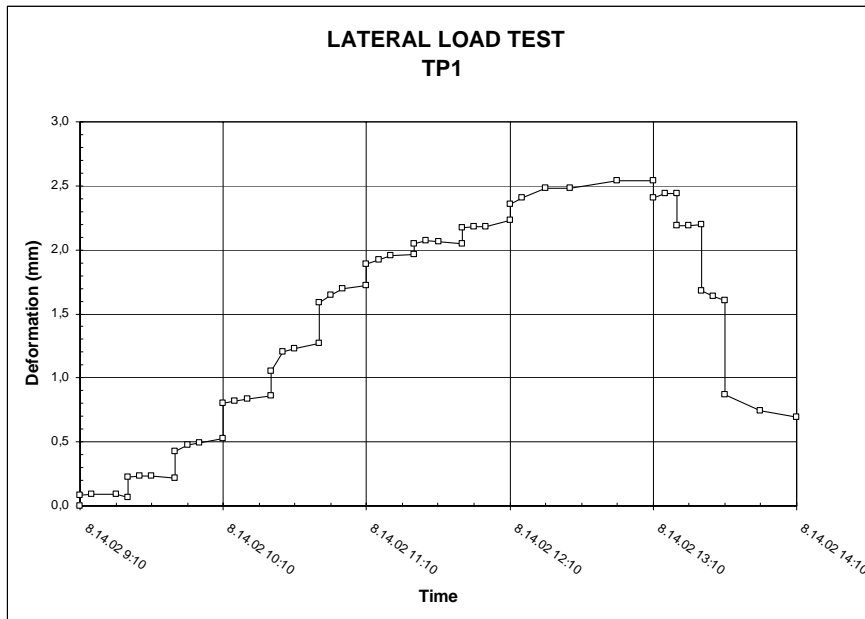


**Figure 6.19:** Time- Deformation test graph

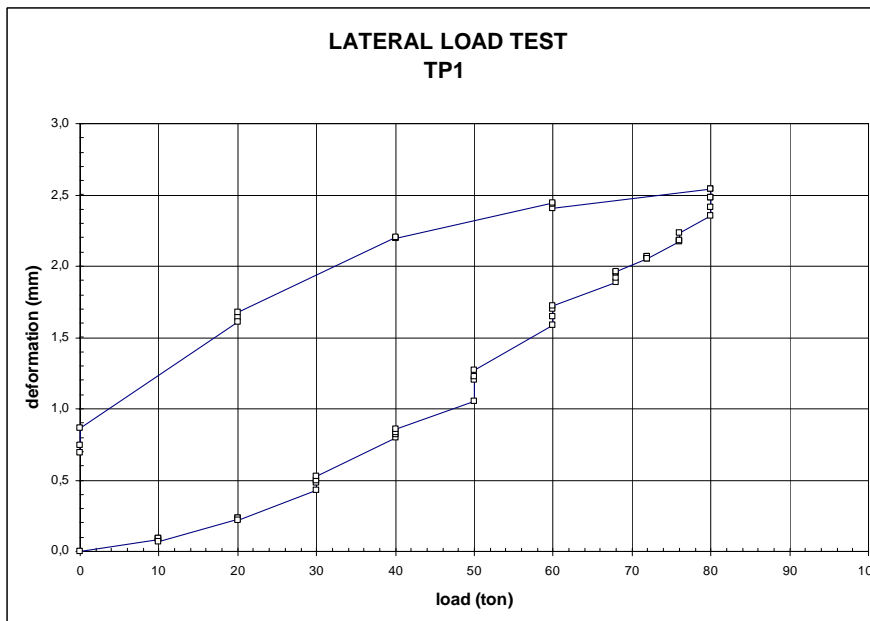


**Figure 6.20:** TP1 Load-Deformation test graph

### 6.1.3 OpenseesPL result

In this section, behaviour of lateral loading of a single pile in different soils will be investigated using Openseespl program. The most important issue is to model the problem correctly. Therefore, attention should be paid in each step of the model. Each parameter should be considered carefully. However, it is difficult to model both

the loading 3 step and correct parameter together. In the Openseespl program, most attention is given to the types of elements used and soil properties.

In this work, the effect of the length of the pile on its behaviour wanted to be researched. Especially, the program is sensitive to changes in the length and soil types. Therefore, the effects of lateral loading on a single pile in different soils and with different length were investigated.

In the analysis cohesionless soils dense or loose and clayey soils soft and stiff were used. The soil parameters used are given in Table 6.2.

In evaluating the results of the lateral loading test, a ground model is formed; giving the measured lateral displacement value at the top of the pile, a possible soil profile at each layer is achieved by computer analyses. At this model lateral loading is applied and lateral displacement is computed at the top. By trial and error method, the computed displacement and measured displacement is made similar and recommended for each layer within the statement. It is possible to determine moments, shear forces and lateral displacements, using these program values by means of similar calculations for different depth or piles under different loading conditions.

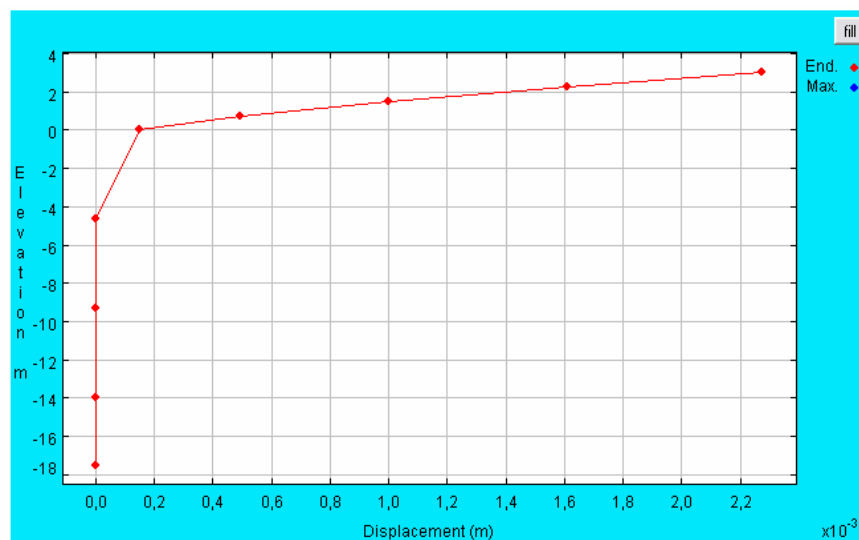


**Figure 6.21:** Aliaga pile displacement result with openseespl program

A real field data obtained from the lateral loading test of a pile in Aliaga was used to validate the program used. In Figure 6.21., the displacement of the pile found by Openseespl programs is shown. The displacement calculated is 2.25 mm and the measured one is 2.5 mm. The results are close and the openseespl program can be used to calculate the pile displacements. Sandy and clayey soils parameters are given in Table 6.1 and 6.2. are used in the analysis done.

**6.1.3.1 Cohesionless soils analysis**

In the analysis of Openseespl program loose and dense sands were examined. The effect pile length was investigated in the cases of loose and dense sand soil layers. In this research with OpenseesPL program only the effect of changing the length of the pile and the soil parameters were investigated. Pile lengths were chosen as 20.5 m, 15 m, 10 m and 6m. The results will be compared with each other to see these effects. The results of Aliaga case history was compared with the results obtained for this case history with the result obtained from Openseespl program.

The results for the various pile lengths of the pile in loose sands are shown in Figures 6.22, 6.23, 6.24 and 6.25. Under 80 ton lateral loading, the pile displacement observed at the pile head is 2.79mm for 20.5m long pile as seen in Figure 6.22. In Fig. 6.23 the 15m pile displacement seen is 2.81mm. 10m pile displacement is calculated 3.25 mm as shown in Fig. 6.24. Also the pile displacement calculated for the 6m pile is 3.4 mm shown in Fig. 6.25. It is observed that as the pile length decreases, the pile displacement increases.

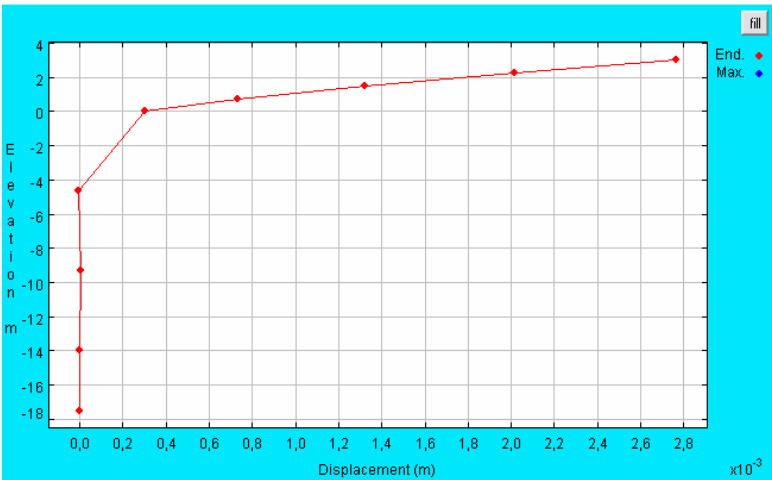


**Figure 6.22:** Loose sandy soils L: 20.5m Openseespl result

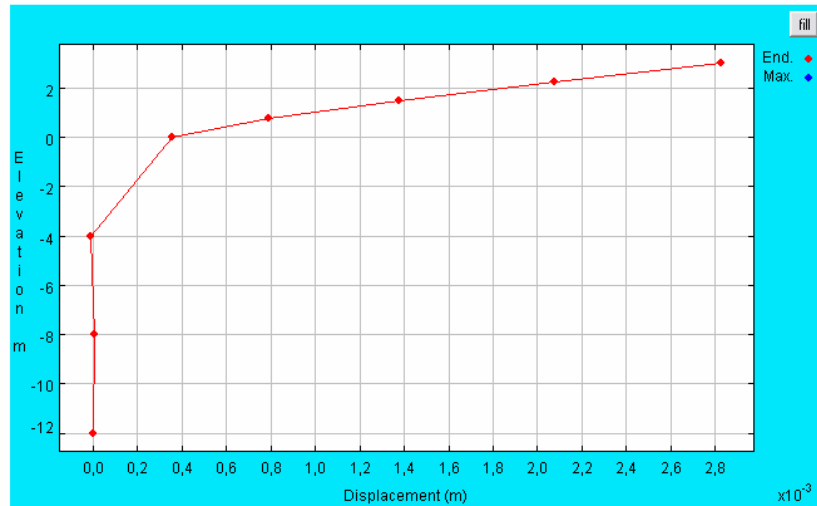


**Figure 6.23:** Loose sandy soils L: 15m Openseespl result

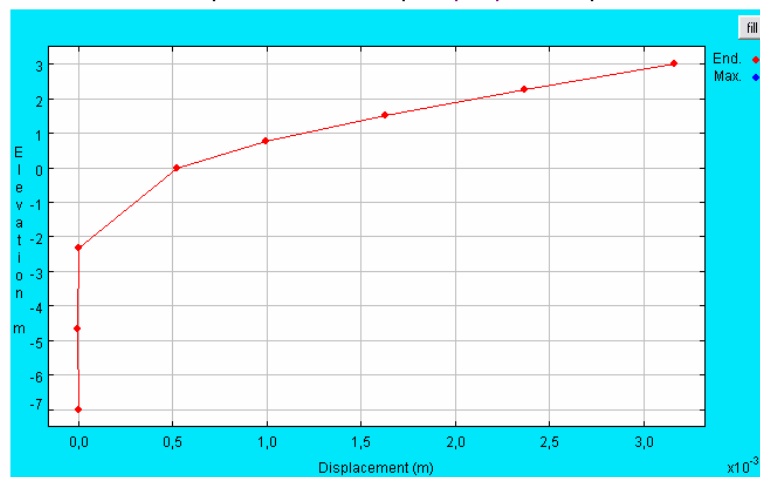


**Figure 6.24:** Loose sandy soils L: 10m Openseespl result

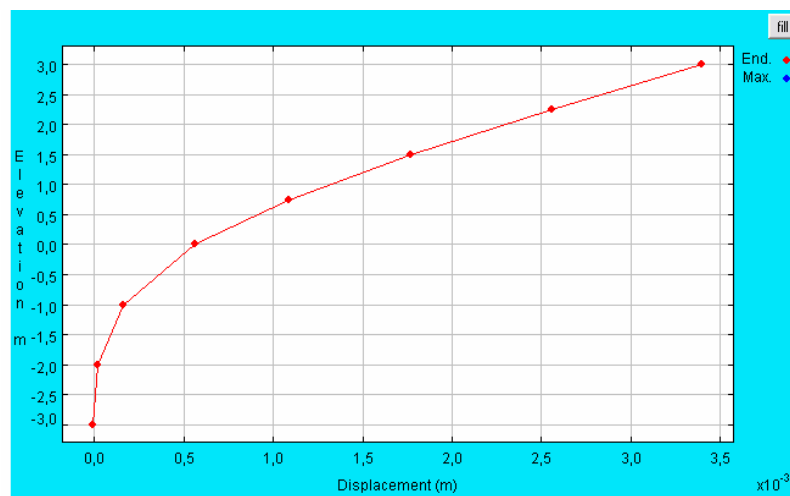


**Figure 6.25:** Loose sandy soils L: 6m Openseespl result

The results for the various pile lengths of the pile in dense sands are shown in Figures 6.26, 6.27, 6.28 and 6.29. Under 80 ton lateral loading, the pile displacement observed at the pile head is 2.23 mm for 20.5 m long pile as seen in Figure 6.26. In Fig.6.27 the 15 m pile displacement is 2.22 mm. 10 m pile displacement is calculated 2.25 mm as shown in Fig. 6.28. Also the pile displacement calculated for the 6m pile is 2.7 mm as seen in Fig. 6.29. It is observed that as the pile length decreases, the pile displacement increases.

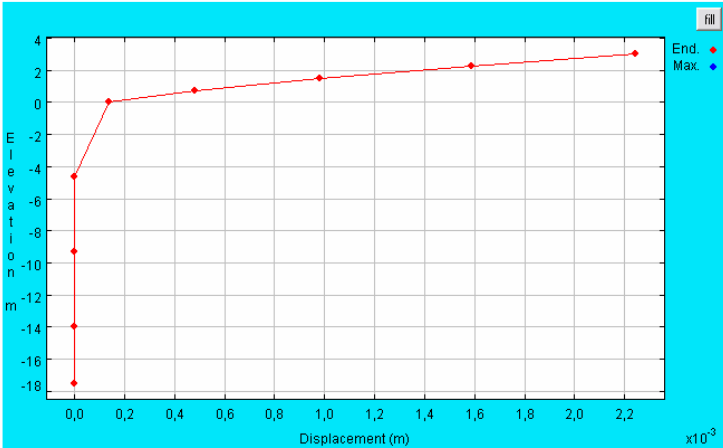


**Figure 6.26:** Dense sandy soils L: 20.5m Openseespl result

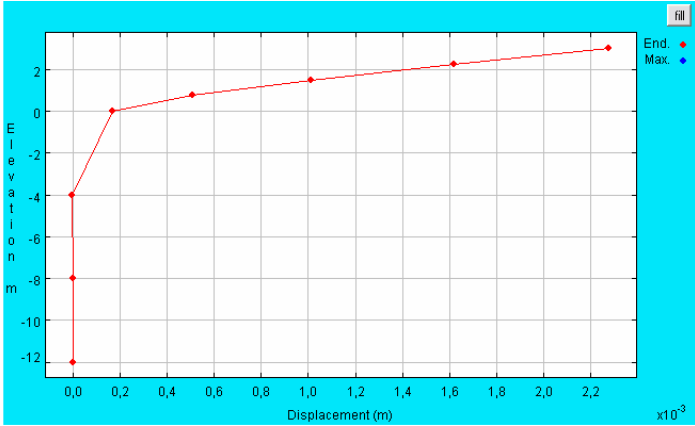


**Figure 6.27:** Dense sandy soils L: 15m Openseespl result

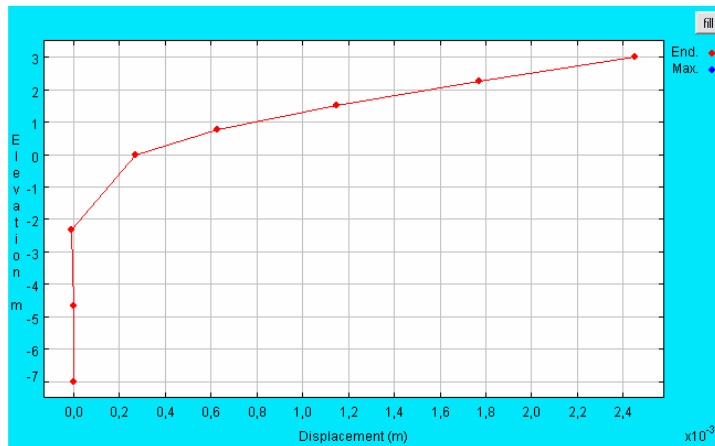


**Figure 6.28:** Dense sandy soils L: 10m Openseespl result

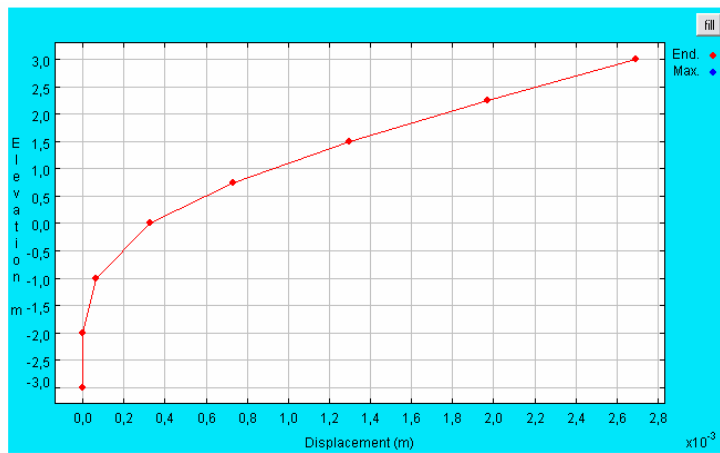


**Figure 6.29:** Dense sandy soils L: 6m Openseespl result

### 6.1.3.2 Analysis of piles in clayey soils

In the analysis of Openseespl program soft and stiff clays were examined. The effect of pile length was investigated in the cases of soft and stiff clay soil layers. In this research with OpenseesPL program only the effect of changing the length of the pile and the soil parameters were investigated. Pile lengths were chosen as 20.5 m, 15 m, 10 m, and 6m. The results will be compared with each other to see these effects.

The results for the various pile lengths of the pile in soft clay are shown in Figures 6.30, 6.31, 6.32 and 6.33. Under 80 ton lateral loading, the pile displacement observed at the pile head is 2.23 mm for 20.5 m long pile as seen in Figure 6.30. In Fig. 6.31, the 15 m pile displacement is seen 2.22 mm. 10 m pile displacement calculated is 2.25 mm as shown Fig. 6.32. Also the pile displacement calculated for

the 6m pile is 2.7 mm shown in Fig. 6.33. It is seen that as the pile length decreases, the displacement increases.

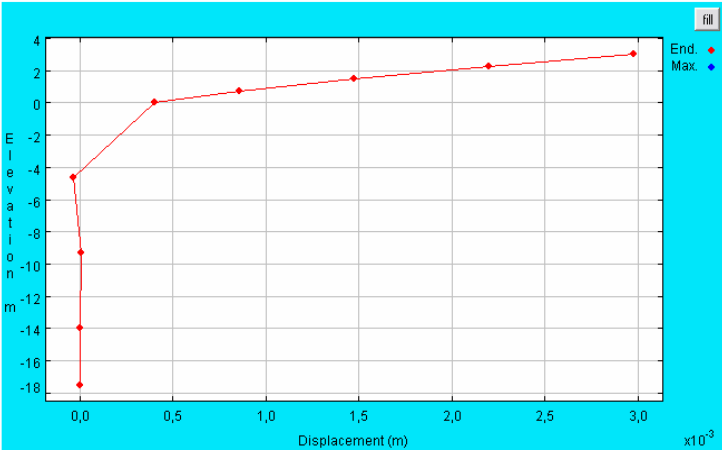


Figure 6.30: Soft clay soils L: 20.5m Openseespl result

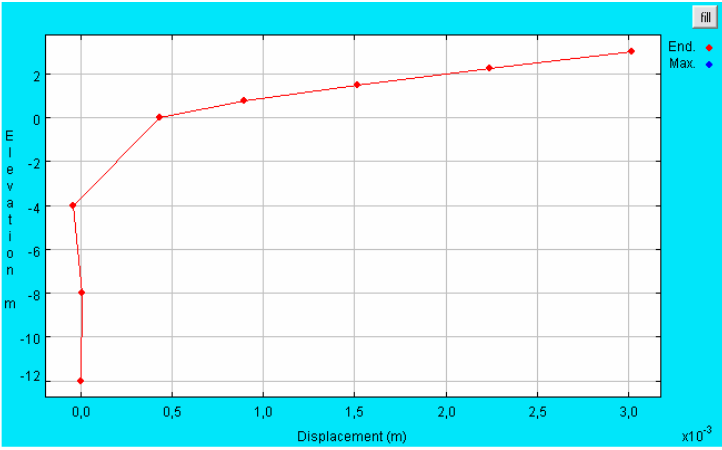


Figure 6.31: Soft clay soils L: 15m Openseespl result

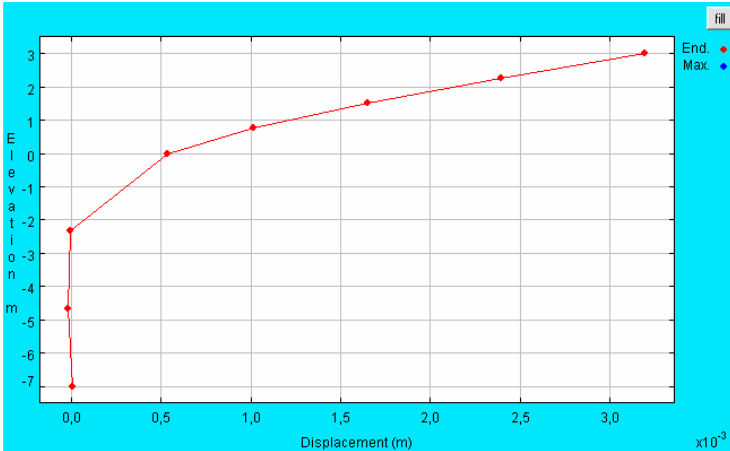
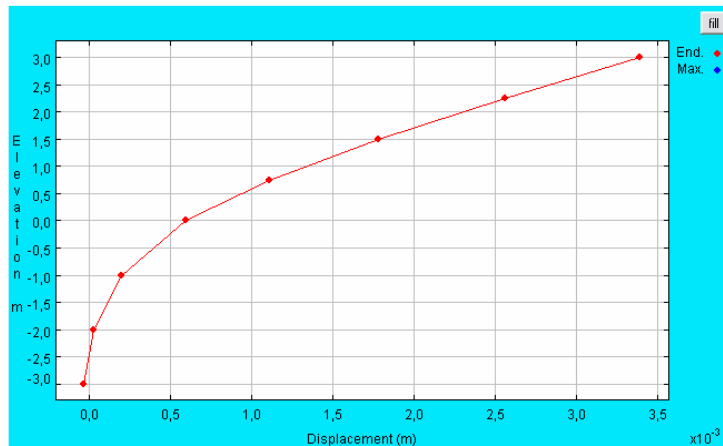
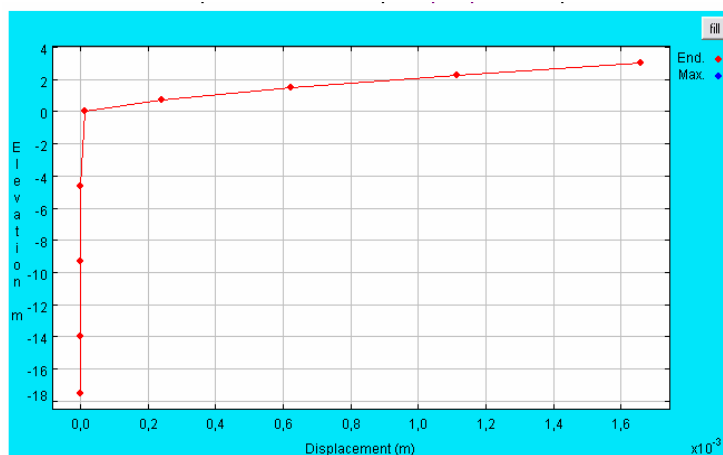


Figure 6.32: Soft clay soils L: 10m Openseespl result



**Figure 6.33:** Soft clay soils L: 6m Openseespl result

The results for the various pile lengths of the pile in stiff clay are shown in Figures 6.34, 6.35, 6.36 and 6.37. Under 80 ton lateral loading, the pile displacement observed at the pile head is 2.23 mm for 20.5 m long pile as seen in Figure 6.34. In Fig.6.35 the 15 m pile displacement seen is 2.22 mm. 10m pile displacement calculated is 2.25 mm as shown in Fig. 6.36. Also the pile displacement calculated for the 6m pile displacement is 2.7 mm as shown in Fig. 6.37. It is seen that as the pile length decreases, the displacement increases.



**Figure 6.34:** Stiff clay soils L: 20.5m Openseespl result

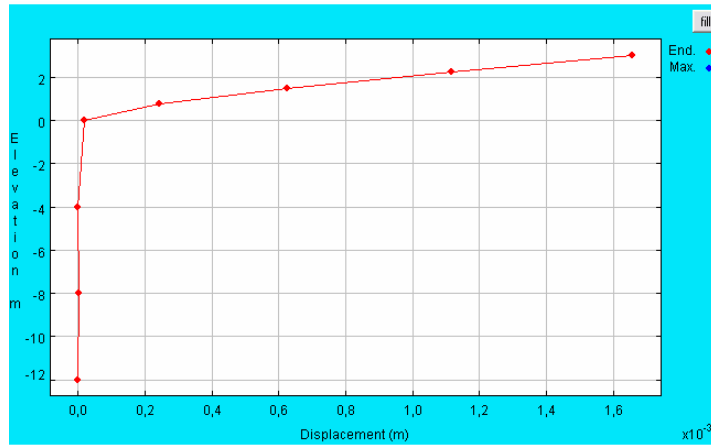


**Figure 6.35:** Stiff clay soils L: 15m Openseespl result

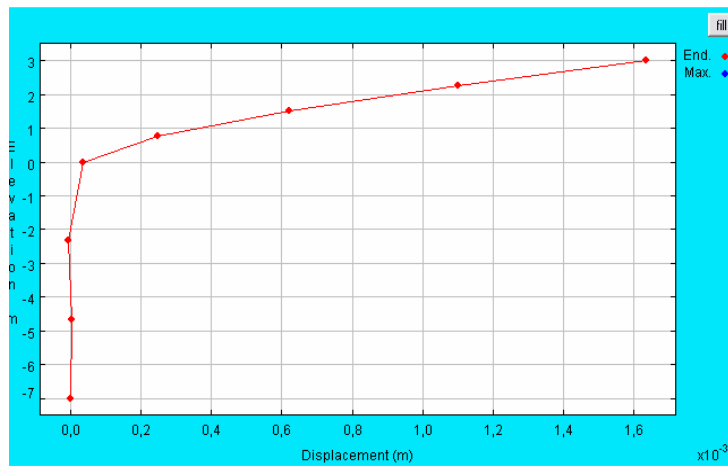


**Figure 6.36:** Stiff clay soils L: 10m Openseespl result

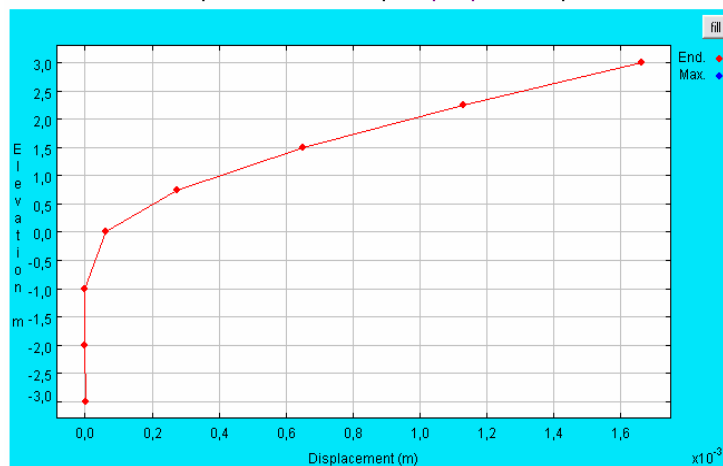


**Figure 6.37:** Stiff clay soils L: 10m Openseespl result

## 7. CONCLUSION

The aim of this study is to analyse laterally loading deformation of piles due to loaded piles deformation in different soils. It is very difficult to analyse piles in lateral spreading fields. The example pile which was lateral loaded single piles has been analysed for the case history in Aliaga, Izmir.

A real field data obtained from the lateral loading test of a pile in Aliaga was used to validate the program used. The displacement calculated by Openseespl program is 2.25mm and the measured one is 2.5mm. The results are close and the Openseespl program can be used to calculate the pile displacements. Although results obtained from the program are realistic, they have to be controlled by a lateral loading test.

With openseespl program lateral displacement of a single pile in sandy and clayey soil layers were analysed and the lateral displacement results are shown in Tables 7.1 and 7.2. In all types of soils, as the pile length decreases, the pile displacement increases. This could be due to the length of the pile resistance in soils. Long piles have more advantages than shorth piles. Therefore, pile must be socketted to stiffer or denser soil structures.

In the application of lateral loading onto piles, as the geological loads increases, the load on the pile increases with depth. Hence, shear force developed along the pile and internal friction angle of soil increases. The load that the piles would transfer to the soil increases. In this study, influence of increment of pile length, perimeter area and friction was investigated. It was observed that as the length of pile increased, the friction force per unit area has decreased which reduces the load on a pile. In long piles, displacements are less than the shorter piles due to the frictional forces around the piles. In a laterally loaded pile, the load transfer from the pile to the soil is easier with frictional forces. As the frictional forces increases, the pile movement decreases especially in long piles. In different soil conditions, the friction between granulars change. For example, in loose sand, the pile displacement calculated is 2.79mm, in

soft clay it has increased to 3mm. From the results, it was observed that as the pile length increased, the movement, displacement and the rotation of the pile has decreased.

**Table 7.1:** Sandy soils deflection results

Pile length (m)	Pile displacement (mm)	
	Sand	
	Loose	Dense
20.50	2.79	2.23
15.00	2.23	2.24
10.00	3.25	2.50
6.00	3.45	2.70

Lateral displacement in soils in clayey soils results are shown in Table 7.2

**Table 7.2:** Clayey soils deflection results

Pile length (m)	Pile displacement (mm)	
	Clay	
	Soft	Stiff
20.5	3.00	1.70
15.00	3.01	1.71
10.00	3.25	1.72
6.00	3.40	1.73

Tables 7.3 and 7.4 show the pile rotation at the pile head in 4 different soil type and 4 different pile length obtained from the analysis. In all type of soils as the pile length decreases, the pile rotation increases.

**Table 7.3:** Sandy soils rotation results from Openseespl program

Pile length (m)	Pile rotation * 10 <sup>-3</sup>	
	Sand	
	Loose	Dense
20,50	1,01	0.89
15.00	1,01	0.89
10.00	1,06	0.91
6.00	1,40	0.99

**Table 7.4:** Clayey soils rotation results from Openseespl program

<b>Pile length (m)</b>	<b>Pile rotation * 10<sup>-3</sup></b>	
	<b>Clay</b>	
	<b>Soft</b>	<b>Stiff</b>
<b>20,50</b>	1,05	0.74
<b>15.00</b>	1,05	0.74
<b>10.00</b>	1,07	0.72
<b>6.00</b>	1,20	0.72

Group analysis has to be done and considered when designing as the soil-pile interaction can affect the behaviour of the structure during earthquakes and could dominate its behaviour. In this study, group analysis was not considered as the available program only solved a single pile and the available field data was on one pile as well.



## REFERENCES

- Abrahart, R. J., and See, L., 1998:** Neural Network vs. ARMA Modelling: Constructing Benchmark Case Studies of River Flow Prediction. In GeoComputation '98. Proceedings of the Third International Conference on GeoComputation, University of Bristol, United Kingdom, 17–19 September (CD-ROM).
- Artak D. Mirzoyan, 2007:** Lateral Resistance of Piles at the Crest of Slopes in Sand.
- Ahmed Elgamal, Liangcai He, Jinchi Lu, Akio Abe, Tarek Abdoun, Ricardo Dobry, Masayoshi Sato, Kohji Tokimatsu, and Thomas Shantz, 2006:** Liquefaction-Induced Lateral Load On Piles.
- Ahmed Elgamal and Jinchi Lu , 2007:** Finite Element Analysis of Caltrans 42" Cidh Pile Using Opensees For General Comparison With Lpile (With Default p-y Multiplier = 1.0)
- Bhattacharya S. and Bolton M., 2004:** Errors in design Leading To Pile Failures During Seismic Liquefaction”, Proc. Fifth International Conference on Case Histories in Geotechnical Engineering, New York, NY, April 13-17,2004,Paper No. 12A-12.
- B. Ghosh, S.P.G. Madabhushi, 2004:** Centrifuge Modelling of Dynamic Soil Structure Interaction In Layered and Inhomogeneous Liquefiable Soil, 2004. paper no: 12A-13-ghosh
- D. A. Brown, Auburn University Auburn, AL, M. W. O'Neill University of Houston Houston, TX, M. Hoit, M. Mcvay University of Florida Gainesville, FL, M. H. El Nagggar University of Western Ontario Ontario, Canada and S. Chakraborty Auburn University Auburn, Al, 2001:** Static and Dynamic Lateral Loading of Pile Groups. National Cooperative Highway Reserch Program.
- D. W. Wilson, 1999:** Soil-Pile-Superstructure Interaction In Liquefying Sand and Soft Clay. Research supported by the California Department of Transportation under Contract Number 65V495. The contents of this report reflect the views of the author who is responsible for the facts and the accuracy of the data presented herein. The contents do not necessarily reflect the official views or policies of the STATE OF CALIFORNIA or the FEDERAL HIGHWAY ADMINISTRATION. This report does not constitute a standard, specification, or regulation.
- D. Ghosh Roy, M.F. Bransby and G.J. Yun Division of Civil Engineering, University of Dundee Dundee, UK. , 2004:** Centrifuge investigation of the lateral response of pile groups in sand.

- Frank McKenna University of California, Berkeley, 2009:** OpenSees Dynamic API.
- J. Matthew Walsh, 2005:** Full-Scale Lateral Load Test of A 3x5 Pile Group In Sand.
- Kyle M. Rollins, Steven R. Johnson Civil, Environmental Engineering, Brigham Young University Provo, Utah, USA Kris T. Petersen Region, Utah Dept. of Transportation Salt Lake City, Utah, USA Thomas J. Weaver Civil Engineering Dept., University of Idaho Moscow, Idaho, USA, 2003 :** Static and Dynamic Lateral Load Behavior of Pile Groups Based on Full-Scale Testing.Proceedings of The Thirteenth (2003) International Off shore and Polar Engineering Conference Honolulu, Hawaii,USA.
- Lianyang Zhang, Francisco Silva and Ralph Grismala, 2005:** Analysis of Pile Foundations under Seismic Loading, Jayram Ramachandran, CBE Institute 2005: Final Report
- Miguel A. Pando, Carl D. Ealy, George M. Filz, J.J. Lesko, and E.J. Hoppe, 2006:** FHWA-HRT-04-043
- Mohammed A. Gabr, P.E Roy H. Borden, P.E. ,Kook Hwan Cho, Shane Clark, Joseph B. Nixon, 2002:** P-y Curves for Laterally Loaded Drilled Shafts Embedded in Weathered Rock, 2002
- Priyanshu Singh, Scott J. Brandenburg, Ross W. Boulanger, Bruce L. Kutter, ASCE/AEG/UMKC Geotechnical Conference April 6, 2002 University Center, Pierson Auditorium University of Missouri at Kansas City:** Behavior of Pile Foundations in Liquefied and Laterally Spreading Ground.**Poulos H.G, Davis, E.H, 1980:** Series in geotechnical Engineering, Pile Foundation Analysis And Design,
- Reed L. Mosher and William P. Dawkins, 2000:** Theoretical Manual for Pile Foundations November 2000
- Reese LC, Impe WFV, 2001:** Single Piles and Pile Groups Under Lateral Loading (pg. 7-9) (U.S. Department of Transportation – Analyses of the lateral load tests at the Route 351 Bridge)
- Scott J. Brandenburg, R W. Boulanger, Bruce L. Kutter, Dongdong Chang, 2005:** Behavior of Pile Foundations in Laterally Spreading Ground during Centrifuge Tests.
- S.K. Haigh, S.P.G. Madabhushi University of Cambridge, UK,** Centrifuge Modelling of Lateral Spreading Past Pile Foundations.
- Scott J. Brandenburg, Ross W. Boulanger, Bruce L. Kutter, Dan W. Wilson, Dongdong Chang, 2004:** Load Transfer Between Pile Groups and Laterally Spreading Ground During Earthquakes
- Shamsher Prakash, Vijay K. Puri, 2003:** Liquefaction of Silts and Silt-Clay Mixture.

**Subhamoy Bhattacharya, S.P.G.Madabhushi and Malcolm Bolton Cambridge Geotechnical Research Group, University of Cambridge (U.K), 2003:** Pile Instability during Earthquake Liquefaction. ASCE Engineering Mechanics Conference (EM2003), Seattle, 16-18th July, 2003.

**Shamsher Prakash and Hari D. Sharma,1990:** Pile Foundations In Engineering Practice.

**Timber Pile Design and Construction Manual,2002:** Timber Piling Council American Wood Preservers Institute, James G. Collin, PH.D., P.E. The Collin Group, Ltd.

**Url-1**[http://www.th.gov.bc.ca/WilliamRBennettBridge/photo\\_galleries/Graving\\_Dock/2006/March11-24\\_06/032406-2.jpg](http://www.th.gov.bc.ca/WilliamRBennettBridge/photo_galleries/Graving_Dock/2006/March11-24_06/032406-2.jpg) (24.01.2009).

**Url-2** <http://www.conklinsteel.com/Images/pilepoint1.gif> (24.01.2009).



## **APPENDICES**

### **APPENDIX A.1 : Openseespl results grafic**

APPENDIX A.1

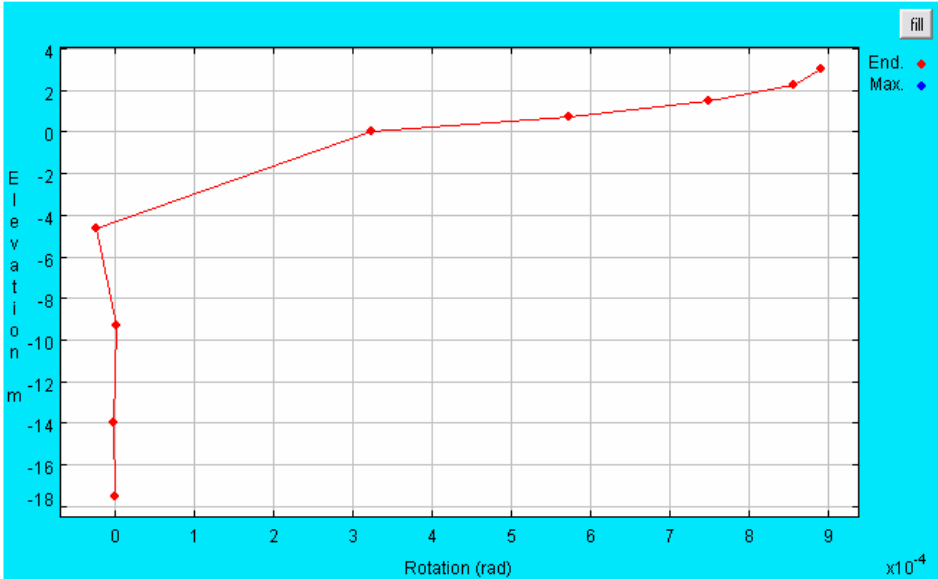


Figure A. 1: Rotation of the pile in the soil Aliaga

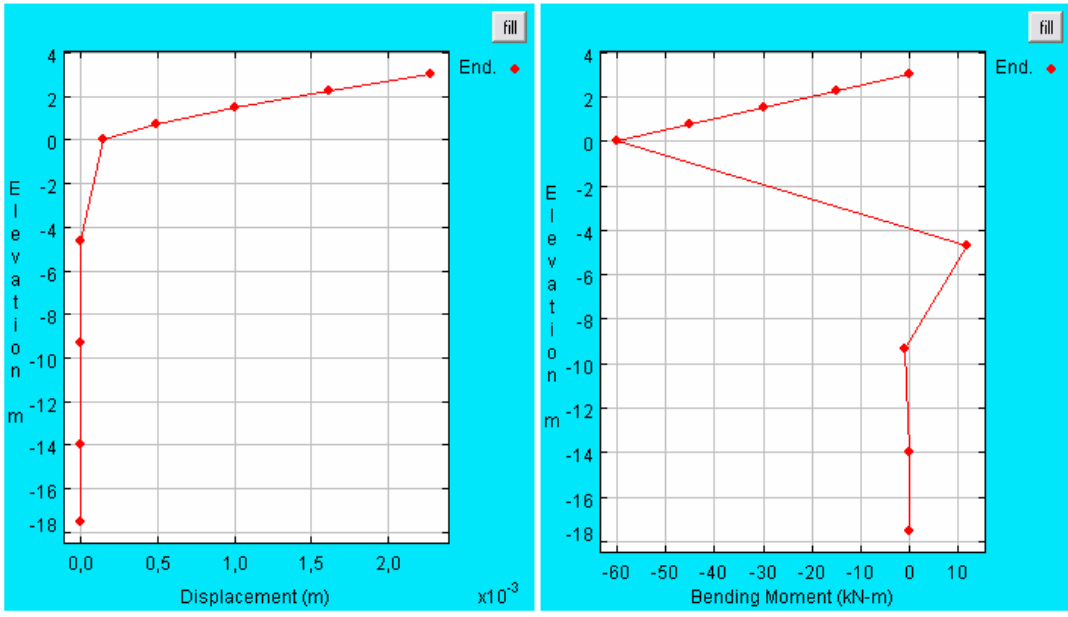
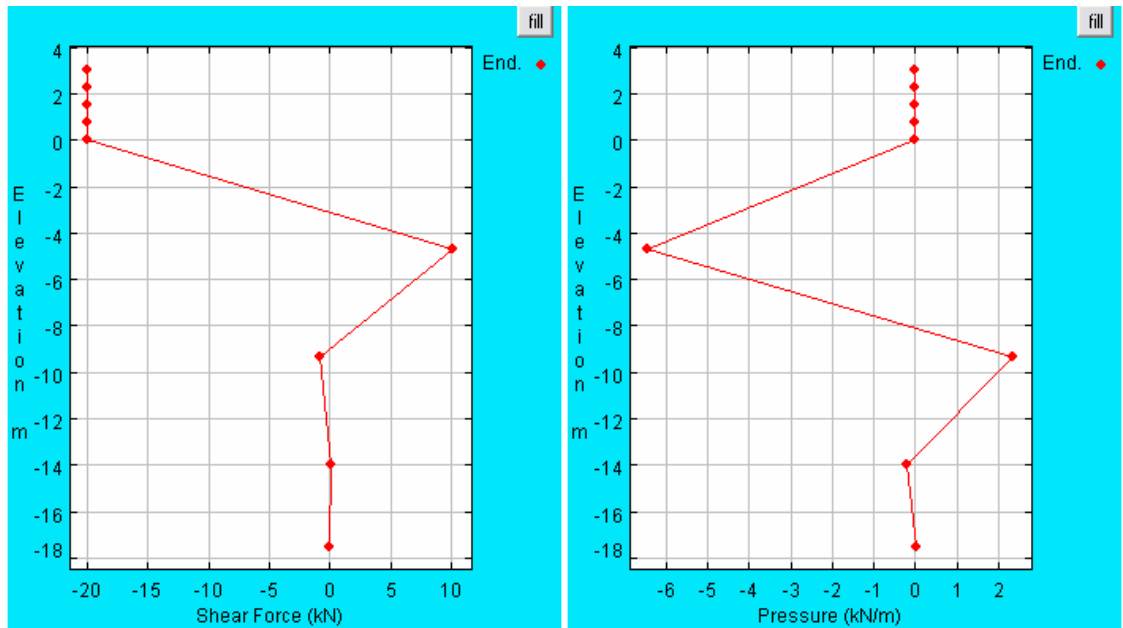
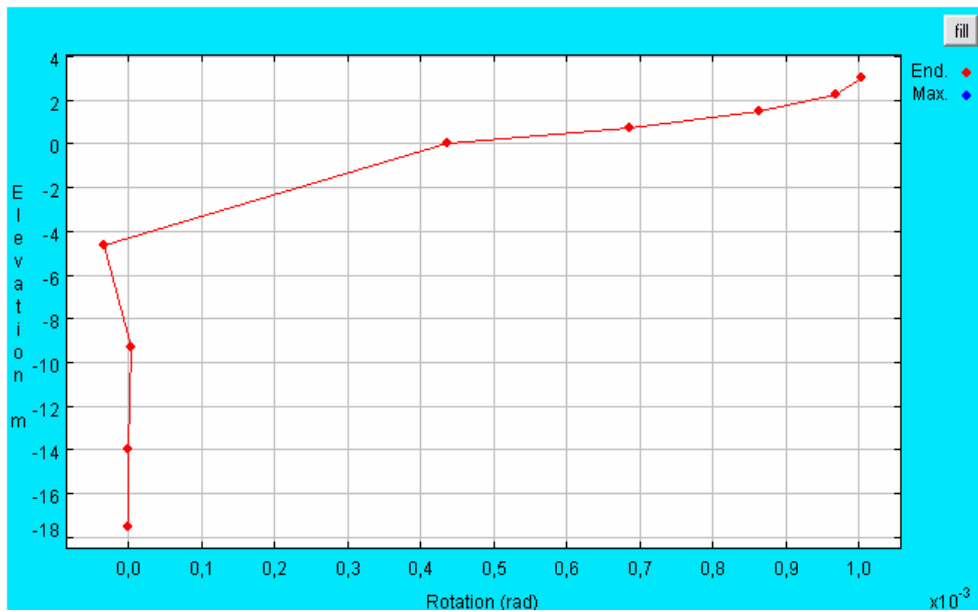


Figure A. 2 : a) Displacement of the pile in the soil Aliaga, b) Bending Moment of the pile in the soil Aliaga



**Figure A. 3 :** a) Shear force of the pile in the soil Aliaga, b) Pressure of the pile in the soil Aliaga



**Figure A. 4 :** Rotation of the 20.5 m pile in loose sandy soil.

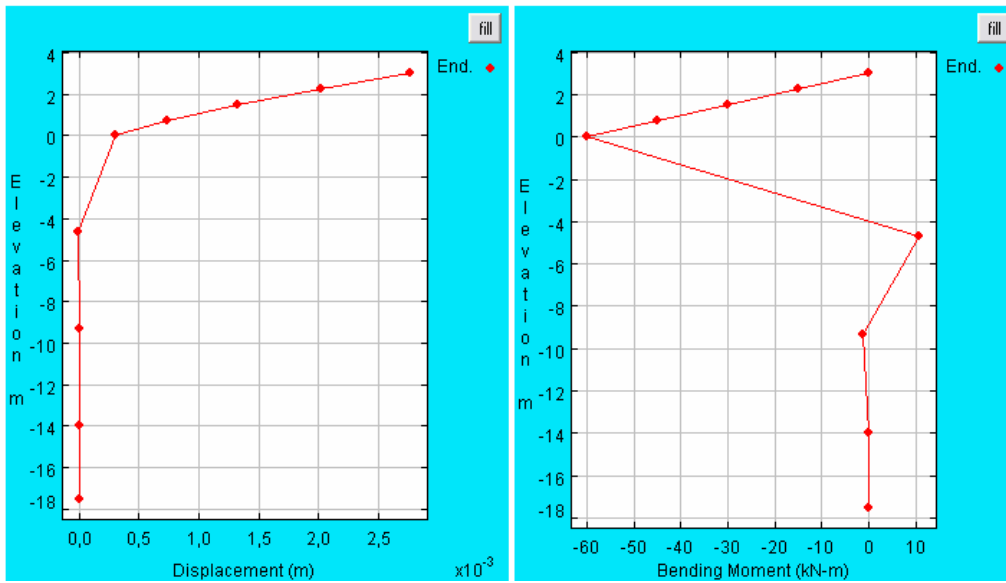


**Figure A. 5 :** a) Displacement of the 20.5 m pile in loose sandy soil., b) Bending moment of the 20.5 m pile in loose sandy soil.

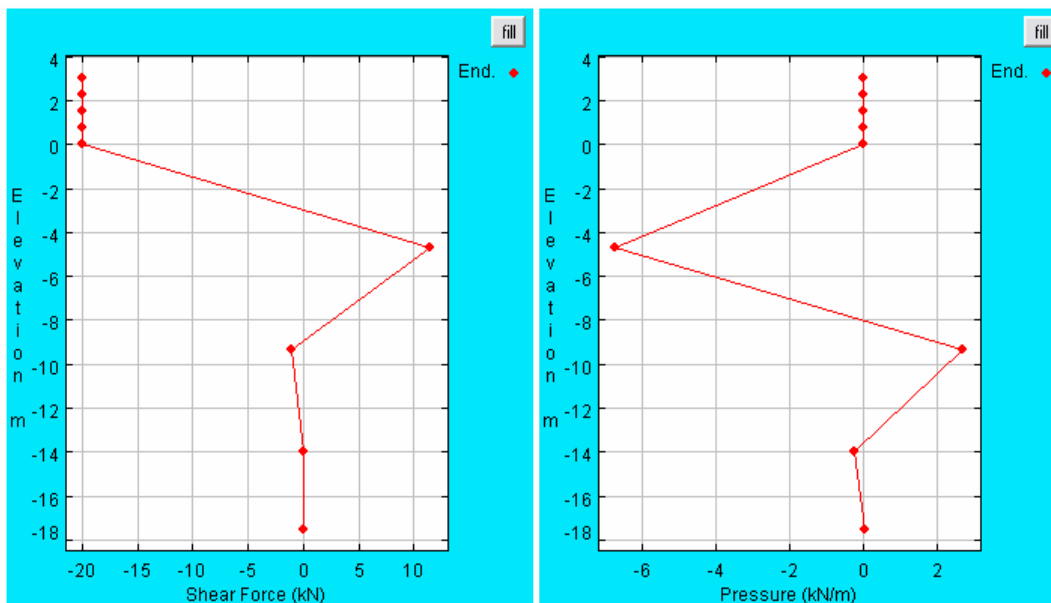


**Figure A. 6 :** a) Shear force of the 20.5 m pile in loose sandy soil., b) Pressure of the 20.5 m pile in loose sandy soil.

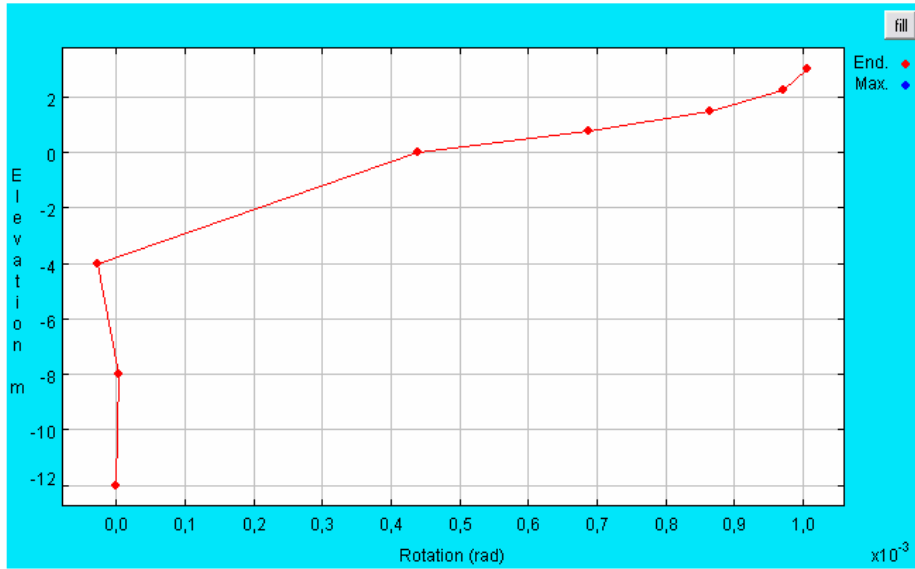


**Figure A. 7 :** Rotation of the 15 m pile in loose sandy soil.

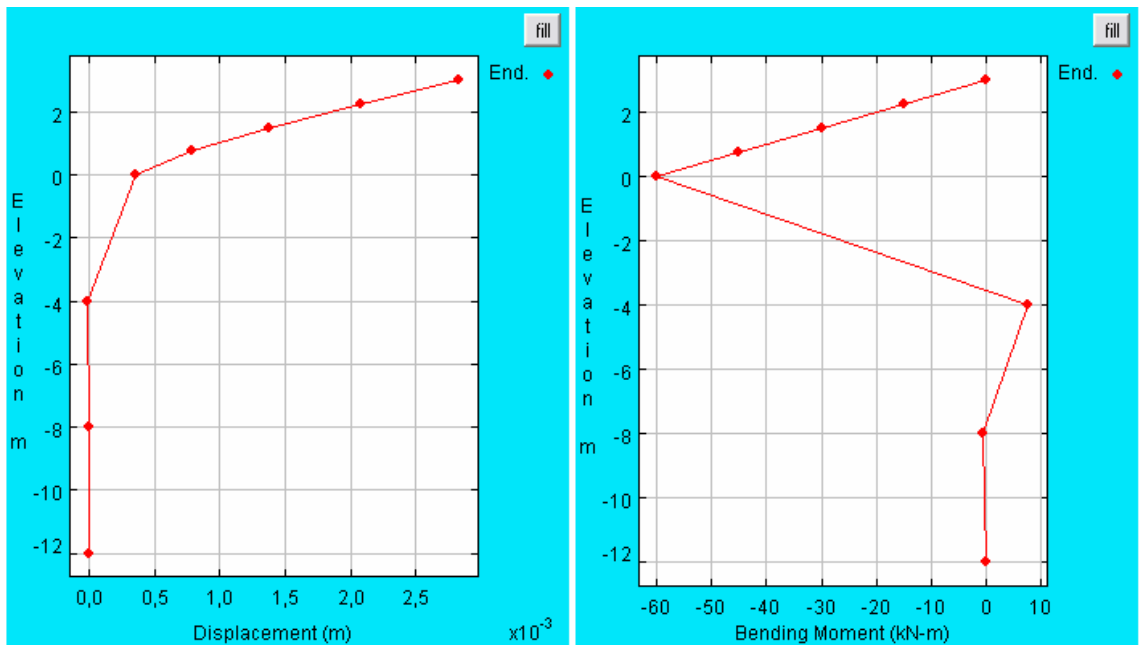


**Figure A. 8 :** a) Displacement of the 15 m pile in loose sandy soil. b) Bending moment of the 15 m pile in loose sandy soil.

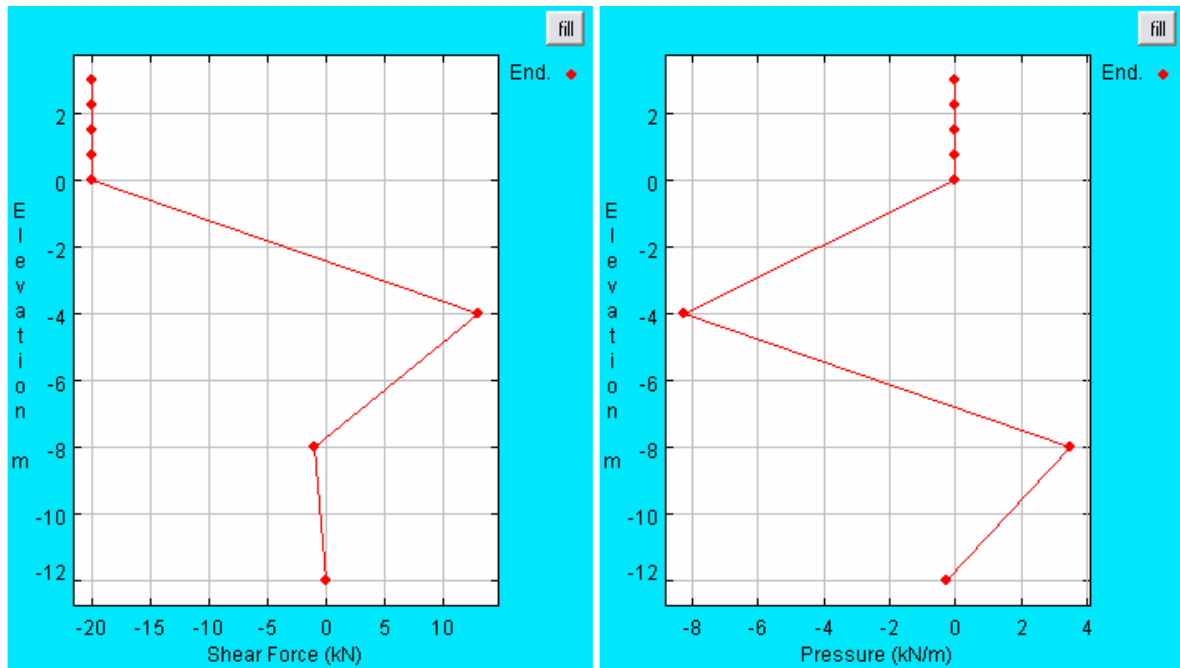


**Figure A. 9 :** a) Shear force of the 15 m pile in loose sandy soil. b) Pressure of the 15 m pile in loose sandy soil.

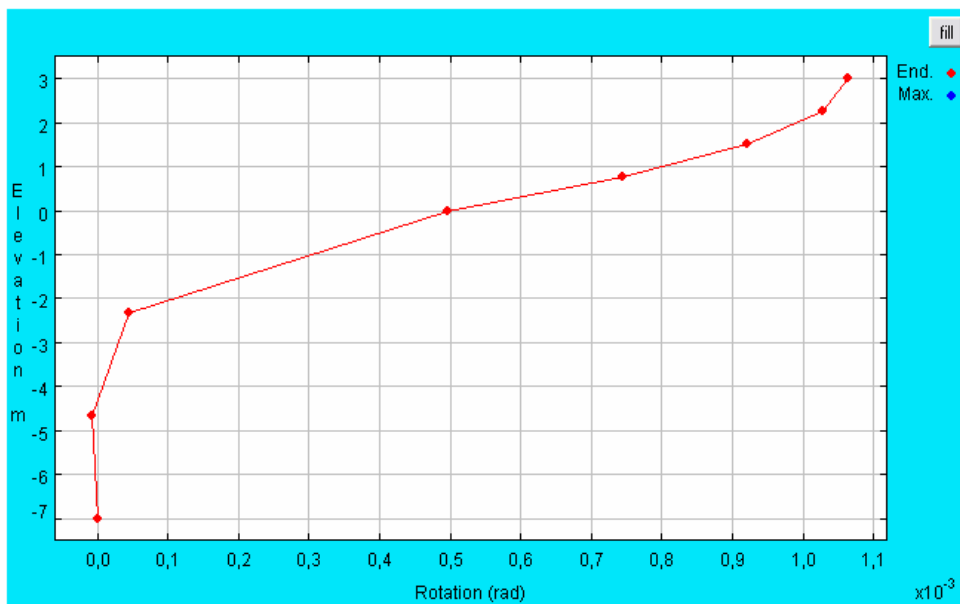


**Figure A. 10 :** Rotation of the 10 m pile in loose sandy soil.

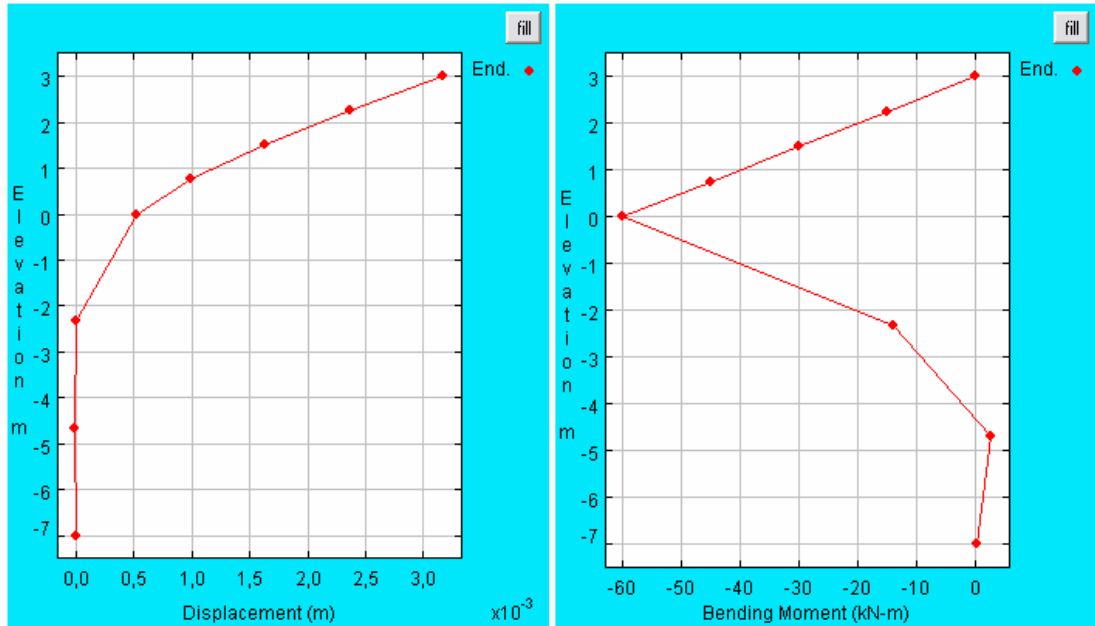


**Figure A. 11 :** a) Displacement of the 10 m pile in loose sandy soil. b) Bending moment of the 10 m pile in loose sandy soil.

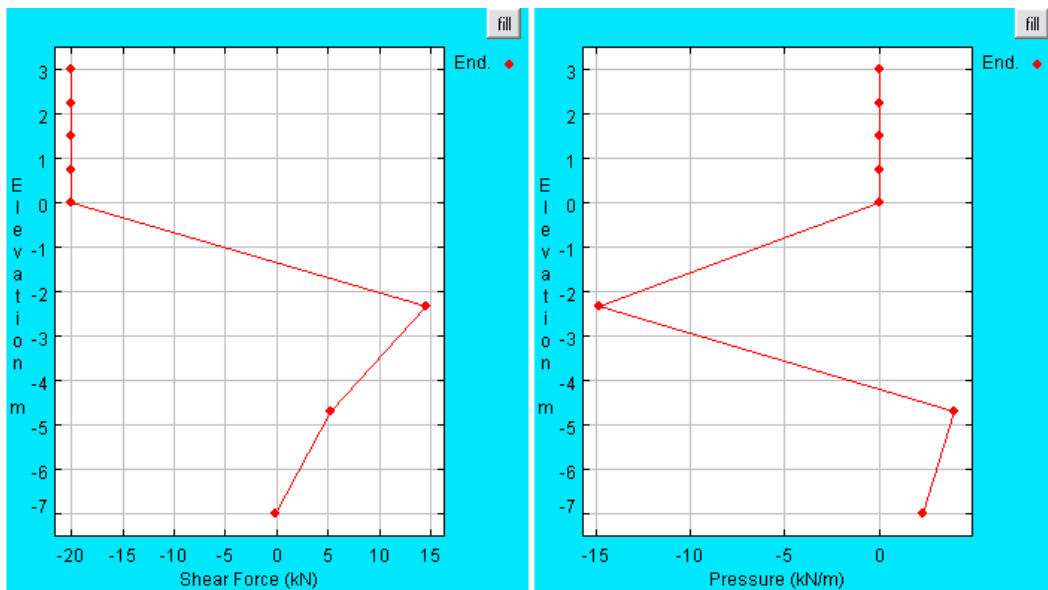


**Figure A. 12 :** a) Shear Force of the 10 m pile in loose sandy soil. b) Pressure of the 10 m pile in loose sandy soil.

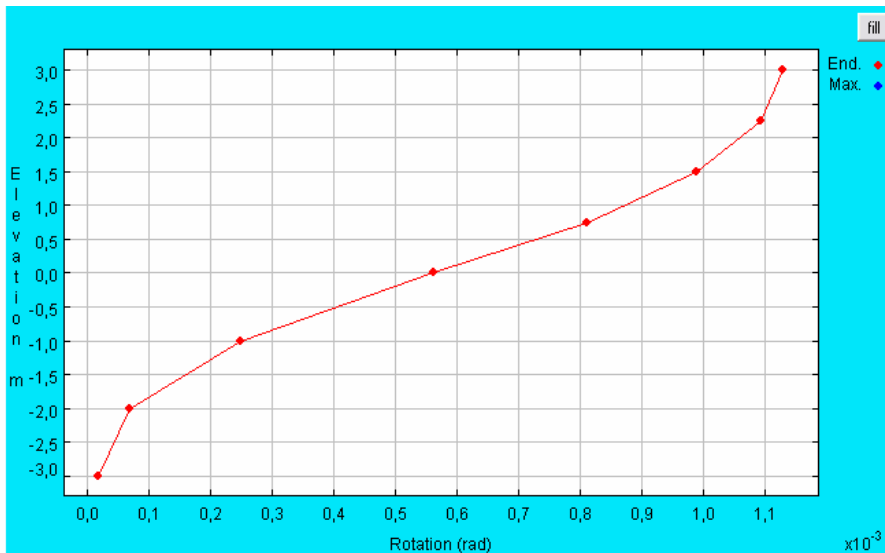


**Figure A. 13 :** Rotation of the 6 m pile in loose sandy soil.

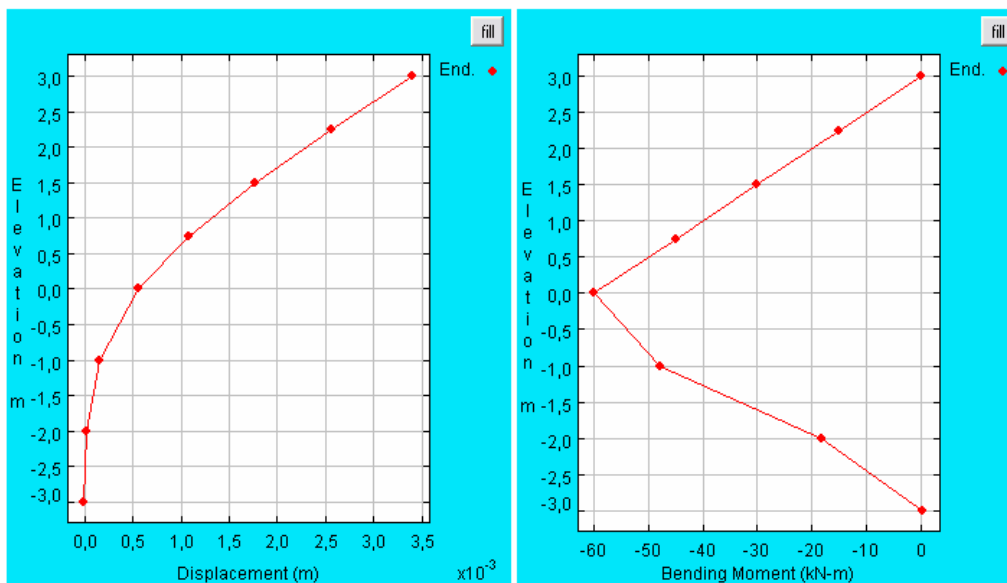


**Figure A. 14 :** a) Displacement of the 6 m pile in loose sandy soil. b) Bending moment of the 6 m pile in loose sandy soil.

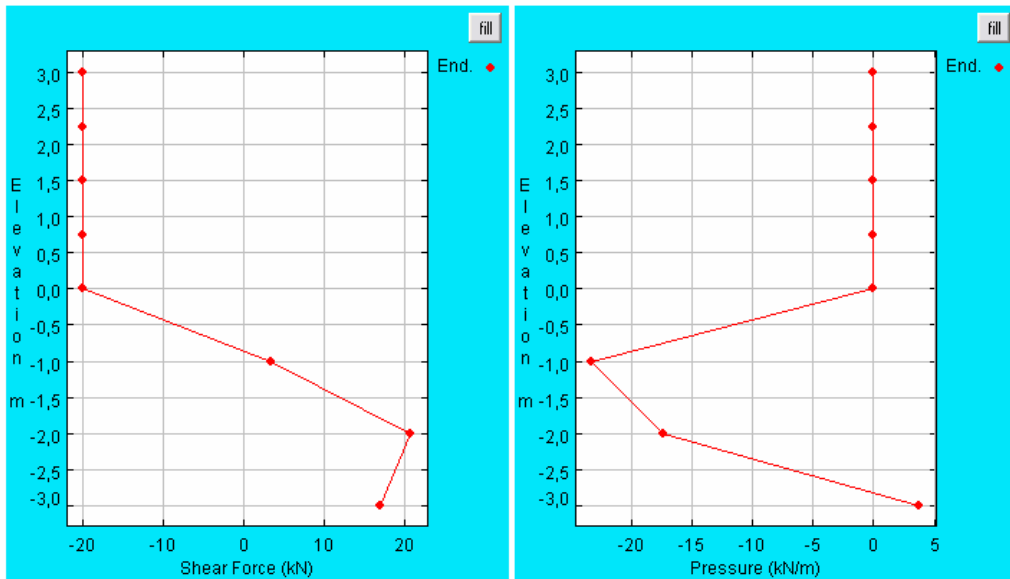


**Figure A. 15 :** a) Shear Force of the 6 m pile in loose sandy soil. b) Pressure of the 6 m pile in loose sandy soil.

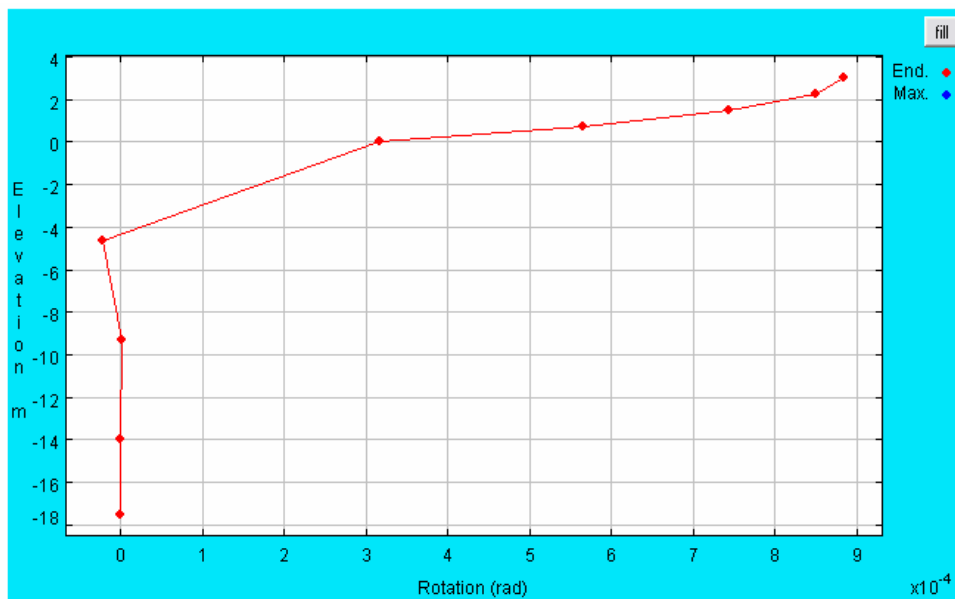


**Figure A. 16 :** Rotation of the 20.5 m pile in dense sandy soil.

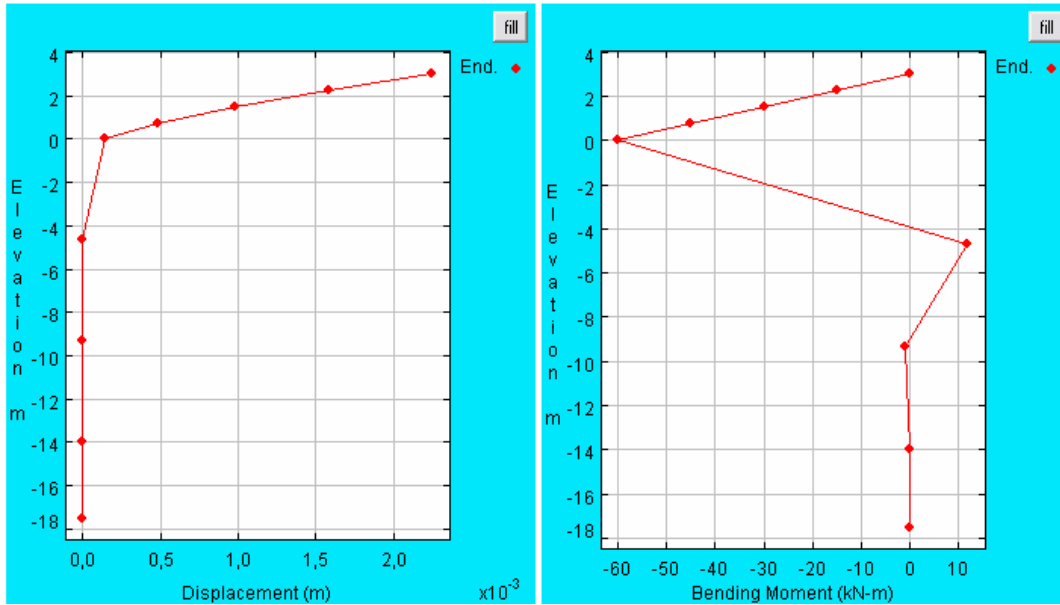


**Figure A. 17 :** a) Displacement of the 20.5 m pile in dense sandy soil. b) Bending moment of the 20.5 m pile in dense sandy soil.

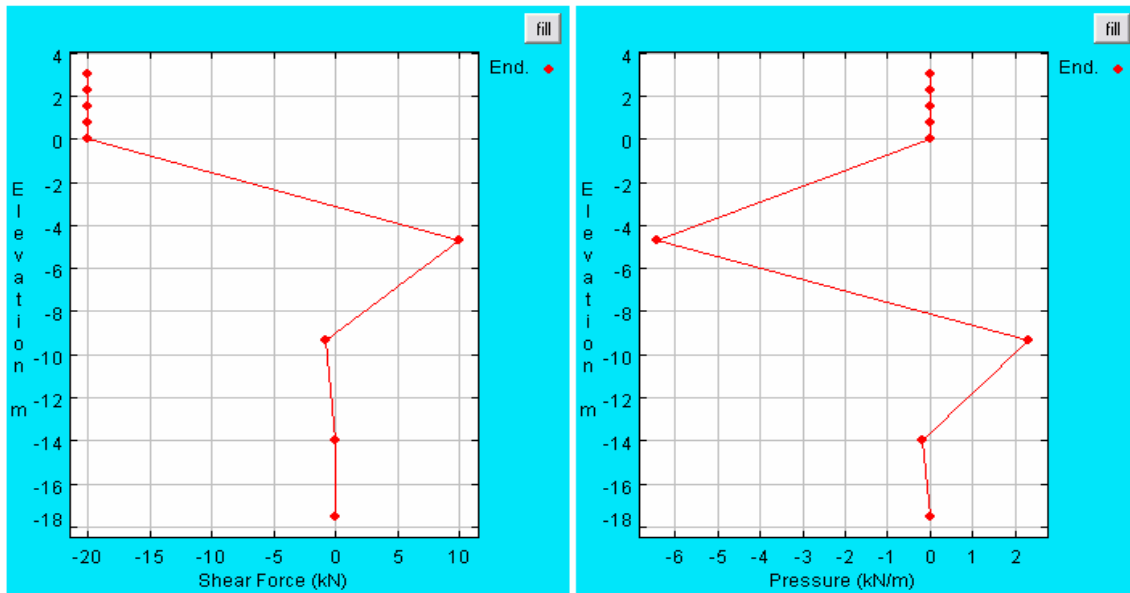


**Figure A. 18 :** a) Shear Force of the 20.5 m pile in dense sandy soil. b) Pressure of the 20.5 m pile in dense sandy soil.

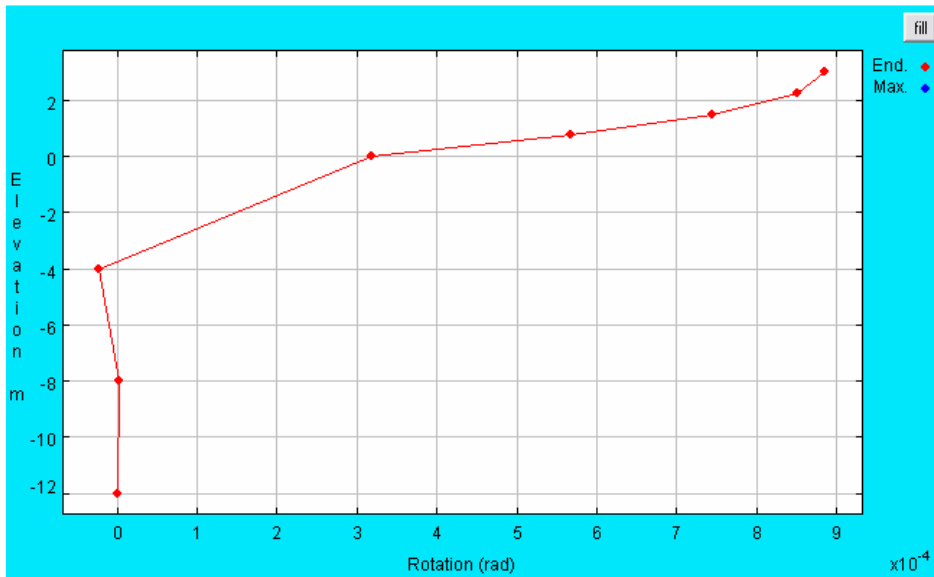


**Figure A. 19 :** Rotation of the 15 m pile in dense sandy soil.

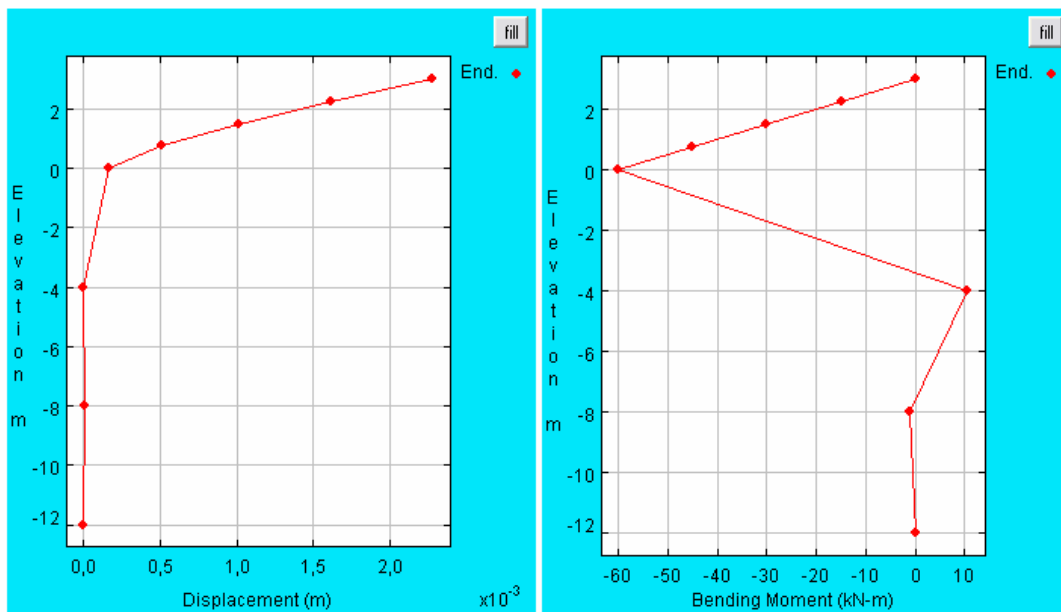


**Figure A. 20 :** a) Displacement of the 15 m pile in dense sandy soil. b) Bending moment of the 15 m pile in dense sandy soil.

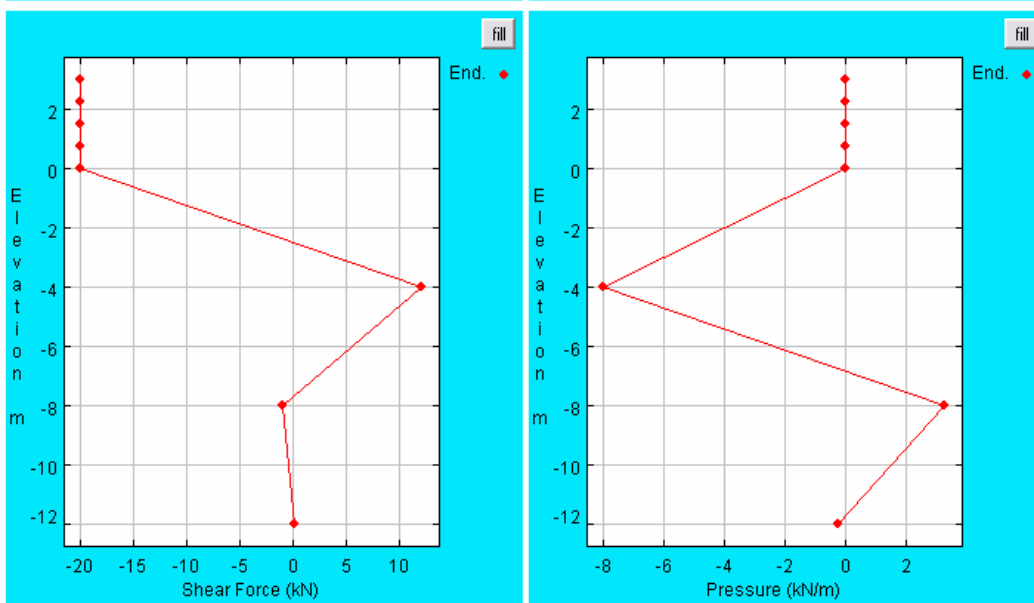


**Figure A. 21 :** a) Shear Force of the 15 m pile in dense sandy soil. b) Pressure of the 15 m pile in dense sandy soil.

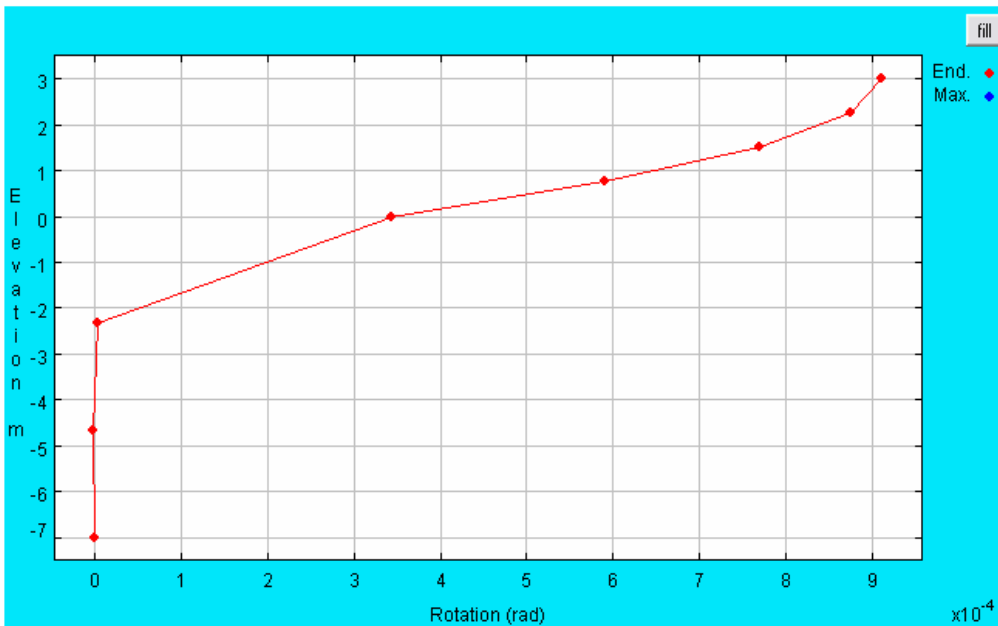


**Figure A. 22 :** Rotation of the 10 m pile in dense sandy soil.

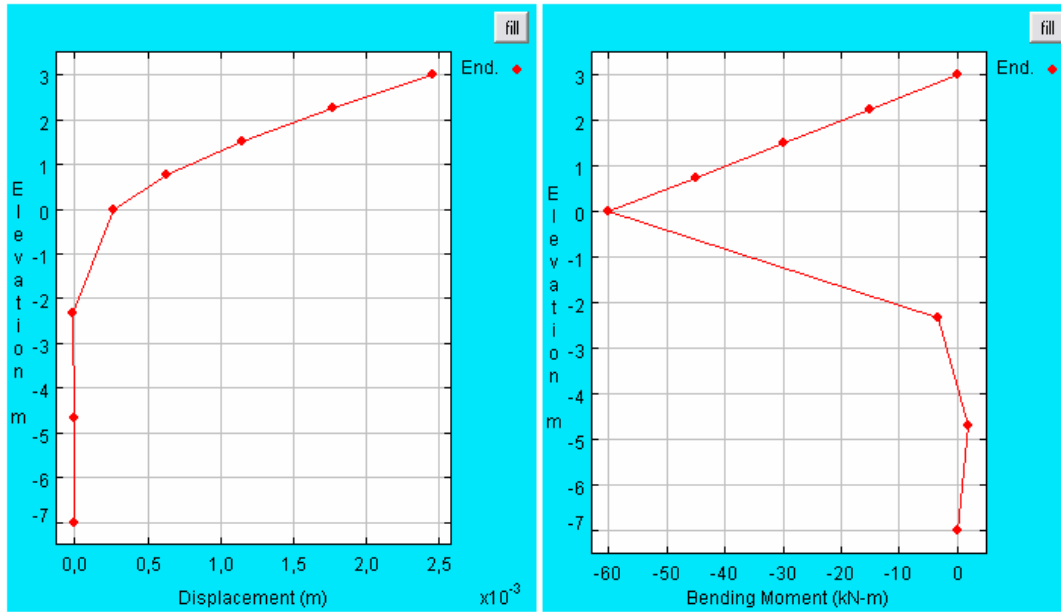


**Figure A. 23 :** a) Displacement of the 10 m pile in dense sandy soil. b) Bending moment of the 10 m pile in dense sandy soil.

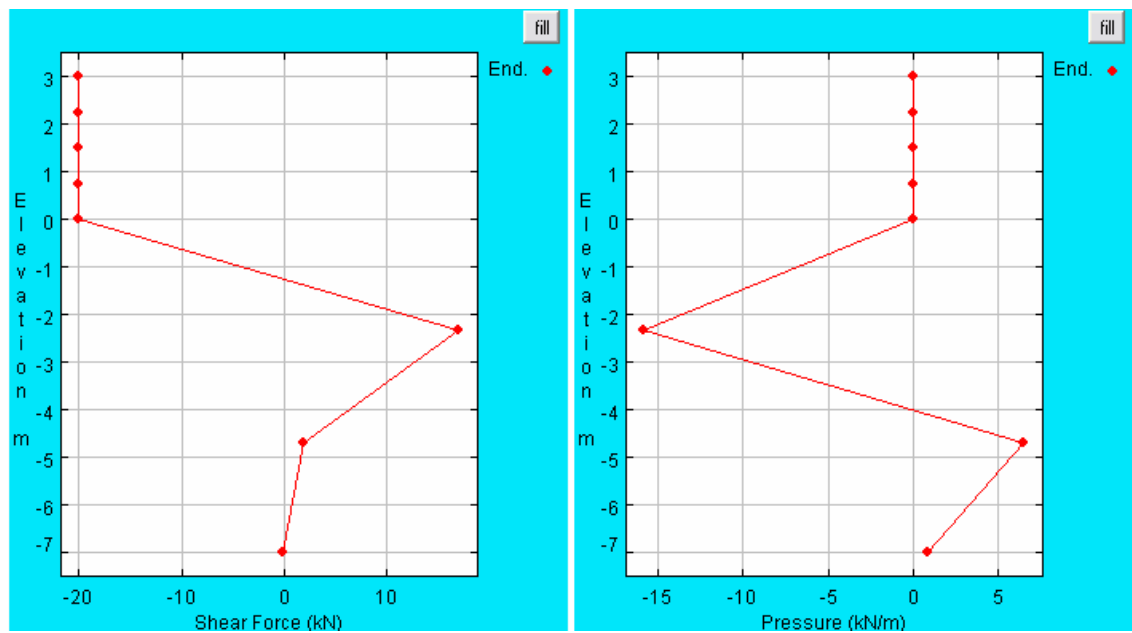


**Figure A. 24 :** a) Shear Force of the 10 m pile in dense sandy soil. b) Pressure of the 10 m pile in dense sandy soil.

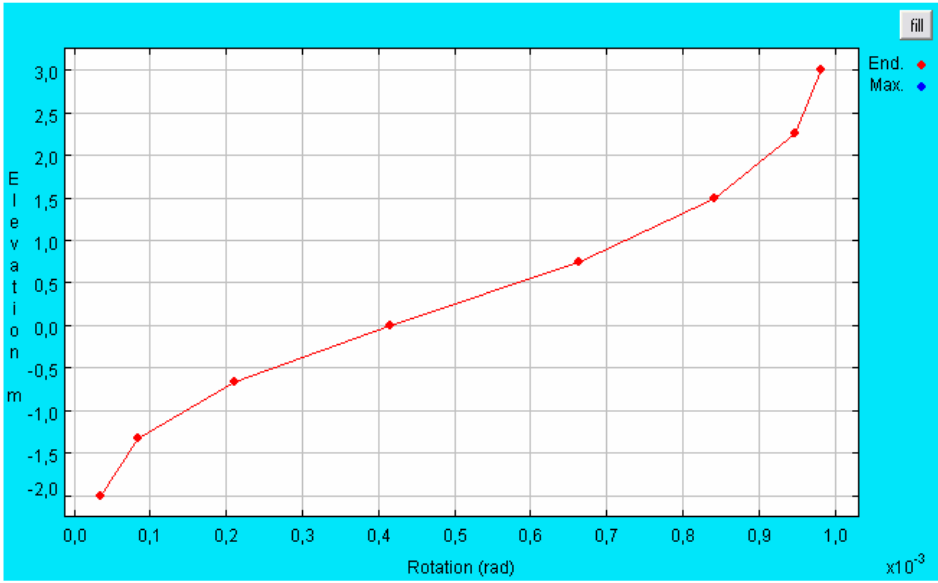


**Figure A. 25 :** Rotation of the 6 m pile in dense sandy soil.

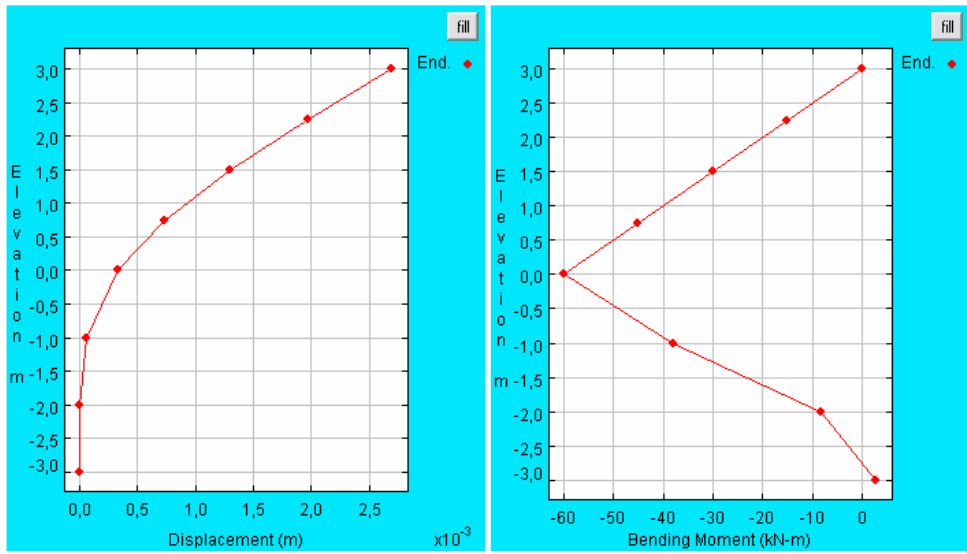


**Figure A. 26 :** a) Displacement of the 6 m pile in dense sandy soil. b) Bending moment of the 6 m pile in dense sandy soil.

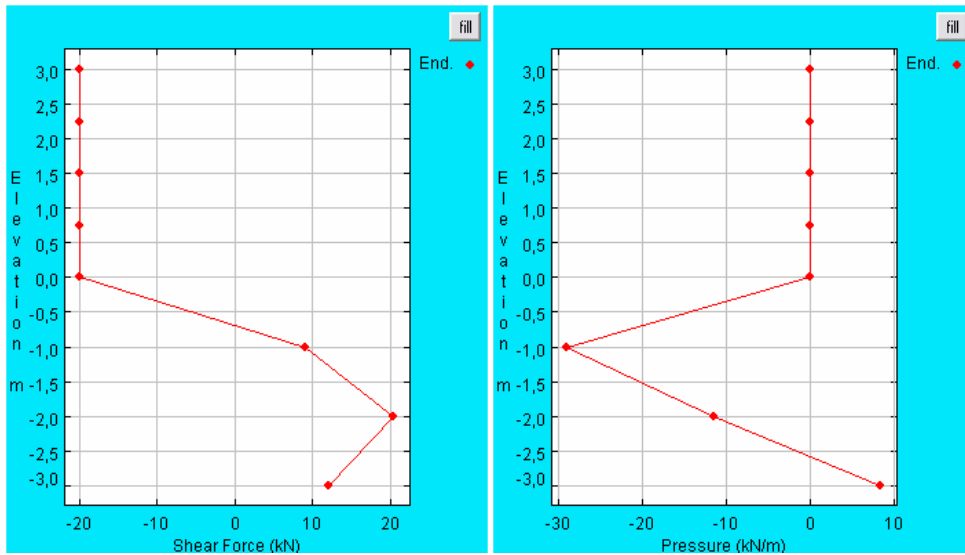


**Figure A. 27 :** a) Shear Force of the 6 m pile in dense sandy soil. b) Pressure of the 6 m pile in dense sandy soil.

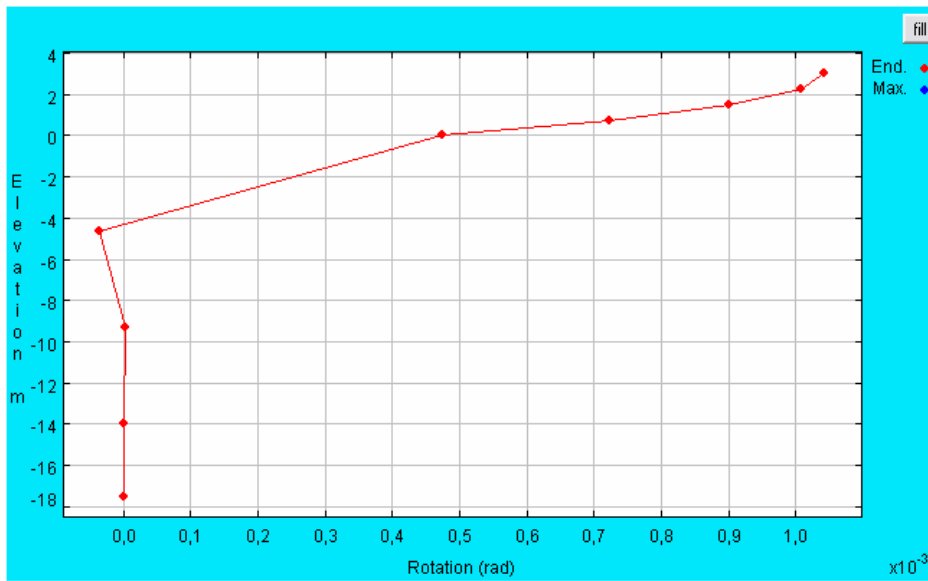


**Figure A. 28 :** Rotation of the 20.5 m pile in soft clayey soil.

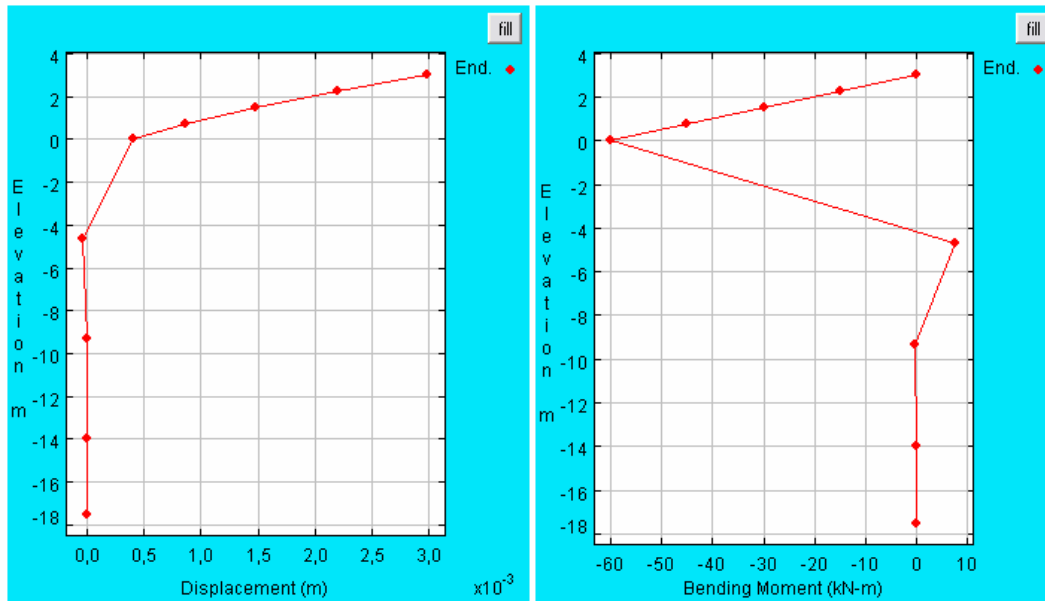


**Figure A. 29 :** a) Displacement of the 20.5 m pile in soft clayey soil. b) Bending moment of the 20.5 m pile in soft clayey soil.

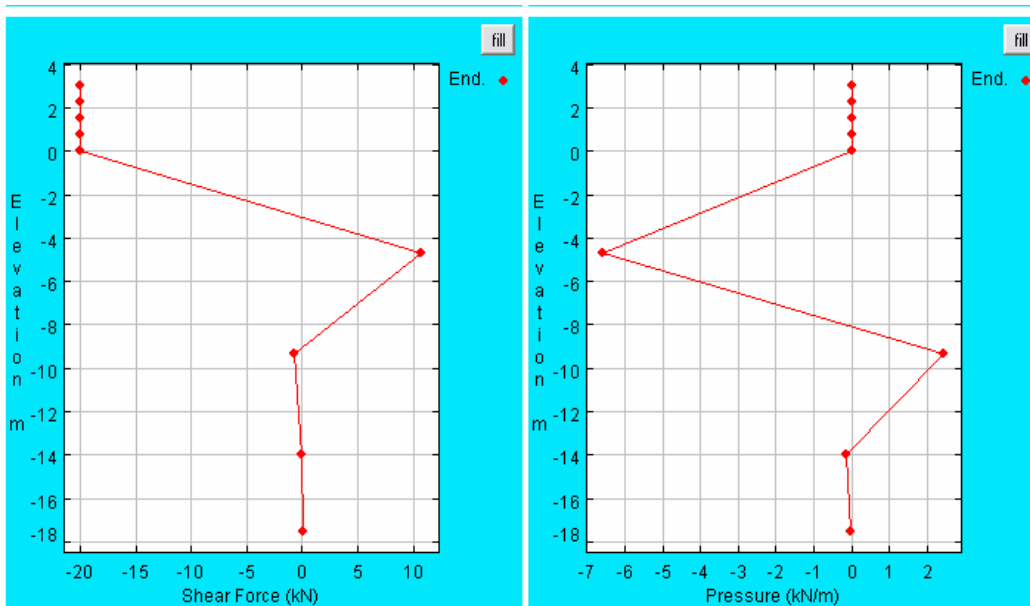


**Figure A. 30 :** a) Shear Force of the 20.5 m pile in soft clayey soil. b) Pressure of the 20.5 m pile in soft clayey soil.

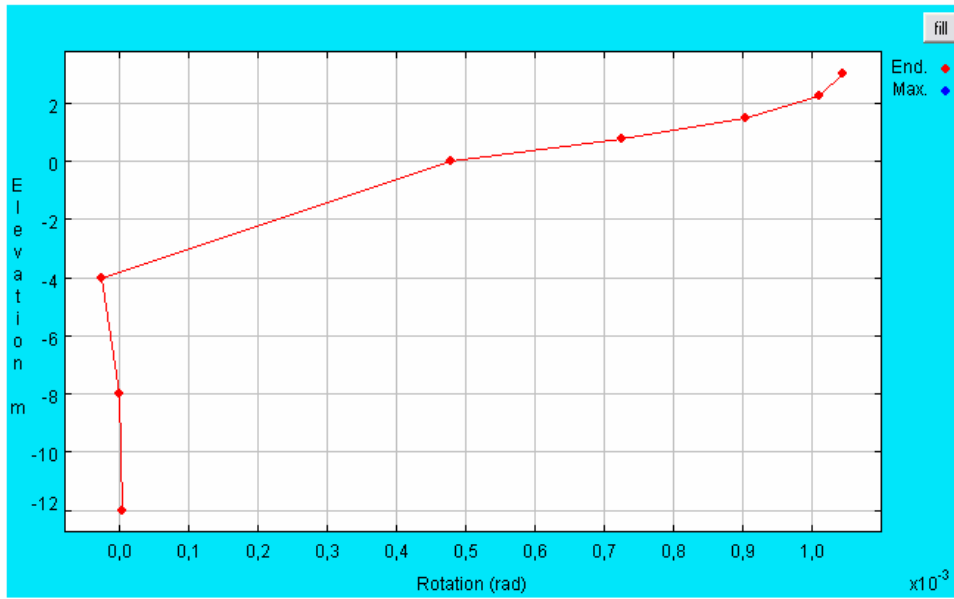


**Figure A. 31 :** Rotation of the 15 m pile in soft clayey soil.

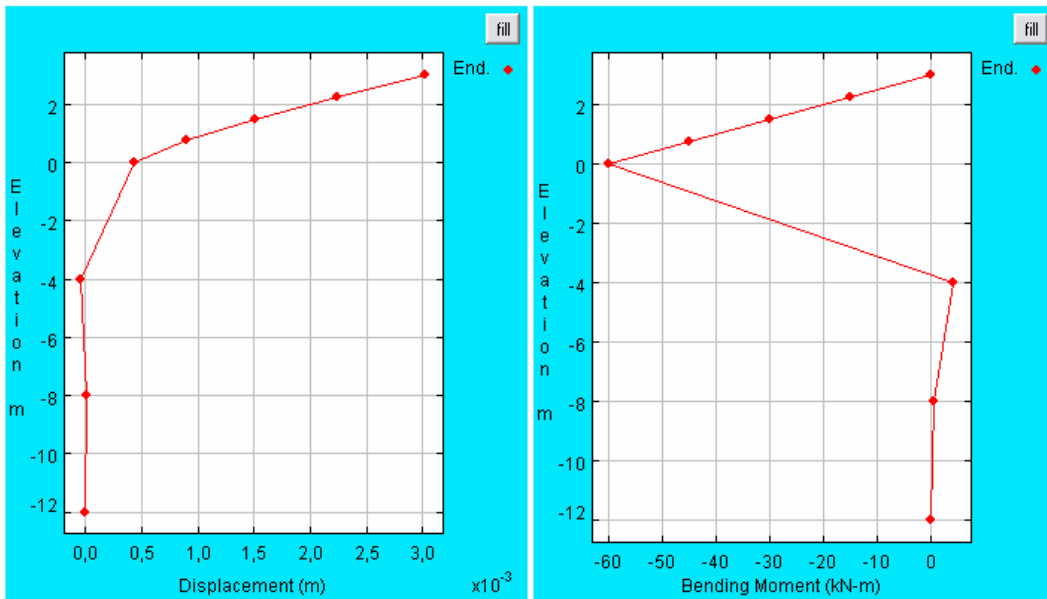


**Figure A. 32 :** a) Displacement of the 15m pile in soft clayey soil. b) Bending moment of the 15 m pile in soft clayey soil.

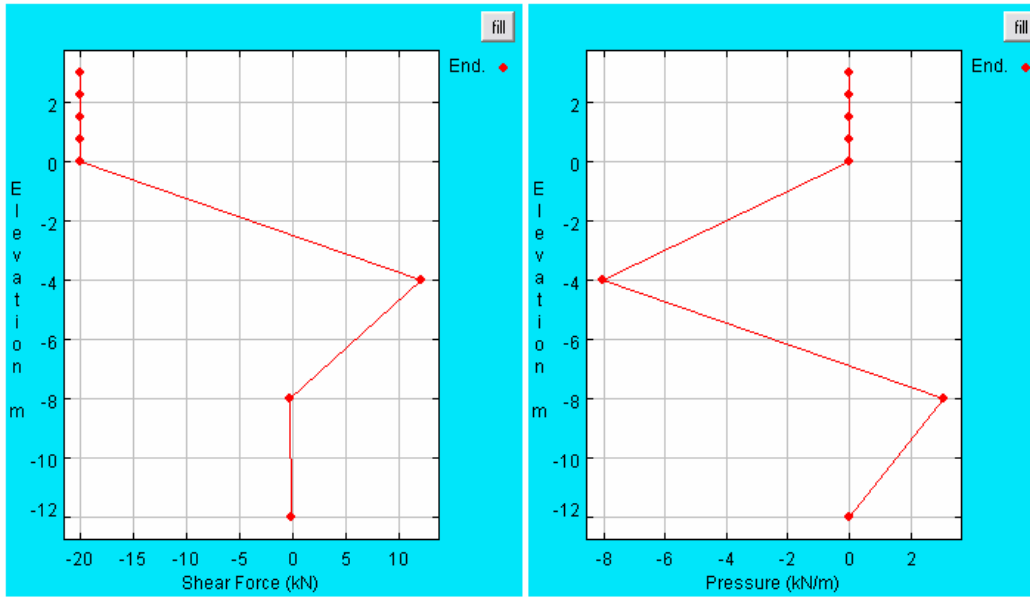


**Figure A. 33 :** a) Shear Force of the 15 m pile in soft clayey soil. b) Pressure of the 15 m pile in soft clayey soil.

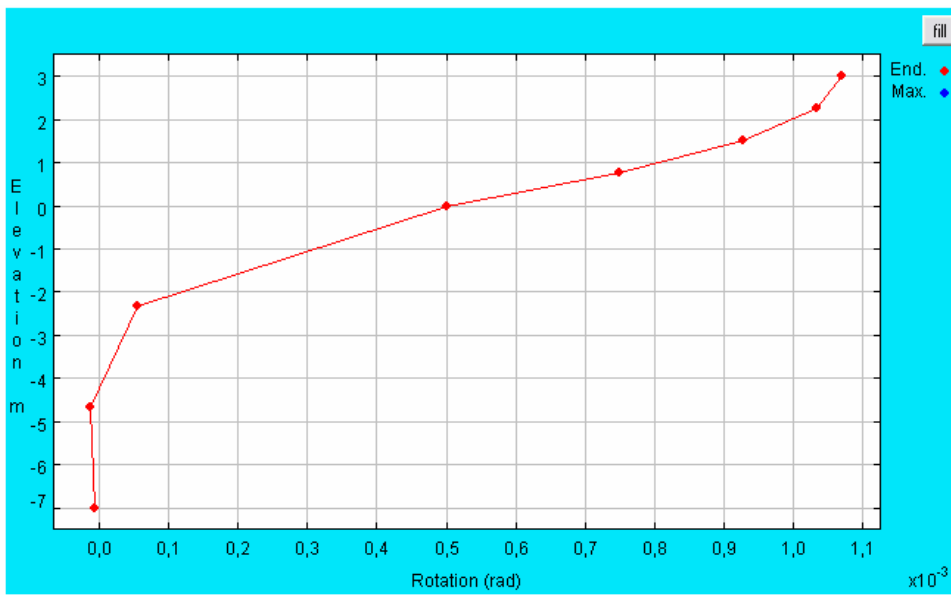


**Figure A. 34 :** Rotation of the 10 m pile in soft clayey soil.

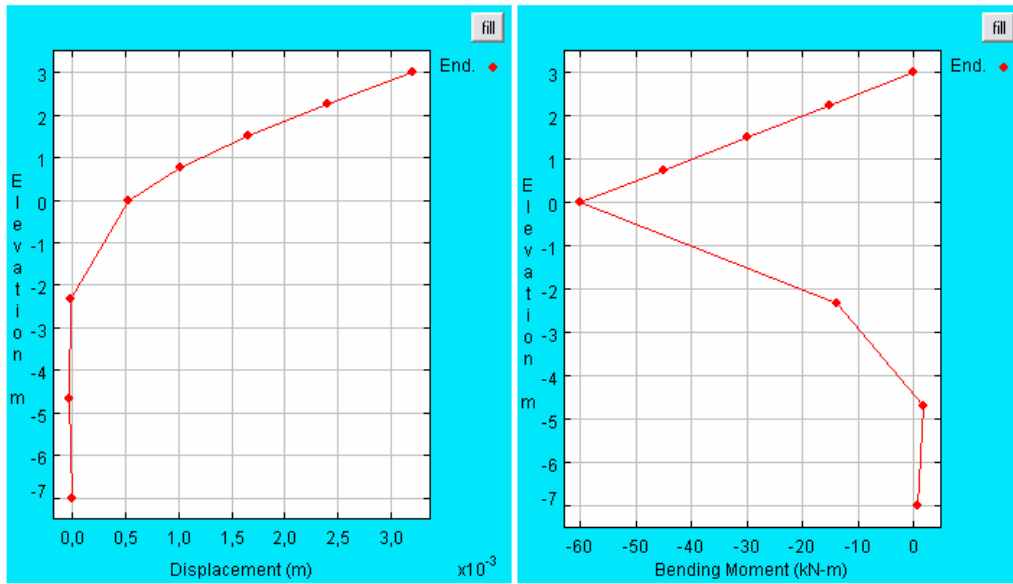


**Figure A. 35 :** a) Displacement of the 10 m pile in soft clayey soil. b) Bending moment of the 10 m pile in soft clayey soil.

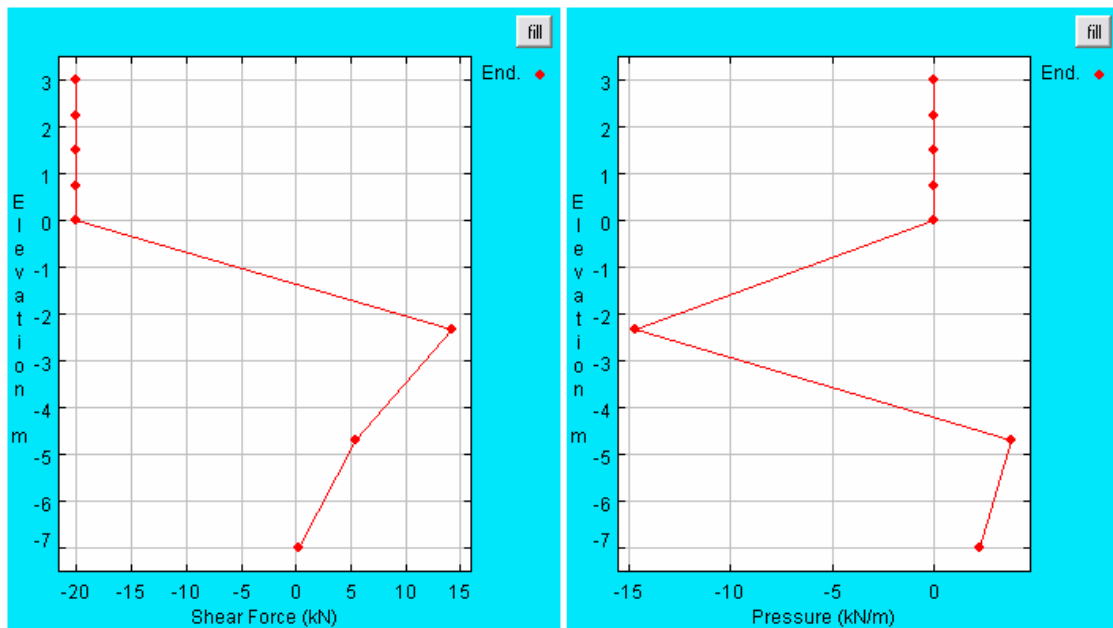


**Figure A. 36 :** a) Shear Force of the 10 m pile in soft clayey soil. b) Pressure of the 10 m pile in soft clayey soil.

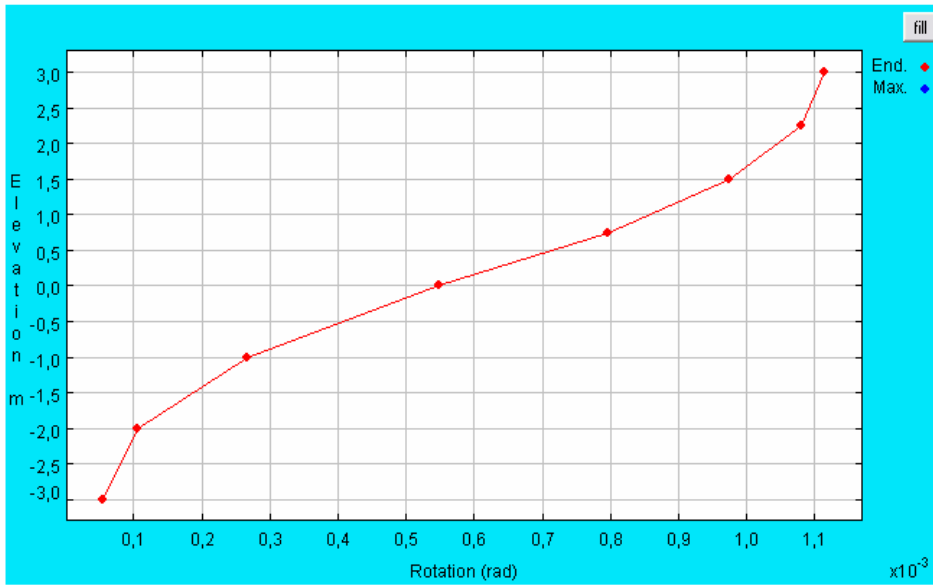


**Figure A. 37 :** Rotation of the 6 m pile in soft clayey soil.

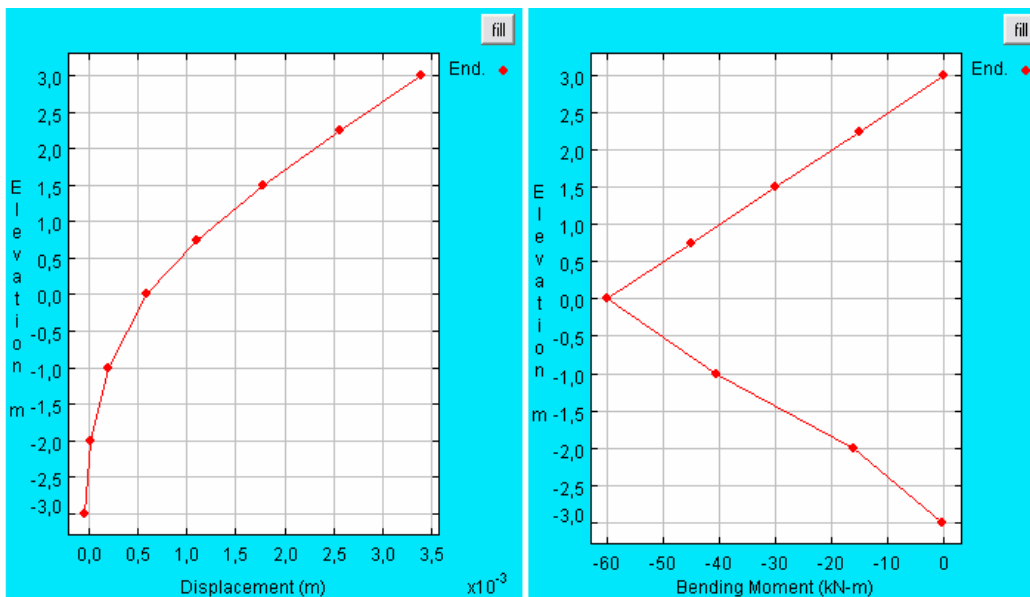


**Figure A. 38 :** a) Displacement of the 6 m pile in soft clayey soil. b) Bending moment of the 6 m pile in soft clayey soil.

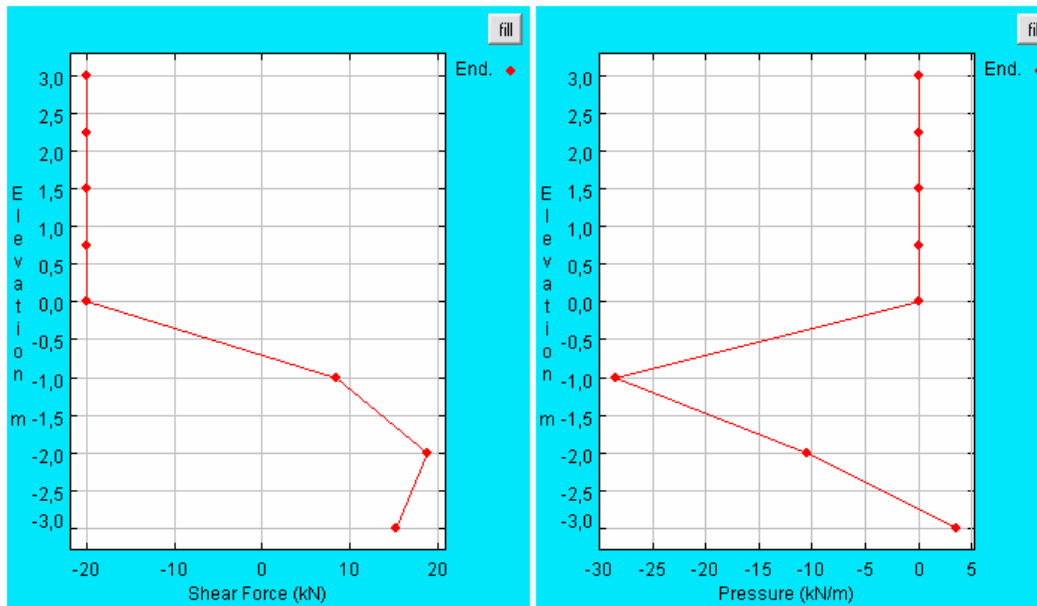


**Figure A. 39 :** a) Shear Force of the 6 m pile in soft clayey soil. b) Pressure of the 6 m pile in soft clayey soil.

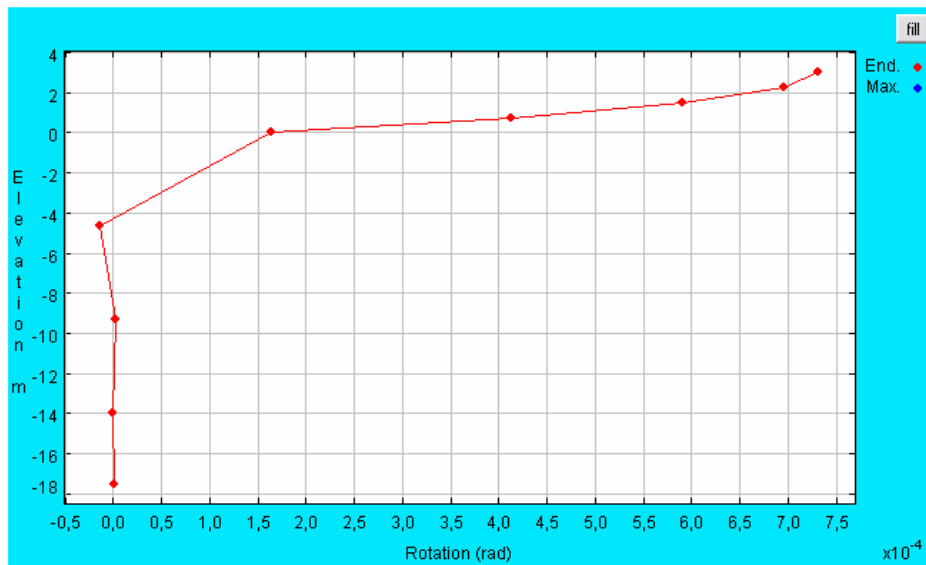


**Figure A. 40 :** Rotation of the 20.5 m pile in stiff clayey soil.

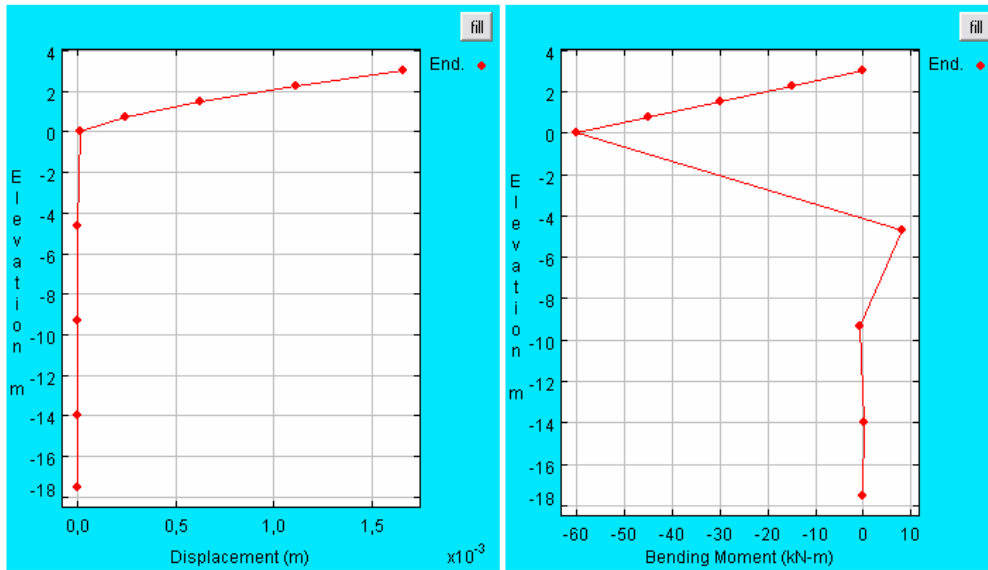


**Figure A. 41 :** a) Displacement of the 20.5 m pile in stiff clayey soil. b) Bending moment of the 20.5 m pile in stiff clayey soil.

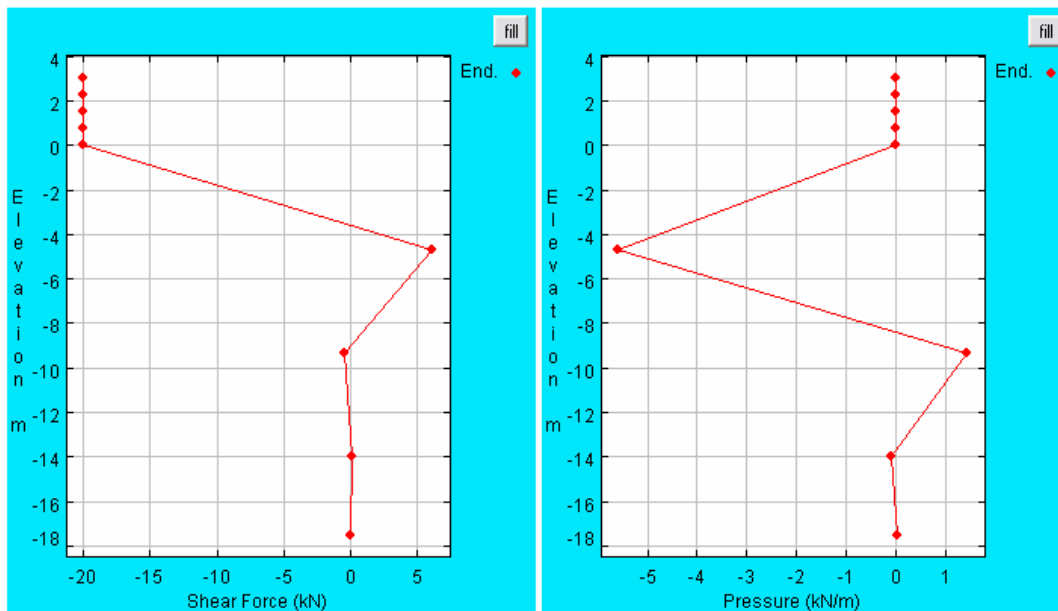


**Figure A. 42 :** a) Shear Force of the 20.5 m pile in stiff clayey soil. b) Pressure of the 20.5 m pile in stiff clayey soil.

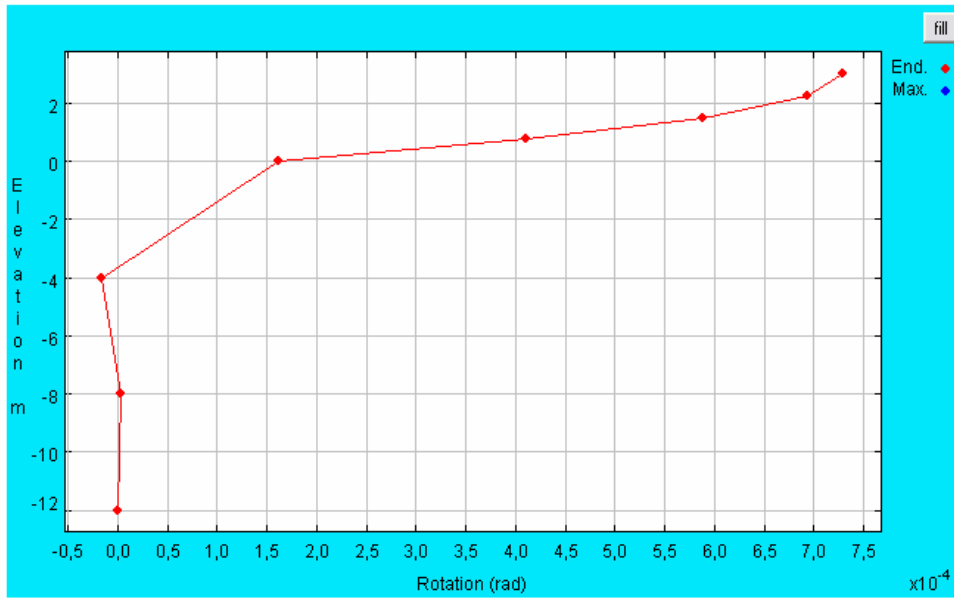


**Figure A. 43 :** Rotation of the 15m pile in stiff clayey soil.

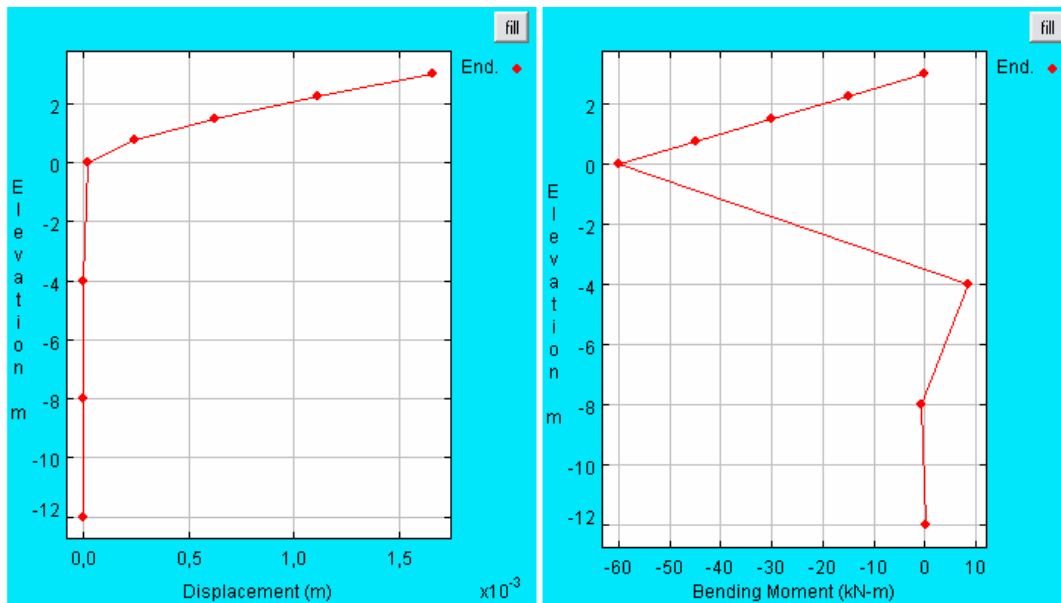


**Figure A. 44 :** a) Displacement of the 15 m pile in stiff clayey soil. b) Bending moment of the 15 m pile in stiff clayey soil.

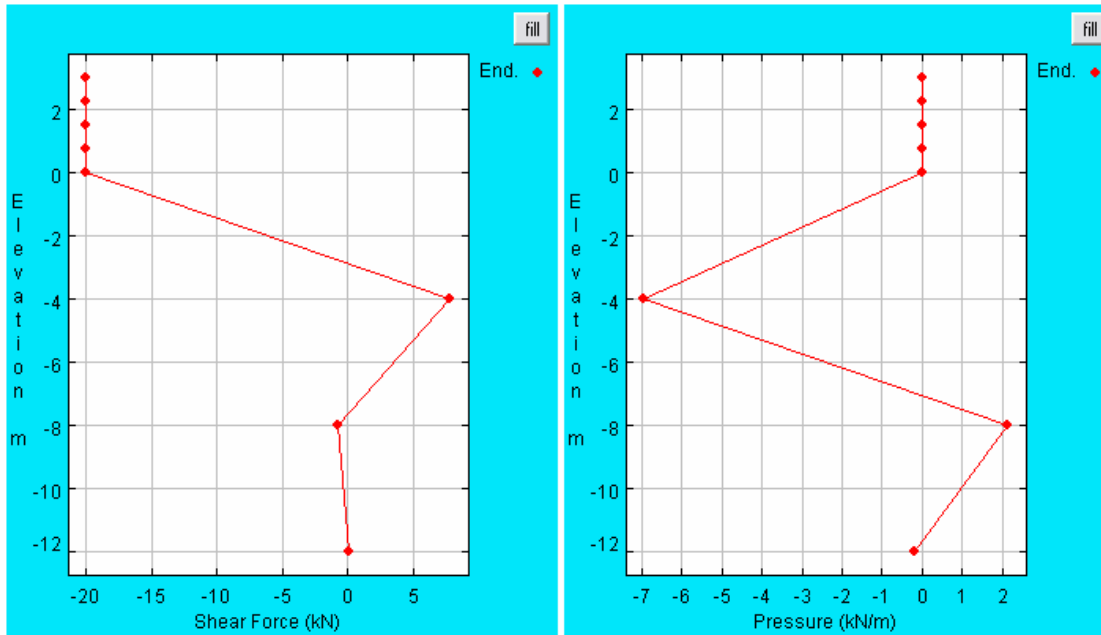


**Figure A. 45 :** a) Shear Force of the 15 m pile in stiff clayey soil. b) Pressure of the 15 m pile in stiff clayey soil.

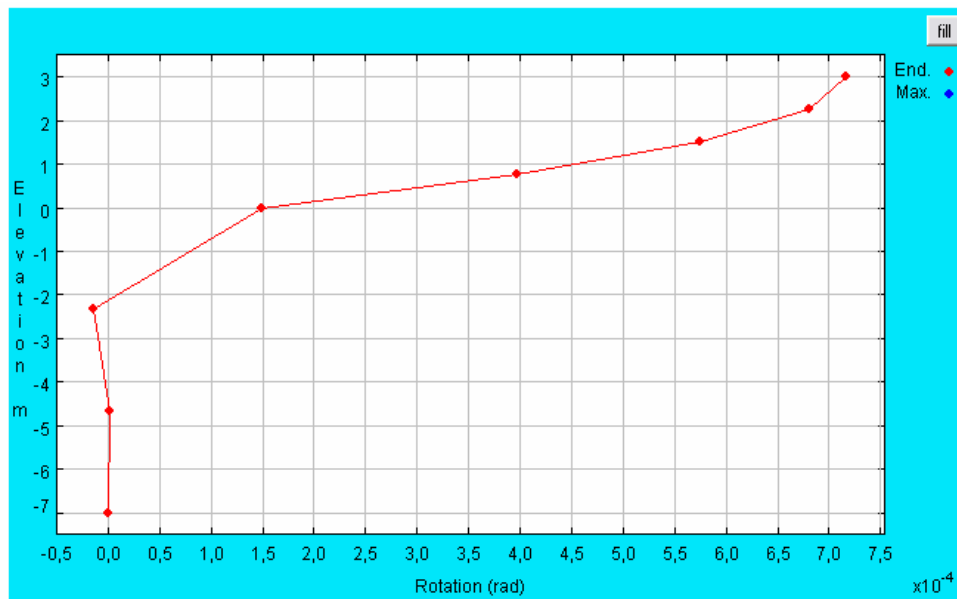


**Figure A. 46 :** Rotation of the 10 m pile in stiff clayey soil.

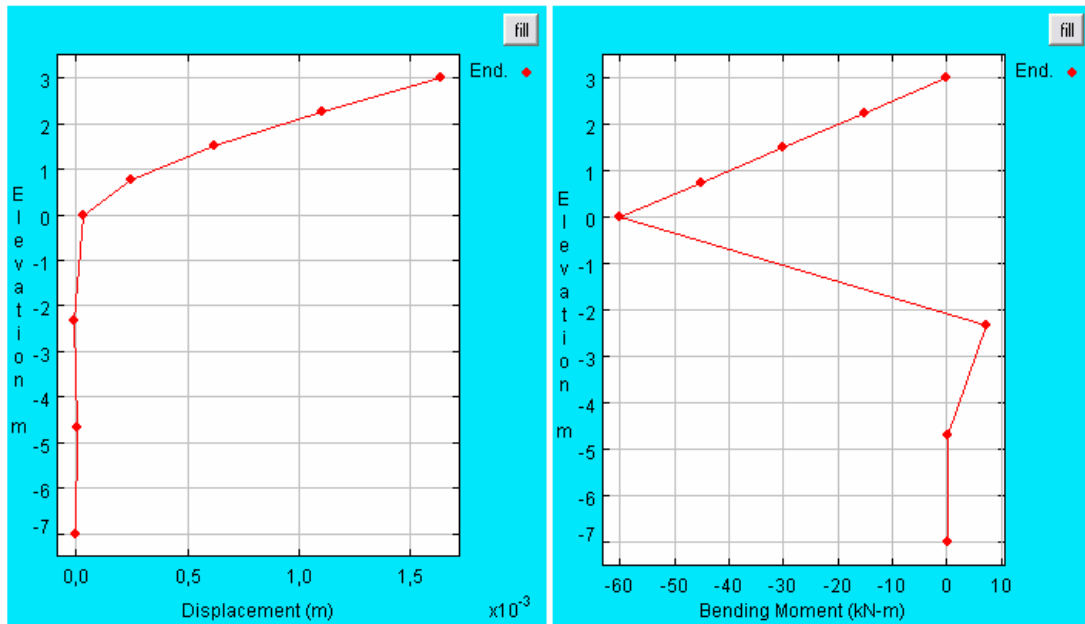


**Figure A. 47 :** a) Displacement of the 10 m pile in stiff clayey soil. b) Bending moment of the 10 m pile in stiff clayey soil.

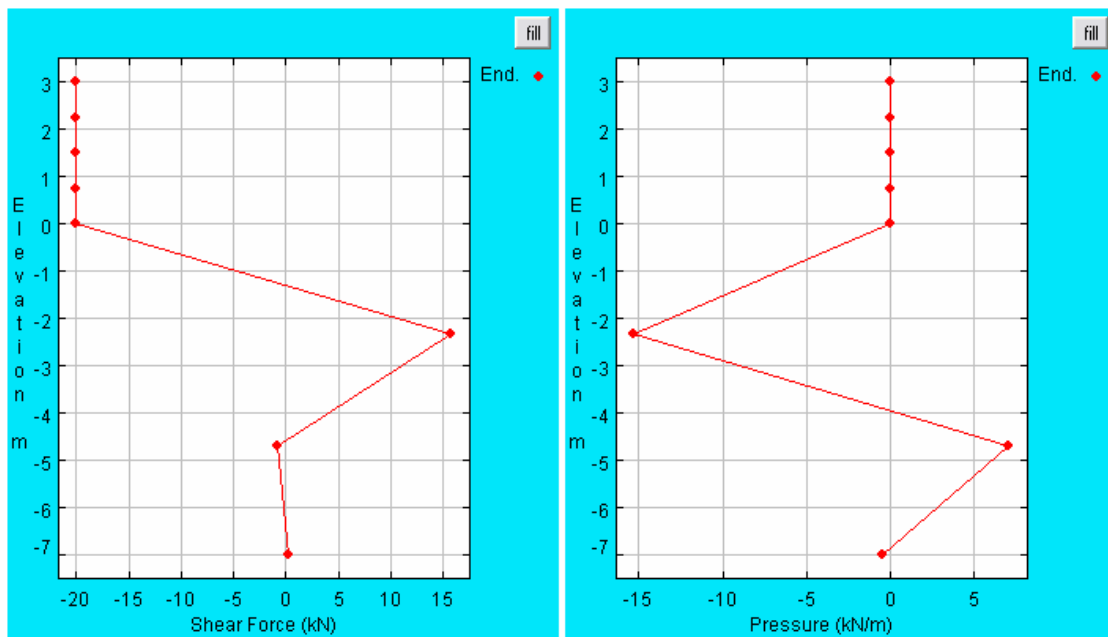


**Figure A. 48 :** a) Shear Force of the 10 m pile in stiff clayey soil. b) Pressure of the 10 m pile in stiff clayey soil.

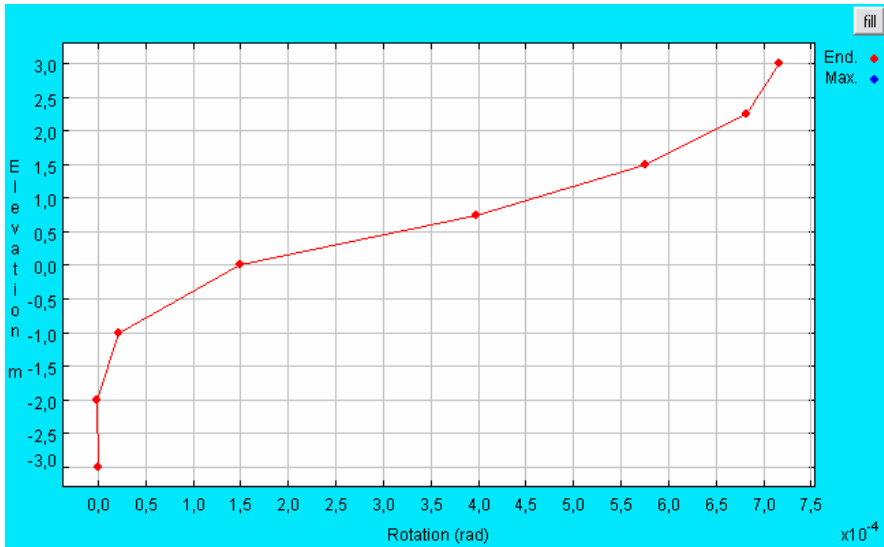


**Figure A. 49** : Rotation of the 6 m pile in stiff clayey soil.

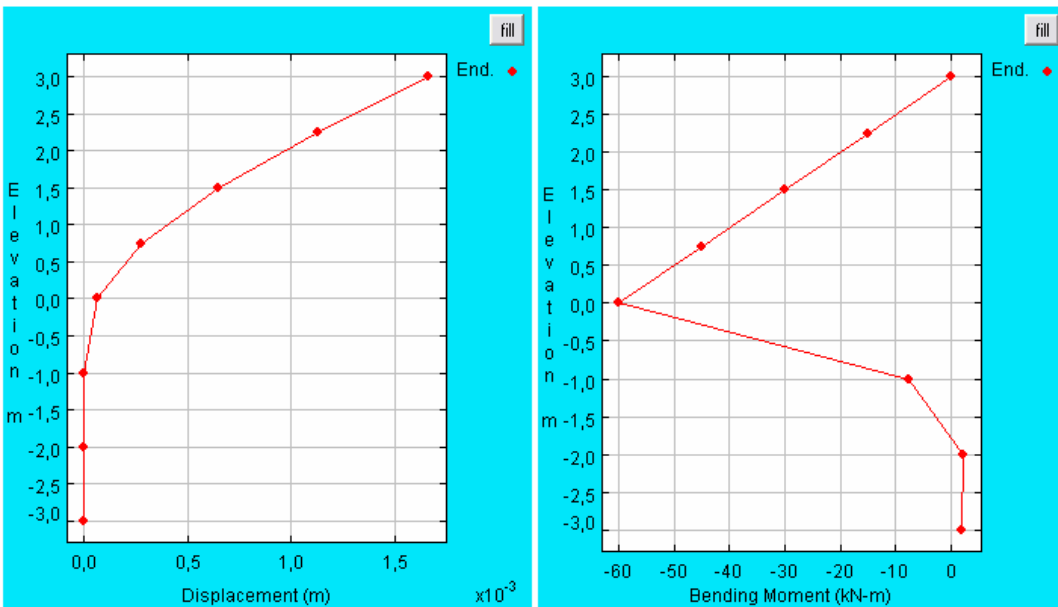


**Figure A. 50** : a) Displacement of the 6 m pile in stiff clayey soil. b) Bending moment of the 6 m pile in stiff clayey soil.

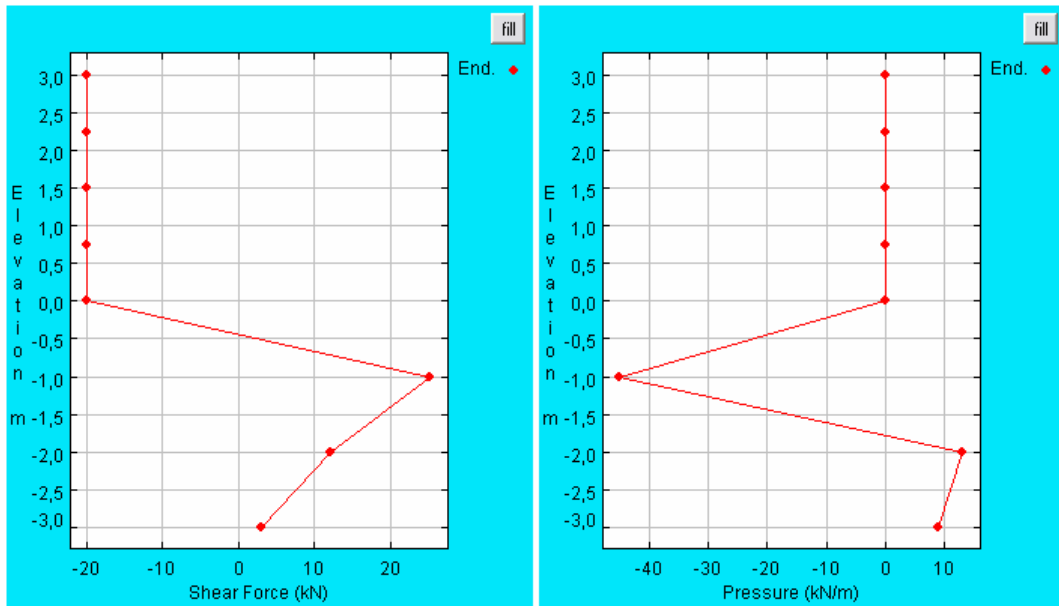


**Figure A. 51:** a) Shear Force of the 6 m pile in stiff clayey soil. b) Pressure of the 6 m pile in stiff clayey soil.

**Table A 1:** Aliaga test data.

Real time	test	Stage	Load ton	cm <sup>2</sup>	1	2	3	Average deformation	Rotation
09:10		00:00	0		0	0	0	0,00	0
09:10	00:00	00:00	10	32,28	0,09	0,08	0,08	0,08	0,01
09:15	00:05	00:05	10		0,1	0,09	0,085	0,09	0,01
09:25	00:15	00:10	10		0,095	0,09	0,09	0,09	0,015
09:30	00:20	00:20	10		0,065	0,08	0,05	0,07	0,025
09:30	00:20	00:00	20	64,56	0,25	0,22	0,21	0,23	0,045
09:35	00:25	00:05	20		0,26	0,23	0,22	0,24	0,05
09:40	00:30	00:10	20		0,26	0,22	0,21	0,23	0,055
09:50	00:40	00:20	20		0,26	0,21	0,19	0,22	0,075
09:50	00:40	00:00	30	92,36	0,48	0,42	0,39	0,43	0,1
09:55	00:45	00:05	30		0,525	0,47	0,44	0,48	0,11
10:00	00:50	00:10	30		0,545	0,48	0,46	0,50	0,12
10:10	01:00	00:20	30		0,58	0,52	0,48	0,53	0,13
10:10	01:00	00:00	40	123,2	0,87	0,79	0,74	0,80	0,155
10:15	01:05	00:05	40		0,882	0,81	0,77	0,82	0,16
10:20	01:10	00:10	40		0,9	0,82	0,78	0,83	0,171
10:30	01:20	00:20	40		0,93	0,85	0,8	0,86	0,19
10:30	01:20	00:00	50	148,8	1,13	1,04	0,99	1,05	0,21
10:35	01:25	00:05	50		1,28	1,19	1,14	1,20	0,22
10:40	01:30	00:10	50		1,305	1,22	1,16	1,23	0,23
10:50	01:40	00:20	50		1,34	1,27	1,21	1,27	0,245
10:50	01:40	00:00	60	176,8	1,66	1,59	1,51	1,59	0,26
10:55	01:45	00:05	60		1,72	1,65	1,57	1,65	0,265
11:00	01:50	00:10	60		1,77	1,7	1,63	1,70	0,295
11:10	02:00	00:20	60		1,785	1,72	1,65	1,72	0,32
11:10	02:00	00:00	68	200	1,96	1,88	1,82	1,89	0,332
11:15	02:05	00:05	68		1,99	1,92	1,85	1,92	0,35
11:20	02:10	00:10	68		2,023	1,95	1,89	1,95	0,37
11:30	02:20	00:20	68		2,03	1,95	1,905	1,96	0,415
11:30	02:20	00:00	72	212	2,12	2,04	1,99	2,05	0,42
11:35	02:25	00:05	72		2,14	2,06	2,01	2,07	0,43
11:40	02:30	00:10	72		2,13	2,06	2,01	2,07	0,452
11:50	02:40	00:20	72		2,1	2,06	1,99	2,05	0,49
11:50	02:40	00:00	76	224,3	2,23	2,16	2,12	2,17	0,5
11:55	02:45	00:05	76		2,25	2,17	2,13	2,18	0,51
12:00	02:50	00:10	76		2,25	2,17	2,13	2,18	0,53
12:10	03:00	00:20	76		2,3	2,22	2,18	2,23	0,555
12:10	03:00	00:00	80	236,1	2,43	2,34	2,3	2,36	0,565
12:15	03:05	00:05	80		2,48	2,4	2,35	2,41	0,57
12:25	03:15	00:15	80		2,55	2,47	2,42	2,48	0,59
12:35	03:25	00:25	80		2,555	2,47	2,42	2,48	0,6
12:55	03:45	00:45	80		2,61	2,53	2,485	2,54	0,63
13:10	04:00	01:00	80		2,61	2,53	2,485	2,54	0,65
13:10	04:00	00:00	60	176,8	2,57	2,35	2,31	2,41	0,65
13:15	04:05	00:05	60		2,57	2,39	2,35	2,44	0,64
13:20	04:10	00:10	60		2,57	2,4	2,36	2,44	0,64
13:20	04:10	00:00	40	123,2	2,36	2,12	2,1	2,19	0,62
13:25	04:15	00:05	40		2,36	2,12	2,1	2,19	0,615
13:30	04:20	00:10	40		2,36	2,14	2,1	2,20	0,61
13:30	04:20	00:00	20	64,56	1,74	1,65	1,64	1,68	0,58
13:35	04:25	00:05	20		1,7	1,62	1,6	1,64	0,57
13:40	04:30	00:10	20		1,66	1,59	1,57	1,61	0,57
13:40	04:30	00:00	0	0	0,91	0,84	0,85	0,87	0,52
13:55	04:45	00:15	0	0	0,79	0,73	0,72	0,75	0,52
14:10	05:00	00:30	0	0	0,73	0,67	0,67	0,69	0,53

## **CIRRICULUM VITA**

**Candidate's full name: Zeynep Şekerer**

**Place and date of birth: Mersin and 19.02.1979**

**Mail Address: zeynepsekerer@gmail.com**

**Universities and Colleges attended: Eastern Mediterranean University**

